1998

Paleoseismic recurrence investigation of the Santa Cruz Mountains segment of the San Andreas fault near Watsonville, California

Gordon Frank Heingartner
San Jose State University

INFORMATION TO USERS

This manuscript has been reproduced from the microfilm master. UMI films the text directly from the original or copy submitted. Thus, some thesis and dissertation copies are in typewriter face, while others may be from any type of computer printer.

The quality of this reproduction is dependent upon the quality of the copy submitted. Broken or indistinct print, colored or poor quality illustrations and photographs, print bleedthrough, substandard margins, and improper alignment can adversely affect reproduction.

In the unlikely event that the author did not send UMI a complete manuscript and there are missing pages, these will be noted. Also, if unauthorized copyright material had to be removed, a note will indicate the deletion.

Oversize materials (e.g., maps, drawings, charts) are reproduced by sectioning the original, beginning at the upper left-hand corner and continuing from left to right in equal sections with small overlaps. Each original is also photographed in one exposure and is included in reduced form at the back of the book.

Photographs included in the original manuscript have been reproduced xerographically in this copy. Higher quality 6" x 9" black and white photographic prints are available for any photographs or illustrations appearing in this copy for an additional charge. Contact UMI directly to order.

UMI

A Bell & Howell Information Company
300 North Zeeb Road, Ann Arbor MI 48106-1346 USA
313/761-4700 800/521-0600

PALEOSEISMIC RECURRENCE INVESTIGATION OF THE SANTA CRUZ MOUNTAINS SEGMENT OF THE SAN ANDREAS FAULT NEAR WATSONVILLE, CALIFORNIA

A Thesis

Presented to

The Faculty of the Department of Geology

San Jose State University

In Partial Fulfillment

of the Requirements for the Degree

Master of Science

by

Gordon Frank Heingartner

May 1998

APPROVED FOR THE DEPARTMENT OF GEOLOGY

Dr. Deborah R. Harden

Dr. David W. Andersen

Dr. David P. Schwartz, U.S. Geological Survey

APPROVED FOR THE UNIVERSITY

ABSTRACT

PALEOSEISMIC RECURRENCE INVESTIGATION OF THE SANTA CRUZ MOUNTAINS SEGMENT OF THE SAN ANDREAS FAULT NEAR WATSONVILLE, CALIFORNIA

by Gordon F. Heingartner

Exploratory trenches excavated in the southern Santa Cruz Mountains 5 km east of Watsonville, California, provide information on the timing of paleo-earthquakes and the behavior of the Santa Cruz Mountains segment of the San Andreas fault. Faulting of alluvial deposits extending to within 35-40 cm of the ground surface is interpreted to record 1906 surface rupture, and analysis of 88 radiocarbon samples places the age of a previous episode of warping and faulting between 1434 and 1667 A.D. No direct evidence was found for large displacements equal to or greater than approximately 1-2 m associated with the 1836, 1838, or 1865 earthquakes, all of which have been proposed to have ruptured this segment. Age constraints for the penultimate event closely match those from other sites to the north, suggesting either a large 1906-type event in the mid-1600's or a sequence of closely-timed but discrete events along adjacent segments of the northern San Andreas fault. The minimum recurrence time of 239-271 years between the 1906 and penultimate events is considerably longer than most previous recurrence estimates and suggests that the Santa Cruz Mountains segment may rupture primarily in conjunction with other segments, rather than as an independent unit.

ACKNOWLEDGEMENTS

I would like to thank Deborah Harden, my principal advisor, for her enthusiastic encouragement with this project, and for all of the helpful suggestions that she made. I would like to thank David Schwartz of the USGS for all of his support, financial and otherwise, and for giving me the opportunity to take on this project. I would like to thank Dave Andersen for his helpfulness, and for his many invaluable suggestions.

I would like to express my gratitude to John Baldwin for teaching me the basics of paleoseismic research, and for the many hours of camaraderie we shared in the trenches. I would like to thank Tom Fumal of the USGS for imparting upon me some of his paleoseismic wisdom, John Hamilton of the USGS for his surveying expertise and production of the topographic maps, Daniela Pantosti of the USGS for her kind and timely assistance with the production of the figures, Carol Prentice of the USGS for providing me with the opportunity to gain valuable paleoseismic experience at the Survey, and Mike Rymer of the USGS for his support and encouragement.

Thanks to Allen Tucker of the Department of Physics for providing me the opportunity to work at Lawrence Livermore National Laboratory (LLNL), and John Southon of LLNL for allowing me to analyze my radiocarbon samples at no cost to the project, for sharing with me some of his vast knowledge of radiocarbon dating, and for his invaluable assistance in the data interpretation.

My gratitude goes to Ed Kelly, Jean Kelly, Colleen Kelly, and Tamia Marg-Anderson of the Kelly-Thompson Ranch for allowing me unlimited access to their property, and for being so kind and accommodating in the process. In addition, I would like to express my gratitude to Paul Gnehm and Joe Morris of the Kelly-Thompson Ranch for the assistance that they provided.

Many thanks to Bob Bogar, John Shipstead, Eric Eddlemon, Malia Burrows, Regina Bussard, Eric Sivers, and Lisa McBee for their invaluable field assistance, and to Fred Silva for his backhoe expertise. Finally, I would like to thank my wife, Ann, for her tireless support, patience, and encouragement. Without the assistance and kindness of all of the above-mentioned individuals, this project would not have been possible.

TABLE OF CONTENTS

LIST OF ILLUSTRATIONS

Figure

Plate

Table

PURPOSE AND BACKGROUND

Purpose

A detailed investigation of paleoseismic recurrence on the Santa Cruz Mountains segment of the San Andreas fault was performed between October 1995 and November 1996 at Arano Flat, which is located in the southern Santa Cruz Mountains approximately 5 km east of Watsonville, California (Fig. 1). The objective of the study was to identify and date paleoearthquake events as recorded in recent sediment. In turn, this allowed for the examination of: 1) the average recurrence interval for large-magnitude events on the southern portion of the Santa Cruz Mountains segment; 2) whether the penultimate event of the mid-1600's identified in regions to the north (Cotton and others, 1982; Prentice, 1989; Niemi, 1992; Simpson and others, 1996; Knudsen and others, 1997; Schwartz and others, in press) ruptured as far south as the study site; 3) whether various pre-1900 events -- in particular the 1838 and 1865 earthquakes -- ruptured the Santa Cruz Mountains segment in the vicinity of the study site; 4) whether the Santa Cruz Mountains segment characteristically ruptures as an independent unit, or only in conjunction with other segments, as in 1906; and 5) the nature of the seismic hazards posed by the Santa Cruz Mountains segment.

The field work associated with this study consisted of two phases: 1) excavation, examination, and detailed mapping of exploratory trenches; and 2) surveying of the site and subsequent generation of a detailed topographic map. The efforts put forth in this investigation contribute to our overall

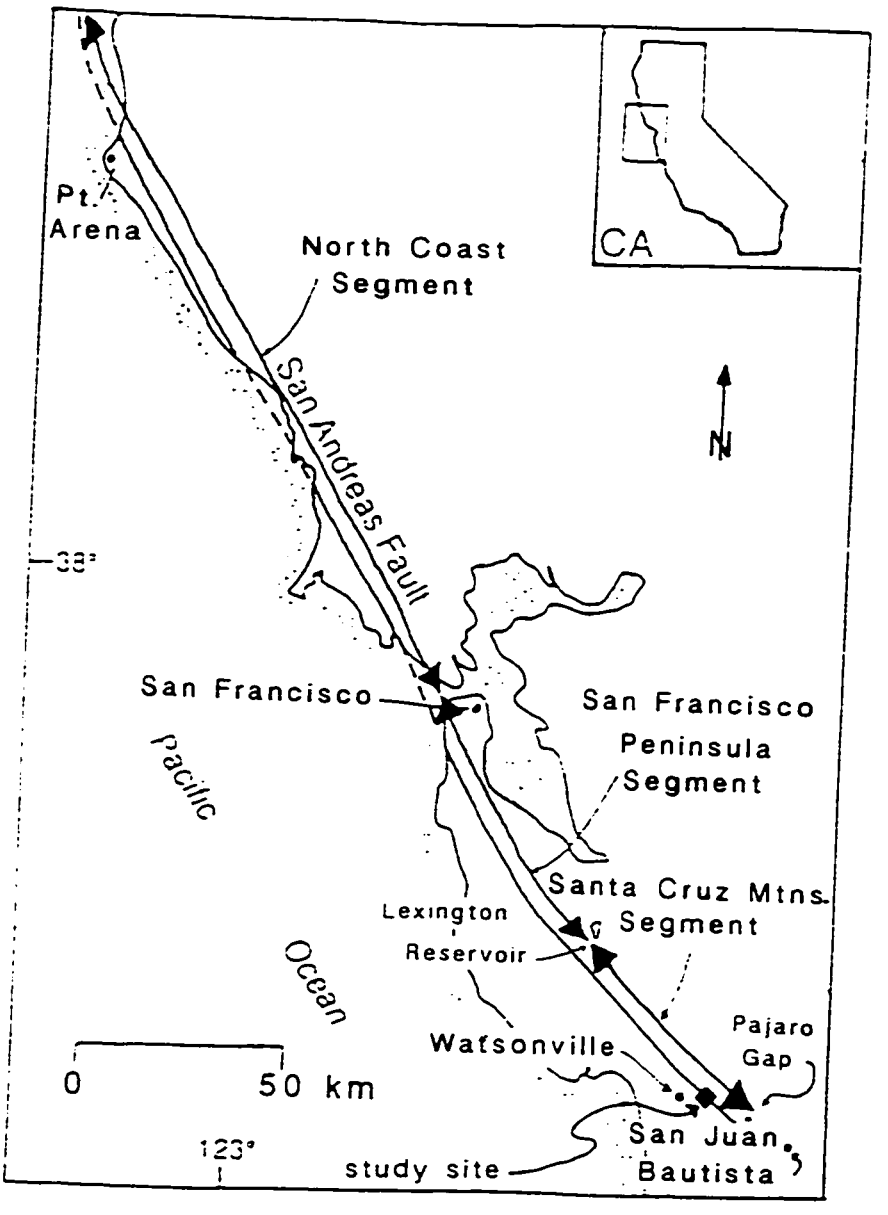

Figure 1. Map of the Northern California section of the San Andreas fault, showing location of the three constituent segments and the study site (modified from Niemi and Hall, in review).

understanding of the behavior and seismic potential of the Santa Cruz Mountains segment of the San Andreas fault.

Background

Paleoseismic investigations represent an important means by which the future seismogenic capabilities of a fault can be characterized. An accurate record of past earthquake events -- both historical and prehistorical -- provides the basis for estimating the magnitude and timing of future events. Since the development of fault segmentation modeling theory (Schwartz and Coppersmith, 1984), in which major faults are divided into discrete segments based on differences in slip rate, amount of coseismic slip, seismicity, and fault geometry, such estimates have been largely segment-specific.

The Northern California section (Hill and others, 1990) of the San Andreas fault (SAF), which represents the portion of the fault that ruptured in the great "San Francisco" earthquake of 1906, extends from Punta Gorda, near Cape Mendocino, to San Juan Bautista (Fig. 2). The Northern California section has been further subdivided into three major segments, primarily on the basis of variations in background seismicity and amount of coseismic slip associated with the 1906 and 1989 earthquakes (Working Group on California Earthquake Probabilities, 1988, 1990). From northwest to southeast, these are: 1) the North Coast segment (NCS; Fig. 1); 2) the San Francisco Peninsula segment (SFPS; Fig. 1); and 3) the Santa Cruz Mountains segment (SCMS; Fig. 1).

It is only within the past several years that detailed paleoseismic investigations -- involving the determination of slip rates, recurrence intervals,

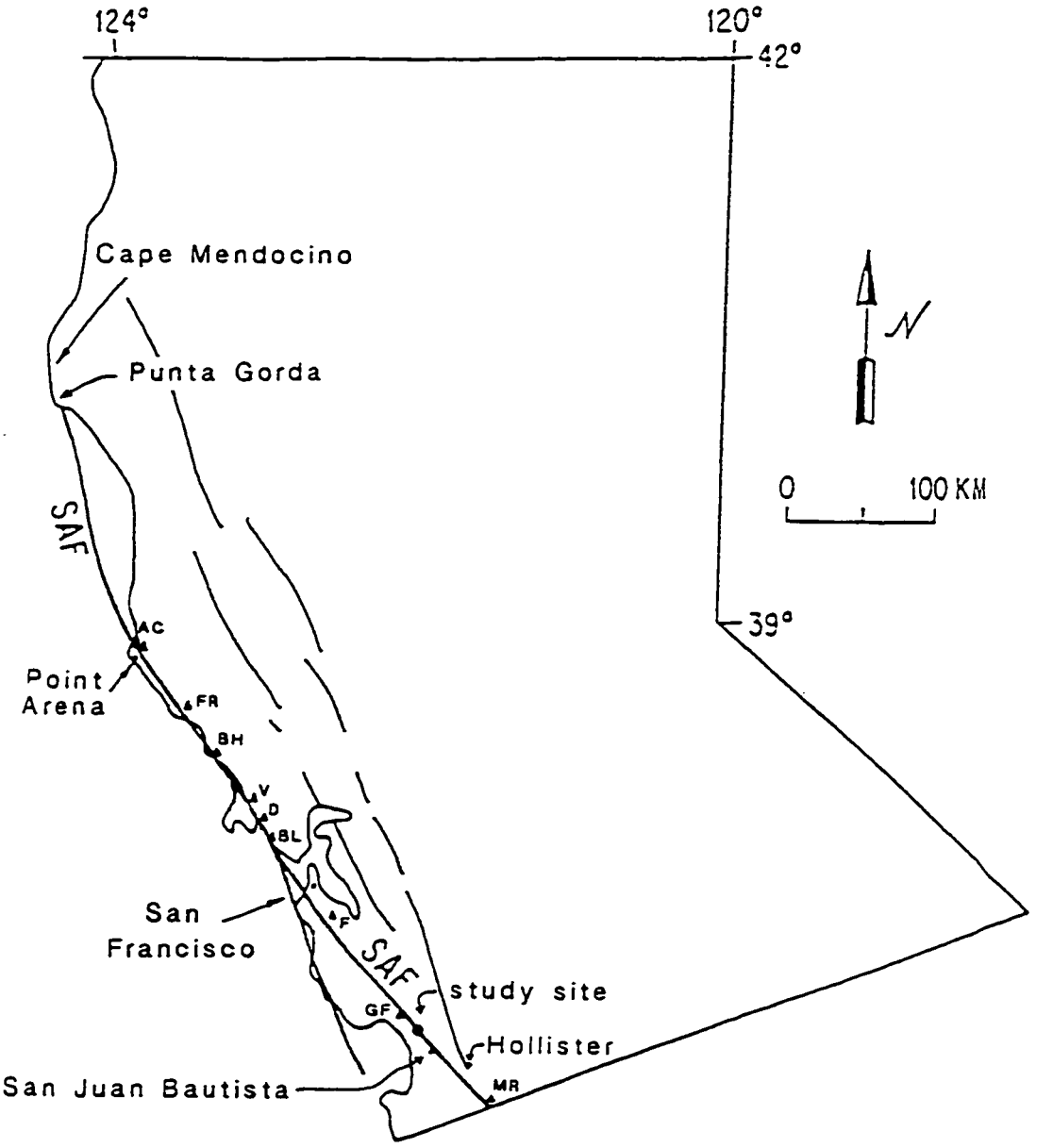

Figure 2. Map of the Northern California section of the San Andreas fault (SAF), showing locations of previous paleoseismic investigations and the study site. Point Arena (Prentice, 1989); AC=Alder Creek site (Baldwin, 1996); FR=Fort Ross (Noller and others, 1994; Simpson and others, 1996); BH=Bodega Harbor (Knudsen and others, 1997); V=Vedanta Wind Gap site (Niemi and Hall, 1992, in review; Niemi, 1992); D=Dogtown (Cotton and others, 1982); BL=Bolinas Lagoon (Knudsen and others, 1997); F=Filoli site (Clahan, 1996); GF=Grizzly Flat (Schwartz and others, in press); MR=Melendy Ranch (Sims, 1991). Modified from Prentice, 1989.

and timing of paleoearthquakes -- have been conducted on any of these segments. Studies of the North Coast segment (NCS) have been performed by Prentice (1989) and Baldwin (1996) near Point Arena, Noller and others (1994) and Simpson and others (1996) at Fort Ross, Niemi and Hall (1992, in review) and Niemi (1992) at the Vedanta Wind Gap site, Cotton and others (1982) at Dogtown, and Knudsen and others (1997) at Bolinas Lagoon and Bodega Harbor. Clahan (1996) conducted an investigation of the SFPS at the Filoli site, and Schwartz and others (in press) recently completed a study of the SCMS at Grizzly Flat, 15 km northwest of the study site (Fig. 2).

The SCMS, upon which this investigation focuses, traverses the southern portion of the Santa Cruz Mountains, much of which is steep, densely vegetated, and sparsely populated. It is, however, situated in close proximity to the population centers of Santa Cruz and Watsonville. Renewed interest in this stretch of the fault was precipitated by the 1989 Loma Prieta earthquake, which was centered in the southern Santa Cruz Mountains. This earthquake was responsible for serious damage sustained by the cities of Santa Cruz, Watsonville, San Francisco, and Oakland. The occurrence of this event and the resulting widespread damage accentuate the need for further study of the potential seismic hazards posed by this segment of the fault.

TECTONIC SETTING

Tectonic Evolution of the San Andreas Fault

The San Andreas fault (SAF) is the primary component of the North American-Pacific plate boundary. This transform boundary is believed to have originated approximately 28-26 Ma when a portion of the Pacific-Farallon spreading ridge collided with the trench at the western edge of North America, initiating dextral displacement between the North American and Pacific plates (Atwater, 1970).

The Farallon plate, which had previously been subducting beneath the North American plate, was fragmented into the Juan de Fuca plate to the north and the Cocos plate to the south; these two plates were connected by the newly formed transform boundary. The boundary lengthened as the Mendocino triple junction, located at the north end of the transform margin, and the Rivera triple junction, located at the south end (MTJ and RTJ, Fig. 3), migrated progressively away from one another (Atwater, 1970; Sedlock and Hamilton, 1991).

The SAF proper was first activated approximately 20-18 Ma, before which time North American-Pacific dextral displacement evidently was accommodated almost exclusively along an offshore fault system located near the toe of the continental slope (Atwater, 1970; Sedlock and Hamilton, 1991). About 8 Ma, the Mendocino triple junction is estimated to have passed the latitude of present-day Watsonville, California, thereby extending the SAF northward into the southern Santa Cruz Mountains (Atwater, 1970). Thus the SCMS, as well as the

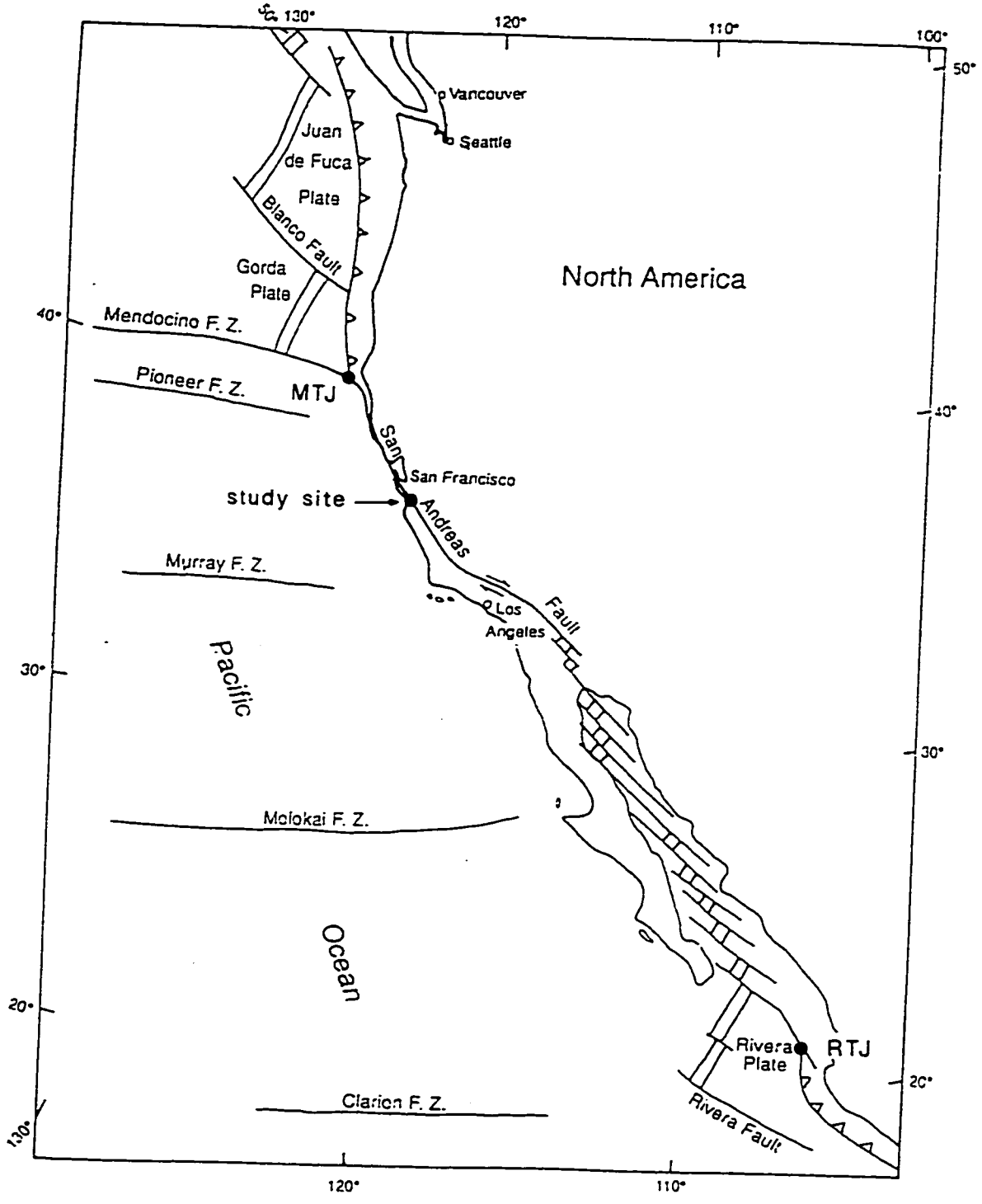

Figure 3. Map of the western margin of North America, showing location of the San Andreas fault, Mendocino Triple Junction (MTJ), Rivera Triple Junction (RTJ), and the study site (modified from Irwin, 1990).

remainder of the SAF to the north, is geologically young, having probably been active only since about latest Miocene time.

Most of the North American-Pacific dextral displacement continued to be accommodated along the offshore fault system until about 5 Ma, when the primary locus of displacement shifted eastward to the SAF (Sedlock and Hamilton, 1991). The present-day San Andreas system is approximately 1300 km long by 100 km wide (Wallace, 1990), encompassing numerous subsidiary faults, such as the Hayward, Calaveras, and San Gregorio, in addition to the SAF itself.

Segmentation of the Northern San Andreas Fault

The SCMS extends from just north of the intersection of the San Andreas fault and Highway 17 (near Lexington Reservoir) to Pajaro Gap, which is located 15 km northwest of San Juan Bautista (Fig. 1). It is about 40 km in length, making it the shortest segment of the northern SAF (Working Group on California Earthquake Probabilities, 1990; Thatcher and others, 1997). The boundaries of this segment correspond with the primary rupture zone of the 1989 Loma Prieta earthquake; prior to 1989, the designated boundaries had been located 15 km to the southeast (Working Group on California Earthquake Probabilities, 1988).

The SCMS is bounded on its south end by the central creeping segment of the SAF, which extends from just north of San Juan Bautista to the town of Parkfield (Fig. 4). The central creeping segment separates the northern SAF from the southern SAF, which was the locus of the great "Fort Tejon" earthquake of 1857 (Fig. 4). The creeping segment experiences continuous slip and an

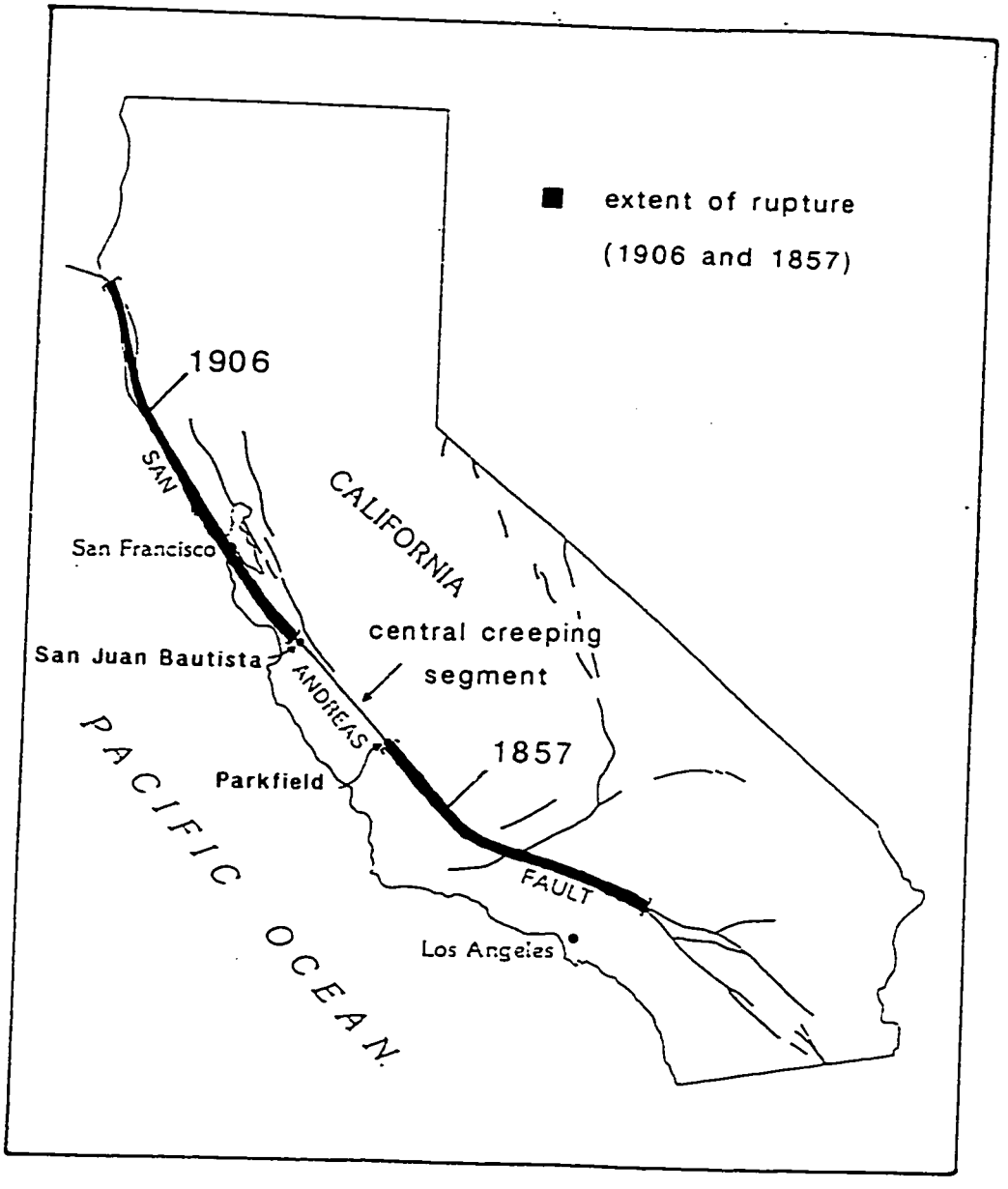

Figure 4. Map of the San Andreas fault, showing extent of 1906 and 1857 ruptures and location of central creeping segment (modified from Wallace, 1990).

abundance of small to moderate earthquakes, but very few large-magnitude events (Hill and others, 1990).

Recent work suggests that the northern boundary of the SFPS, which lies directly north of the SCMS, is located just offshore of the Golden Gate (King and others, 1990; Marshall and others, 1994; Thatcher and others, 1997), whereas previously it was thought to be located in the vicinity of Lower Crystal Springs Reservoir, approximately 40 km to the southeast (Working Group on California Earthquake Probabilities 1988, 1990). Hall and Wright (1993) have proposed the subdivision of the SFPS into a southern Black Mountain sub-segment and a northern Crystal Springs sub-segment, with the boundary between the two lying near the Filoli site (F) shown on Figure 2. The NCS, which is by far the longest of the northern SAF, extends from just west of San Francisco to Punta Gorda, near Cape Mendocino.

Geometry of the Fault Zone in the Southern Santa Cruz Mountains

The SCMS features a long restraining (left) bend and is situated within a broad zone of fault-normal compressional deformation that extends from the coast to the Santa Clara Valley (Schwartz, 1990). The presence of numerous folds and thrust faults in the southern Santa Cruz Mountains is consistent with the horizontal shortening associated with such a restraining bend (Aydin and Page, 1984; Schwartz and others, 1990).

The zone of active deformation associated with the SAF itself may also be considerably wider and more complex in the southern Santa Cruz Mountains than in more northerly regions. Here, numerous discontinuous and en-echelon

lineaments define a broad zone ranging in width from about 1 to 2 km (Sarna-Wojcicki and others, 1975; Thatcher and Lisowski, 1987), whereas the zone of deformation to the north is considerably simpler, and is characterized by a narrow, well-defined fault zone with a width of about 20 to 200 m (Brown and Wolfe, 1972; Thatcher and Lisowski, 1987). However, a detailed re-examination of the geometry and geomorphic expression of the fault zone in the southern Santa Cruz Mountains has led Prentice and Schwartz (1991) to conclude that most of the subsidiary lineaments represent the effects of differential erosion, or of shaking- and gravity-related processes, rather than constituting primary surface ruptures. They proposed that the main fault trace in the southern Santa Cruz Mountains defines a narrow, continuous zone, much as it does in areas to the north.

PREVIOUS INVESTIGATIONS AND IMPLICATIONS

Previous Investigations

The steep slopes, dense vegetation, and abundant landslides that characterize much of the southern Santa Cruz Mountains have impeded efforts to conduct investigations in this region. The only previous paleoseismic investigation of the SCMS was performed by Schwartz and others (in press), making this segment the least-studied of the northern SAF. The results of their investigation, as well as others conducted on nearby segments, are summarized below.

The aforementioned investigation of the SCMS by Schwartz and others (in press) was conducted at Grizzly Flat, a small, elongate alluvial basin located 15 km northwest of the study site (Site GF, Fig. 2). Three trenches were excavated across the fault, revealing evidence for two surface-rupturing earthquakes. The older event occurred prior to 1633-1655 A.D. and after 1016-1209 A.D. The more recent event, which is expressed by faulting extending to within several centimeters of the ground surface, has been interpreted as the 1906 earthquake.

A detailed paleoseismic investigation of the SFPS was recently conducted by Clahan (1996) at the Filoli site, which is located approximately 38 km southeast of San Francisco (Site F, Fig. 2). This study involved the excavation of 13 trenches -- both fault-parallel and fault-normal -- across an alluvial fan surface at the mouth of Spring Creek. A buried channel with an age of 2070±120 years B.P. was offset 30±1.5 m, yielding a preferred late Holocene slip rate of 14.9±2.6 mm/yr. In addition, three younger channels were each offset 2.5 m across the

fault, evidently as a result of coseismic slip associated with the 1906 earthquake. An older buried channel with an age of 530 to 140 years B.P. was offset 4.1±0.5 m; assuming that the additional offset resulted from the June, 1838 earthquake, a coseismic slip value of 1.6 m can be attributed to this event. These findings also suggest that the SFPS may be capable of generating two different types of "characteristic earthquake" (Clahan, 1996).

Investigations of the NCS have been more numerous (Cotton and others, 1982; Prentice, 1989; Niemi, 1992; Niemi and Hall, 1992, in review; Noller and others, 1994; Simpson and others, 1996; Baldwin, 1996; Knudsen and others, 1997), so slip rates, recurrence intervals, and timing of paleoearthquakes have been fairly well constrained for this reach of the fault. Cotton and others (1982) performed the first paleoseismic study of the NCS at Dogtown, which is located approximately 29 km northwest of San Francisco (Site D, Fig. 2). Although the results of their investigation were ambiguous, re-interpretation of their data by Niemi (1992) implies that the penultimate event most likely occurred after 1521-1668 A.D.

At Point Arena, Prentice (1989) obtained a maximum late Holocene slip rate of 25.5±2.5 mm/yr, an average recurrence interval for large magnitude events of 270 to 380 years, and age constraints for at least four pre-1906 surface-rupturing events (Fig. 2). The penultimate event occurred after 1531 A.D., and most likely after 1636 A.D. The previous event occurred between 1040 A.D. and 1644 A.D., and the earliest two events occurred between 89 B.C. and 1384 A.D.

Niemi and Hall (1992) obtained a minimum late Holocene slip rate of 24±3 mm/yr and an average recurrence interval of 181 to 261 years at the Vedanta Wind Gap site, approximately 35 km northwest of San Francisco (Site V, Fig. 2). Niemi (1992) and Niemi and Hall (in review) also identified at least five pre-1906 surface-rupturing earthquakes: the penultimate event, which most likely occurred after 1591-1661 A.D., and four successively older events, which occurred between 1270 A.D. and 1617 A.D., between 869 A.D. and 1211 A.D., between 715 A.D. and 1037 A.D., and prior to 555 A.D., respectively.

At the Archae Camp site, which is located at Fort Ross, approximately 58 km southeast of Point Arena, Noller and others (1994) obtained a preliminary late Holocene slip rate of 19.5±2.5 mm/yr, an average recurrence estimate of 300 to 350 years, and evidence for six or seven surface-rupturing earthquake events during the past 2500 to 3000 years (Site FR, Fig. 2). Simpson and others (1996) obtained age constraints for at least four pre-1906 events at this site. The penultimate event occurred between 1170 A.D. and 1650 A.D., while three progressively older events occurred between 920 A.D. and 1285 A.D., between 555 A.D. and 950 A.D., and prior to 555 A.D., respectively.

Baldwin (1996) obtained a minimum slip rate of 24.5±6 mm/yr, an average recurrence interval of 164 to 270 yrs, and age constraints for one pre-1906 surface-rupturing earthquake at the Alder Creek site, which is located approximately 10 km north of Point Arena (Site AC, Fig. 2). This pre-penultimate event occurred between 1040 A.D. and 1630 A.D.

Knudsen and others (1997) have found evidence for two pre-1906 events, which were identified on the basis of rapid sea level changes recorded in

sediment cores obtained adjacent to the NCS at Bolinas Lagoon and Bodega Harbor (Sites BL and BH, Fig. 2). The age of the penultimate event has been bracketed between 1453 A.D. and 1648 A.D. at Bodega Harbor, while a previous event has been constrained to have occurred prior to 1324 A.D. at Bodega Harbor, and prior to 1300 A.D. at Bolinas Lagoon.

Based on studies to date, the slip rate of the central creeping segment of the SAF is substantially higher than that of the SFPS, and most likely the SCMS as well. Offset alluvial deposits of the San Benito River at Melendy Ranch, which is located about 32 km southeast of Hollister, yield a late Holocene slip rate of 22±5 mm/yr for the northern portion of the central creeping segment (Site MR, Fig. 2). This value matches closely the historic rate of 22 mm/yr recorded by an offset corral fence built on the ranch property in 1945 (Sims, 1991).

The 1988 and 1990 Working Group on California Earthquake Probabilities derived average recurrence intervals for the SCMS of 100±24 years and 96±16 years, respectively, for events exhibiting 2.5 m of slip. In addition, the 1990 Working Group assigned a probability of less than 1 percent to the SCMS for a M_w7 earthquake occurring within the next 30 years. The present investigation examines the question of whether these estimates, and the conceptual models of slip distribution and fault segmentation upon which they are based, are accurate.

Tectonic Implications of Slip Rate Variability along the San Andreas Fault

It is important to derive an estimate for the slip rate of the SCMS in order to accurately characterize the seismic hazards for this region. Currently, there are no independent geologic slip rate data for the SCMS. However, based on

the fact that 1906 coseismic slip magnitudes on the SCMS were somewhat lower than those on the SFPS (Thatcher and Lisowski, 1987; Marshall and others, 1994; Thatcher and others, 1997), as well as on geodetic slip rate and other data obtained along the SCMS, the slip rate can be reasonably estimated as probably no higher than, and quite possibly somewhat lower than, the rate of 14.9±2.6 mm/yr obtained for the SFPS (Clahan, 1996). Savage and others (1979), using a rigid block motion inversion model, derived a geodetically modeled slip rate of 13±2 mm/yr for the SAF in the vicinity of San Juan Bautista, and the Working Group on Northern California Earthquake Potential (1996) obtained a similar estimate of about 14 mm/yr for the SCMS.

The slip rate of the SCMS of the SAF, which, as discussed above, probably is about 13-14 mm/yr, constitutes only a small percentage of the total rate of North American-Pacific plate motion at this latitude. Using the global plate-motion model NUVEL-1, DeMets and others (1990, revised 1994) have obtained a value for North American-Pacific relative motion of 46 mm/yr toward N36°W along the SAF in central California. This value can be resolved into a component of plate margin-parallel slip of 39±2 mm/yr along N30°W±2° as well as the relatively small component of plate margin-perpendicular deformation that is largely responsible for the uplift of the Coast Ranges (DeMets and others, 1990; Argus and Gordon, 1991; Kelson and others, 1992). Thus the SCMS of the SAF appears to accommodate only about 40 percent or less of the total plate margin-parallel slip at this latitude (Schwartz and others, in press), which means that the remainder of slip must be distributed among other faults in the region,

such as the Sargent and Calaveras faults to the northeast and the San Gregorio fault to the southwest (Fig. 5).

Because a portion of San Andreas slip appears to be transferred to the San Gregorio fault south of the Golden Gate (Fig. 5), the proportion of total plate margin-parallel slip accommodated by the SCMS and SFPS is substantially less than that accommodated by the NCS, as evidenced by the significantly higher slip rate of the NCS (Schwartz and others, in press). The higher slip rate along the northern portion of the central creeping segment, which is comparable to that of the NCS, probably results from the additional slip that is transferred from the Calaveras fault (Sims, 1991), which merges with the San Andreas near the town of Hollister (Figs. 2, 5).

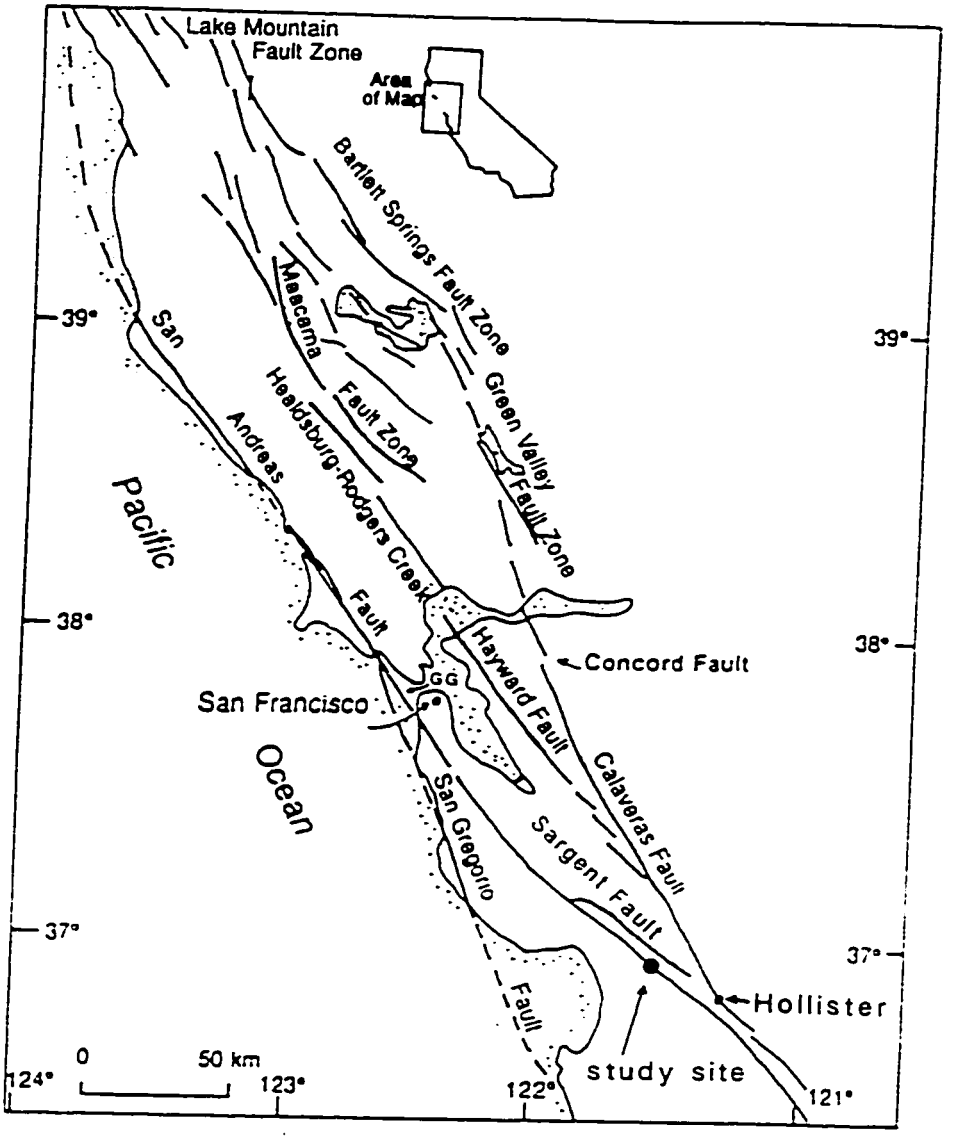

Figure 5. Map of the San Andreas fault system in northern California, showing locations of principal faults and the study site. GG=Golden Gate (modified from Baldwin, 1996).

HISTORICAL SEISMICITY

Records of large historical earthquakes, including information on timing, as well as extent and distribution of damage, can be used to estimate their approximate magnitude, location, and rupture length. Such information is used in the development of seismic hazards assessments. It also represents an important supplement to paleoseismic investigations, because it can help to pinpoint the age of events identified in the sedimentary record that have occurred too recently to be accurately dated using radiocarbon techniques.

A number of moderate- to large-magnitude earthquakes have affected the southern Santa Cruz Mountains in the nineteenth and twentieth centuries, the most prominent of which are discussed below and depicted, with the exception of the 1906 event, on Figure 6. The most recent large event occurring in the vicinity of the SCMS was the M_w6.9 Loma Prieta earthquake of October 17, 1989 (Fig. 6). This event initiated at a point 18 km beneath the surface of the southern Santa Cruz Mountains and ruptured upward to within 4 to 6 km of the ground surface (Oppenheimer, 1990; Working Group on California Earthquake Probabilities, 1990; U.S. Geological Survey Staff, 1990). It did not produce a surface break (Working Group on California Earthquake Probabilities, 1990; U.S. Geological Survey Staff, 1990). The rupture extended a distance of 35 to 40 km along the strike of the fault (Fig. 1), from near Lexington Reservoir to Pajaro Gap (Working Group on California Earthquake Probabilities, 1990). This event involved right-reverse slip along a plane dipping 70° SW, with geodetic data indicating 1.6±0.3 m of dextral slip and 1.2±0.4 m of reverse slip (Lisowski and

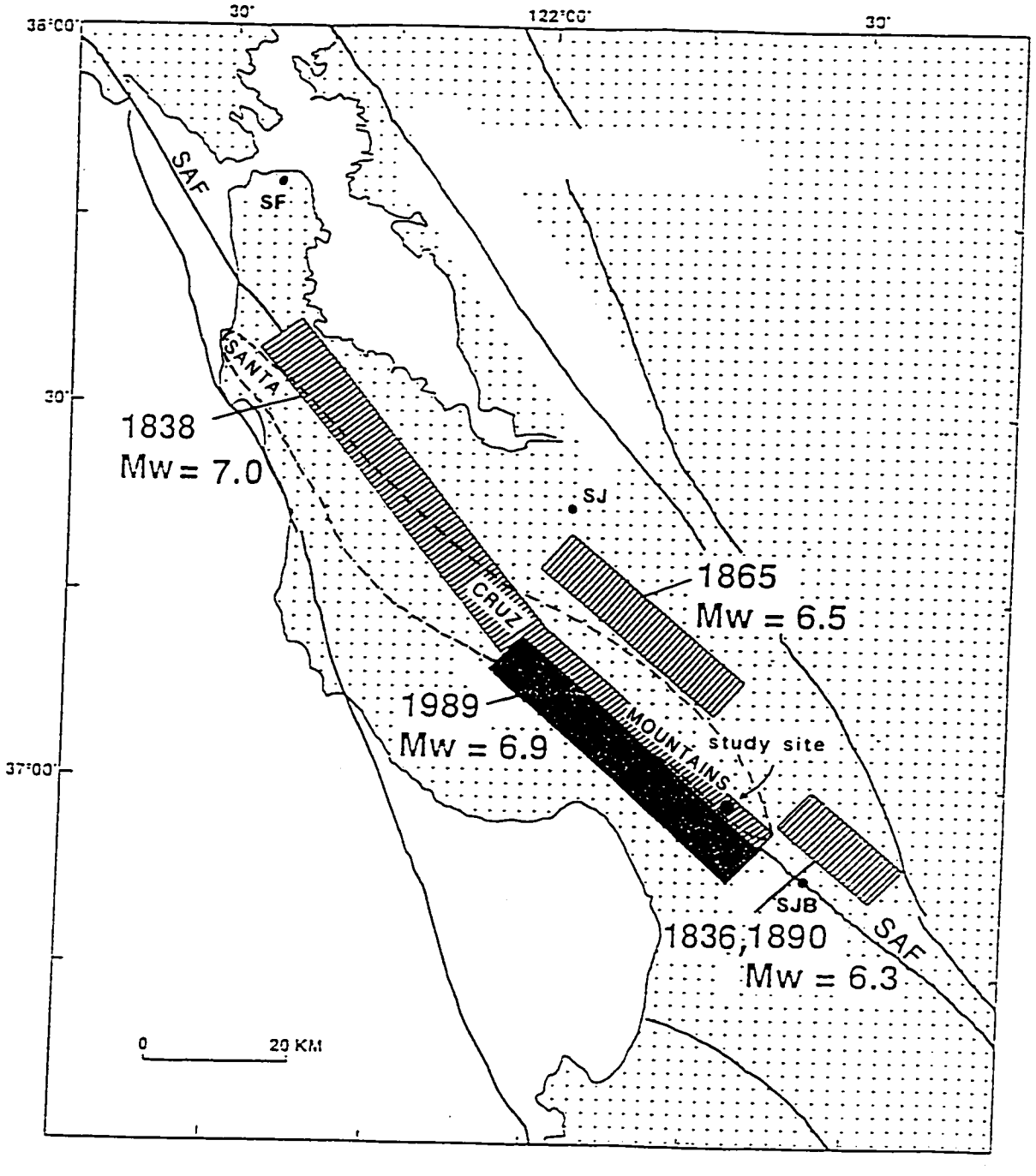

Figure 6. Map of the northern San Andreas fault (SAF) south of 38° latitude, showing inferred locations and rupture extents of 1836, 1838, 1865, 1890, and 1989 earthquakes, all of which are believed to have occurred on or near the Santa Cruz Mountains segment. The location of the study site is also shown. SF=San Francisco; SJ=San Jose; SJB=San Juan Bautista (modified from Tuttle and Sykes, 1992).

others, 1990). The epicentral region is located near the center of the previously mentioned restraining bend in the SCMS of the SAF, which probably accounts in part for the substantial compressional deformation associated with the event (Schwartz and others, 1990).

The Loma Prieta earthquake was unusual in the relatively large component of reverse slip that it exhibited and in the fact that the fault plane was dipping at a 70-degree angle. The 1906 earthquake, by comparison, involved pure strike-slip motion on a vertical San Andreas fault in the vicinity of the Loma Prieta epicenter (Segall and Lisowski, 1990). These inconsistencies have led various workers to conclude that the 1989 event most likely did not occur on the San Andreas fault itself, but rather on a closely associated, oblique-slip blind thrust fault (U.S. Geological Survey Staff, 1990; Dietz and Ellsworth, 1990; Segall and Lisowski, 1990; Marshall and others, 1991; Prentice and Schwartz, 1991; Thatcher and others, 1997).

The previous major earthquake affecting the SCMS was the M_w~8 "San Francisco" earthquake of April 18, 1906 (Fig. 4). Unlike the Loma Prieta earthquake, this event likely involved surface rupture along the entire length of the SCMS, although the evidence for this is not unequivocal. Upon re-evaluating historical reports of 1906 surface offset in the southern Santa Cruz Mountains, Prentice and Schwartz (1991) concluded that surface faulting most likely occurred throughout the region, extending as far south as San Juan Bautista. Near-surface faulting observed at the Grizzly Flat site is consistent with this interpretation (Schwartz and others, in press).

Coseismic slip associated with the 1906 event was substantially less in the southern Santa Cruz Mountains than in regions to the north. Surface offset measurements range from about 1.0 m at the Pajaro River railroad bridge, located approximately 5 km southeast of the study site, to about 1.5 m at Wrights tunnel, located approximately 32 km northwest of the study site (Lawson, 1908). However, these measurements, as well as the others reported in the region, were found upon recent re-examination to be unreliable (Prentice and Schwartz, 1991), leaving little geologic basis for estimating the amount of 1906 slip in the southern Santa Cruz Mountains. A more recent investigation of 1906 slip in the region by Prentice and Ponti (1997) has resulted in a revised estimate for coseismic offset of the Wrights tunnel of at least 1.7-1.8 m.

Geodetic estimates of 1906 coseismic slip in the southern Santa Cruz Mountains are somewhat higher, ranging from about 2.5 m (Segall and Lisowski, 1990) to 2.7 m (Thatcher and Lisowski, 1987; Thatcher and others, 1997), although these values are still considerably lower than those obtained to the north along the SFPS and NCS of about 3.5 m and 5.2 m, respectively (Marshall and others, 1994; Thatcher and others, 1997). Despite the fact that some degree of uncertainty is inherent in these geodetic estimates, they probably represent a much closer approximation of true 1906 slip than do the questionable geologic data.

A number of pre-1900 events also have been documented in or near the southern Santa Cruz Mountains, including the June 1838, October 1865, April 1890, and possibly June 1836 earthquakes (Fig. 6). Unfortunately, information

about these events is limited, so the conclusions drawn must be considered tentative.

Documentation of the M_w~7 June 1838 event is especially sparse. Louderback (1947) assigned it to the San Andreas fault, as did Lindh (1983), the Working Group on California Earthquake Probabilities (1988), and Ellsworth (1990). Based on a comparison of damage reports along the San Francisco Peninsula and Monterey, Louderback (1947) further suggested that it may have ruptured both the SFPS and the SCMS (Fig. 6), a view also held by Toppozada and Real (1981) and Sykes and Nishenko (1984). Lindh (1983) and King and others (1990), on the other hand, limit 1838 rupture to the SFPS, apparently based on the assumption that rupture associated with the 1865 event, which they attributed to the SCMS, abutted against the 1838 rupture zone.

After a detailed review of all the documents, Tuttle and Sykes (1992) concluded that shaking intensities in Monterey were similar in 1838, 1906, and 1989, concurring with Louderback (1947) that the 1838 event ruptured both the SFPS and the SCMS. Toppozada and Borchardt (1996) expanded the boundaries of 1838 rupture even further, suggesting that it extended all the way from San Francisco to San Juan Bautista.

The M_w~6.5 October 1865 event occurred in the general vicinity of the Santa Cruz Mountains. Lindh (1983) assigned the event to the San Andreas fault, as did the Working Group on California Earthquake Probabilities (1988). McNutt and Toppozada (1990) also concluded that the 1865 event occurred on the San Andreas fault, and further suggested that it was almost an exact duplicate of the 1989 Loma Prieta event. However, after detailed re-examination

of the historical documents and comparison of shaking intensities in surrounding areas, Tuttle and Sykes (1992) proposed that this event probably was located northeast of the Loma Prieta rupture zone, possibly on a reverse fault, and in fairly close proximity to the San Jose area (Fig. 6).

An earthquake that occurred in 1890 has been attributed by Toppozada and Real (1981) to the SCMS of the SAF. They suggested that it ruptured a small portion of the fault in the general vicinity of San Juan Bautista. Tuttle and Sykes (1992) agreed with their general location of the event, but suggested that it occurred on one of several subsidiary faults in the region rather than on the San Andreas, thereby resolving the problem of having the same segment of the fault rupture twice within sixteen years -- in 1890 and 1906 (Fig. 6).

The earthquake of June 1836 has traditionally been assigned to the northern Hayward fault (Louderback, 1947; Toppozada and Real, 1981; Lienkaemper and others, 1995). Borchardt and Toppozada (1996) have re-examined the damage reports, comparing the earthquake's felt effects with those of better documented events located within the region that stretches from about 5 km northwest of San Jose to about 40 km southwest of San Juan Bautista. They suggested that the 1836 event actually may have occurred near San Juan Bautista, on or near the San Andreas fault, and was probably of M_w~6.5 (Fig. 6).

The SCMS is currently "locked" and is not exhibiting any significant aseismic creep, as illustrated by the fact that roads and fences crossing the fault more than 5 km northwest of San Juan Bautista show no evidence of offset in the past 40 years (Behr and others, 1990). With the exception of a clustering of events of up to M_w~4 immediately north of Pajaro Gap, recent seismicity along

the SCMS is rather sporadic (King and others, 1990), and is limited primarily to depths of 10 km or greater, with essentially no seismic slip occurring above a depth of about 5 km (Fig. 7). Despite the fact that recent seismicity along the SCMS is well-documented, the question of whether the aforementioned pre-1900 events ruptured this segment has not been completely resolved from a historical perspective, although it is important to do so in order to accurately assess the seismic hazards for this region.

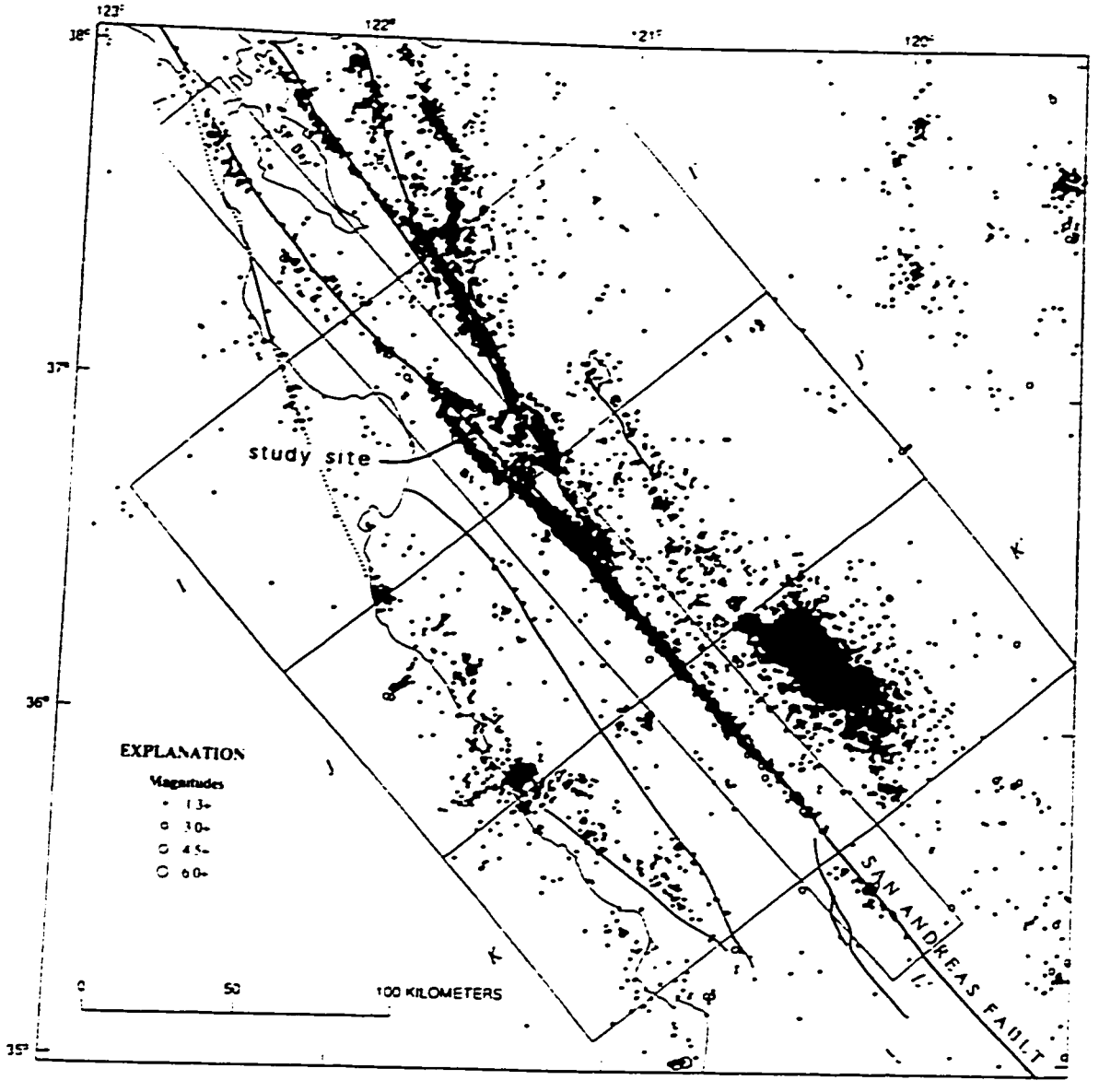

Figure 7. Map showing recent seismicity along the central portion of the San Andreas fault system and the location of the study site (modified from Hill and others, 1990).

GEOLOGIC SETTING OF THE STUDY SITE

The SAF is the predominant geologic feature in the southern portion of the northwest-trending Santa Cruz Mountains. Its trend is slightly more northerly than that of the mountain range, however, as evidenced by the fact that it enters the Santa Cruz Mountains on the east side of the range at the northern end of the SCMS, but crosses over to the west side before it reaches the southern end (Fig. 6). The SAF is geomorphically expressed as a series of well-defined aligned notches, sag ponds, sidehill benches, linear drainages, linear ridges, and offset streams (Sarna-Wojcicki and others, 1975; Prentice and Schwartz, 1991).

In the Santa Cruz Mountains the SAF generally separates plutonic and metamorphic basement rocks of the Salinian block to the southwest from Franciscan basement rocks to the northeast, although the fault itself does not always represent the precise contact between these two terranes (Oakeshott, 1966; Dibblee and Brabb, 1978; McLaughlin and others, 1988; Brabb, 1989). In the southern portion of the range, exposures of Salinian granitic and metasedimentary rocks are primarily limited to the Ben Lomond pluton, which is located approximately 10-15 km southwest of the fault (Brabb, 1989). In the region lying directly southwest of the SAF, Tertiary marine sedimentary rocks, such as the Purisima Formation (Fig. 8), overlie the crystalline basement (Dibblee and Brabb, 1978; Brabb, 1989). In the Pajaro River valley, which lies directly southwest of the southernmost portion of the Santa Cruz Mountains, a series of Pleistocene fluvial and marine terraces (Fig. 8) overlies the Tertiary bedrock (Greene, 1977; Dibblee and Brabb, 1978; Brabb, 1989).

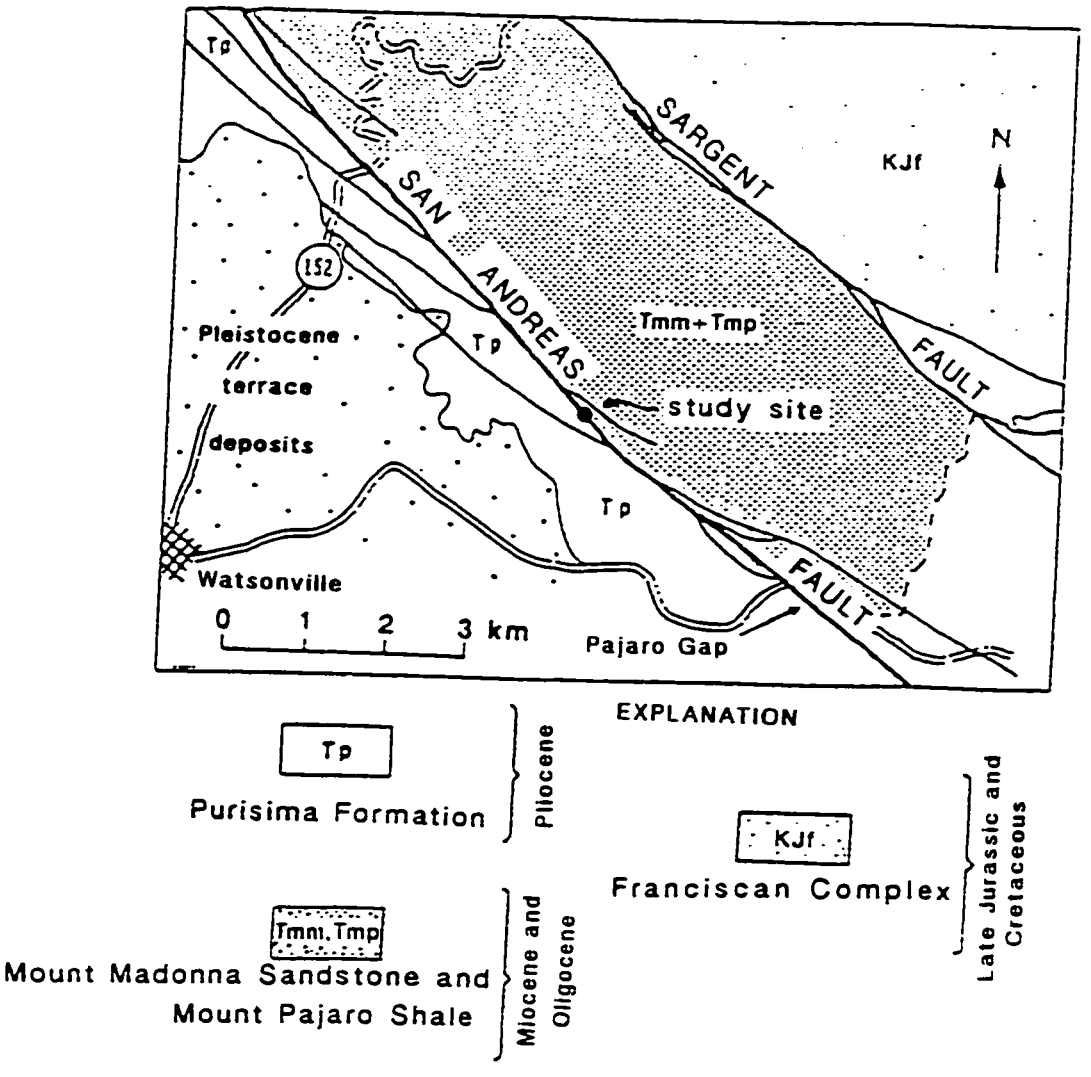

Figure 8. Generalized geologic map of the study site and surrounding area, showing distribution of lithologic units and locations of major faults (modified from Oakeshott, 1966).

Rocks of the Franciscan Complex in the southern Santa Cruz Mountains are exposed only east of the Sargent fault (Dibblee and Brabb, 1978; McLaughlin and others, 1988; Irwin, 1990). A thick sequence of Tertiary marine sedimentary rocks, including the Mount Pajaro Shale and the Mount Madonna Sandstone, occurs in the region between the two faults (Dibblee and Brabb, 1978; McLaughlin and others, 1988; Brabb, 1989); these rocks are quite similar in character to the Tertiary rocks lying directly southwest of the SAF (Fig. 8).

Throughout the Santa Cruz Mountains, evidence of fault-normal shortening is prevalent. This is particularly true of the southern portion of the range, where the Tertiary marine sedimentary rocks on either side of the SAF are tightly folded into a series of anticlines and synclines and cut by numerous thrust faults, most of which are oriented subparallel to the SAF (Dibblee and Brabb, 1978; Aydin and Page, 1984; McLaughlin and others, 1988; Brabb, 1989). The presence of these geologic structures, as well as the Pleistocene terraces, is indicative of recent uplift throughout the region.

In the immediate vicinity of the study site, isolated outcrops of Mount Madonna Sandstone, which consists of a pale orange, arkosic sandstone (Brabb, 1989), are exposed on the steep hillsides directly above and to the northeast of the fault zone. A few outcrops of Mount Pajaro Shale, which consists of a laminated olive-gray to brownish-black, semisiliceous shale (Brabb, 1989), can be seen here as well. Exposures of the Purisima Formation, which consists of a yellowish-gray, tuffaceous siltstone with interbedded sandstone (Brabb, 1989), are more common, and can be found on the topographically lower hillsides directly southwest of the fault zone.

METHODOLOGY

The field work for this investigation consisted of two phases: 1) excavation and logging of exploratory trenches; and 2) generation of a detailed topographic map of the study site. The site was chosen because of the well-defined expression of the fault in this area and the presence of a thick sequence of sediment overlying the fault; the number of sites in the southern Santa Cruz Mountains that satisfy these criteria is relatively small.

Seven trenches, with a cumulative length of about 250 m, were excavated across the fault zone for the purpose of identifying and dating paleoearthquake events. Trench 1 was logged in October of 1995, primarily by John Baldwin of the U.S. Geological Survey. I logged Trench 2 in November of 1995 and all succeeding trenches in 1996, including a widened re-excavation of the fault zone in Trench 1. The logs of the Trench 1 fault zone presented herein, as well as the interpretations derived from them, are based upon this 1996 re-excavation.

The trenches averaged about 2 m in depth, with a maximum depth of about 2.5 m. The presence of groundwater, which was encountered at about 2 m below the ground surface, limited the depths to which the trenches could be extended. Four of the seven trenches were logged (Trenches 1, 2, 3, and 4); the remaining three did not contain suitable exposures of the fault.

The site at which Trenches 1 through 4 were excavated was chosen on the basis of the following factors: 1) its proximity to the linear ridge at the northwest end of the site; 2) its location within the floodplain of Arano Creek, which ensures relatively continuous sedimentation through time and consequent

preservation of paleoearthquake events within the geologic record; and 3) its coincidence with a prominent trace of the fault as mapped by Sarna-Wojcicki and others (1975).

Following excavation of the trenches, the walls were cleaned, and a string grid with 1-m horizontal spacings and 0.5-m vertical spacings was erected on each wall to serve as a reference base for logging. The shears, fractures, and other deformational features comprising the fault zone were logged in detail, as was the stratigraphy of the exposed sedimentary deposits and soil horizons. Units were described in the field. Numerous samples of wood and charcoal, the great majority of which are detrital in nature, were collected for radiocarbon analysis and their locations recorded on the logs. The trenches were logged at scales ranging from one inch equals 0.5 meters to one inch equals 1 meter. With the exception of Trench 2, both walls of the trenches were logged.

A topographic survey of the study site was conducted with the assistance of John Hamilton of the U.S. Geological Survey in order to depict its micro-morphology and to provide a base map for the location of the fault and trenches. A total of 933 survey data points, which includes the perimeters of the four logged trenches, was collected between October, 1995 and November, 1996 using a Wild T2002 combination electronic distance measurer (EDM) and theodolite. A computer-generated topographic map was subsequently produced with a contour interval of 25 cm.

SURFICIAL GEOLOGY AND GEOMORPHOLOGY OF THE STUDY SITE

The study site is located within a broad, fault-controlled, sidehill bench along the western slope of the southern Santa Cruz Mountains, at an elevation of about 183 to 189 m (600 to 620 ft); a detailed topographic map of the site is shown on Plate 1 and in Figure 9. The bench is bisected by Arano Creek, which parallels the fault zone in the vicinity of the study site (Figs. 10, 11). The creek has been right-laterally offset a distance of about 1 km along the fault and has created an extensive flood plain that covers most of the width of the sidehill bench. However, the channel is incised about 4 to 6 m in the vicinity of the study site, making it unlikely that significant flooding has occurred in the recent past.

The location of the principal trace of the fault is clearly delineated by a linear ridge located at the northwest end of the study site (Fig. 9). This ridge comprises the southeasternmost portion of a more extensive alignment of fault-controlled geomorphic features that extend northwestward for a distance of about 0.5 km.

Trenches 1, 3, and 4, which were excavated on the east side of Arano Creek, were situated directly to the southeast of the southeastern termination of the linear ridge, where geomorphic expression of the fault is obscured by thick accumulations of overbank deposits (Figs. 9, 11). These were the only trenches that contained suitable exposures of the fault. An additional trench excavated approximately 6 m northwest of Trench 4 also revealed evidence of faulting, but was situated almost entirely within bedrock. The lack of adequate sedimentary deposits at this locality precluded identification of individual seismic events, so

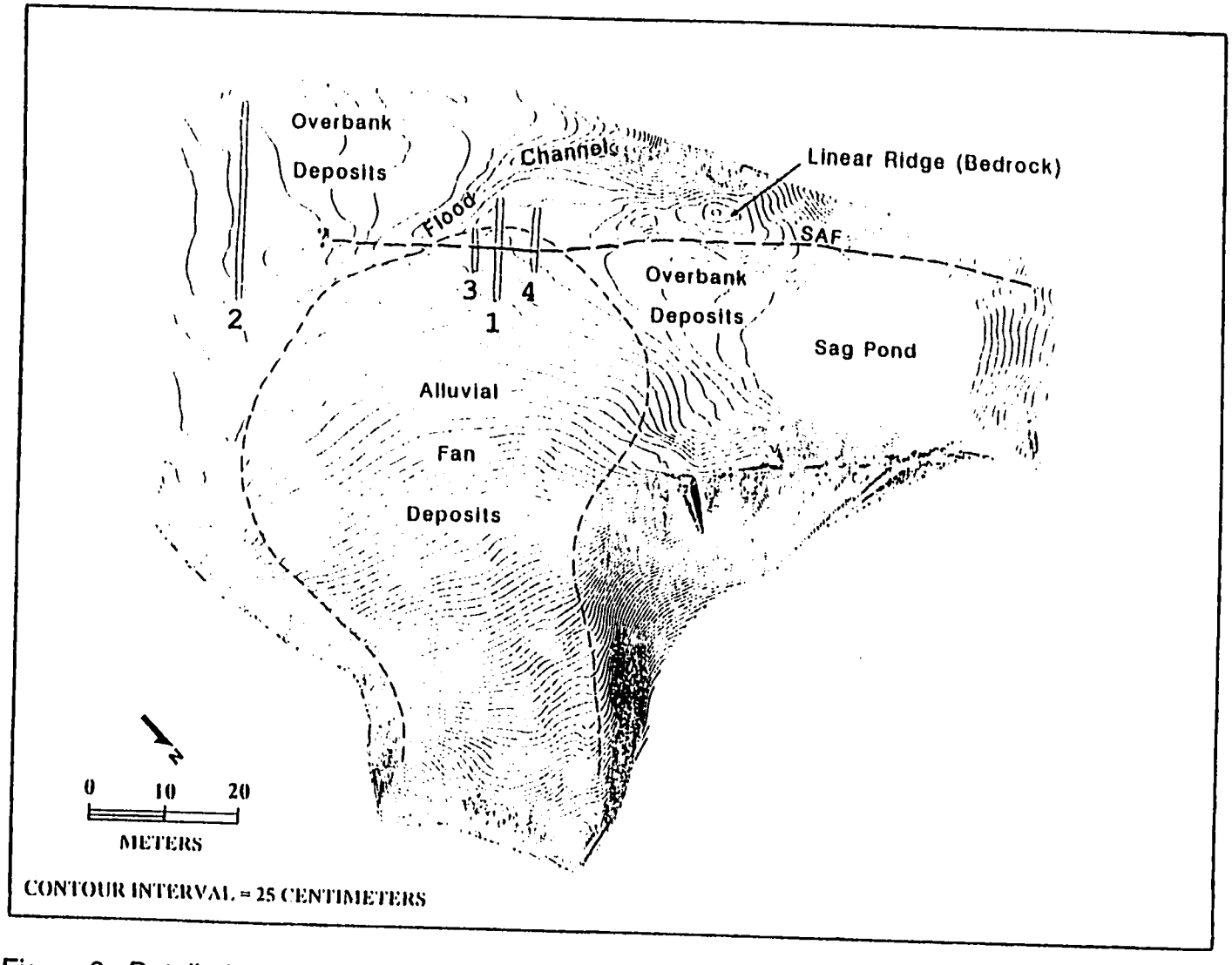

Figure 9. Detailed topographic map of the study site, showing location of the San Andreas fault (SAF), Trenches 1-4, prominent geomorphic features, and distribution of surficial deposits (topographic map created by John Hamilton, U.S. Geological Survey).

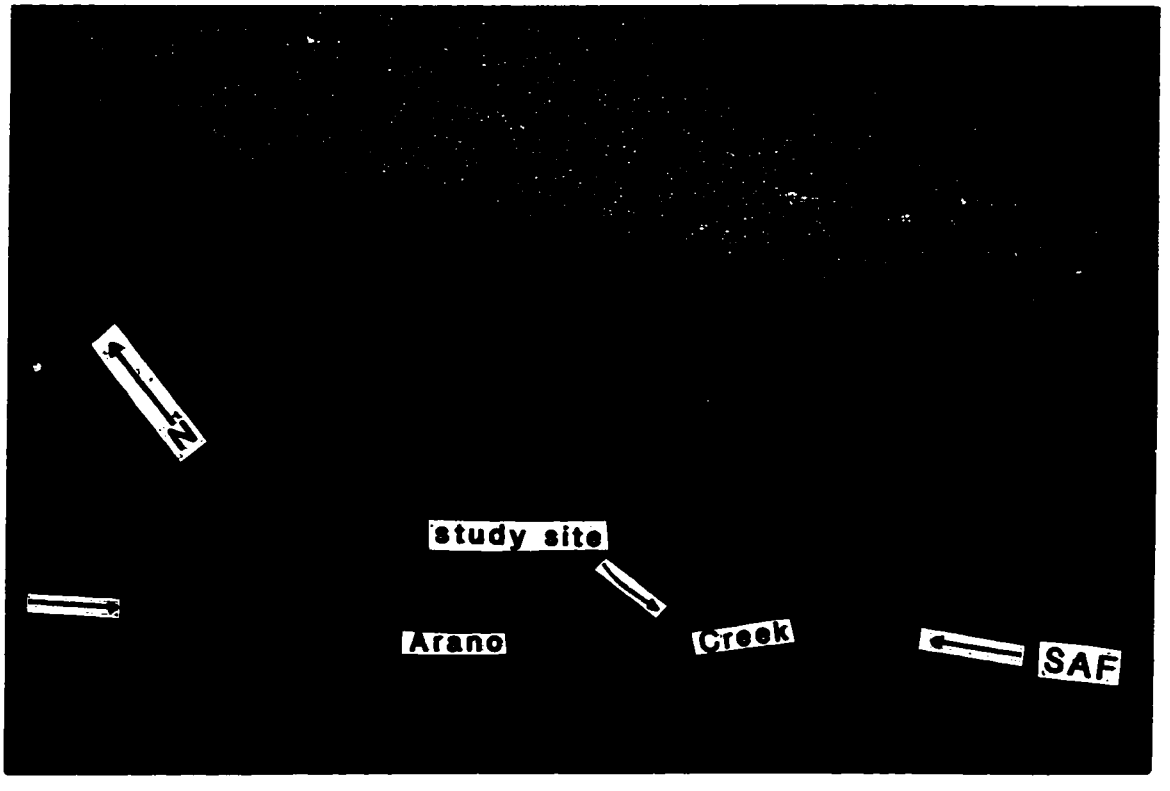

Figure 10. Oblique aerial photograph of the study site and surrounding area looking northeast toward the Santa Clara Valley (photo taken by A.M. Sarna-Wojcicki, U.S. Geological Survey).

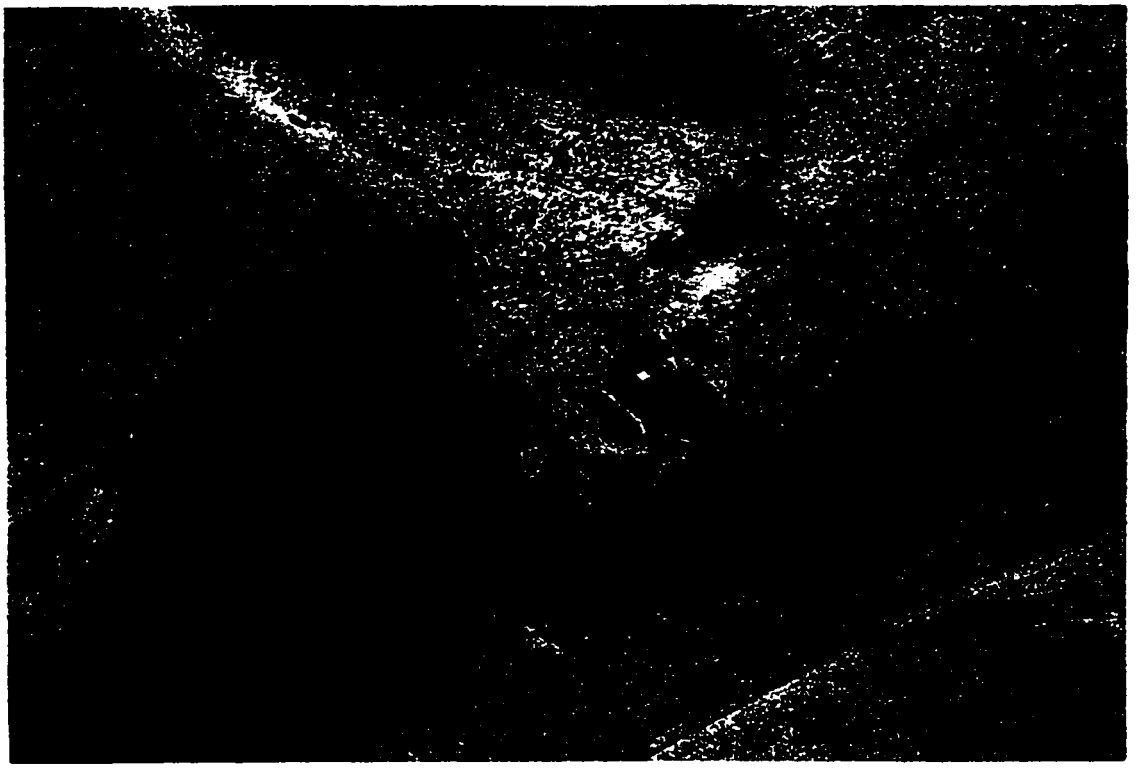

Figure 11. Close-up aerial photograph of the study site, showing location of trenches east of Arano Creek.

this trench was not logged. Trench 2, which was located about 30 to 40 m southeast of the others, did not show any evidence of faulting, a fact that strongly suggests that this trace of the fault ends somewhere between Trench 2 and Trench 3 (Fig. 9, Plate 1).

Southeast of the trenches, the fault is located west of Arano Creek (Sarna-Wojcicki and others, 1975), which implies that the study site is situated within a releasing (right) step-over zone. In order to locate the southeastward continuation of the fault, two additional trenches were excavated directly west of Arano Creek a short distance to the south of Trench 2 (Fig. 12). However, no evidence of the fault was encountered in either of these trenches, so neither was logged. Therefore, in the vicinity of these two trenches, the fault trace must be located either within the creek channel itself, or some distance to the west of the trenches.

The easternmost portion of the sidehill bench encompassing the study site is covered by alluvial fan deposits that emanate from the steep drainages to the east, overlapping the overbank deposits and extending westward to the general vicinity of the main trace of the fault (Figs. 9, 11). During periods of heavy rainfall, such as those that occurred during the winter of 1996-97, large amounts of sediment are added to the fan surfaces, including substantial numbers of cobble- to boulder-sized clasts (Figs. 13, 14). In the vicinity of the study site, these most recent deposits extend to within several meters of the main fault trace, directly east of Trenches 1, 3, and 4. A sag pond lies directly east of the linear ridge a short distance to the north of the trenches, and a flood channel

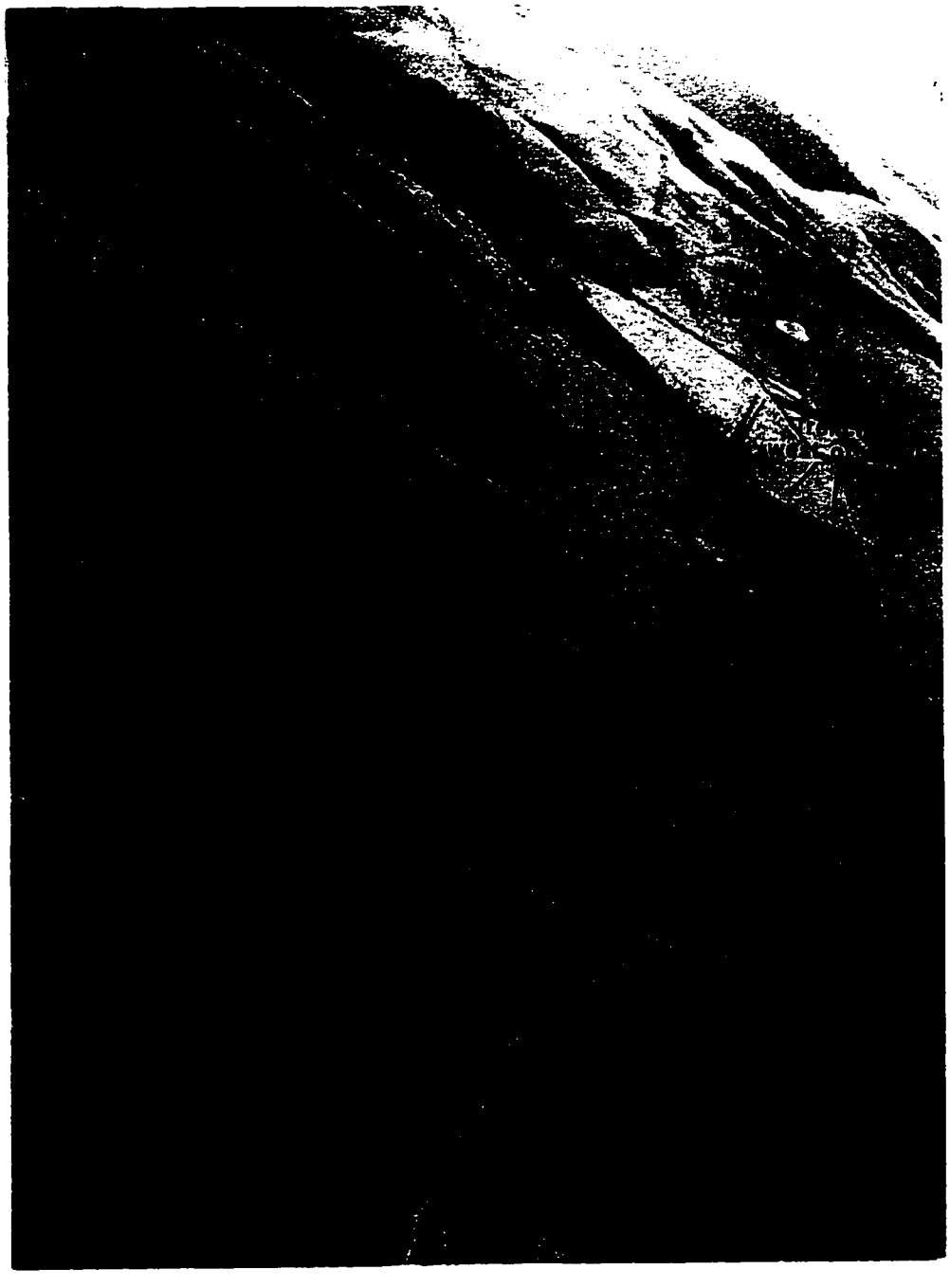

Figure 12. Oblique aerial photograph of the study site, showing location of trenches west of Arano Creek. View to the southwest.

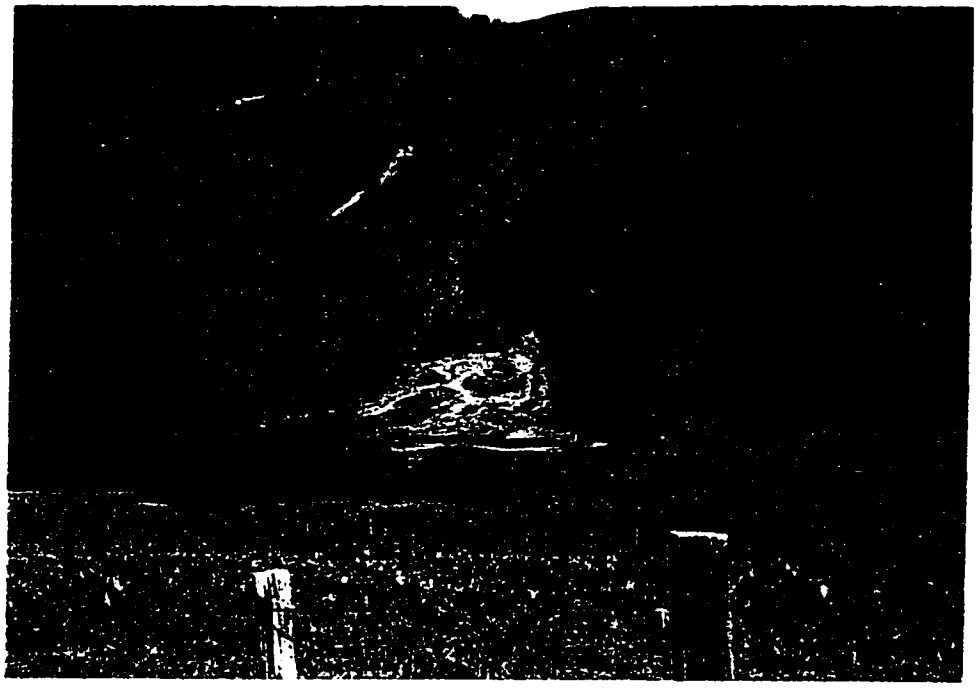

Figure 13. Photograph of alluvial fan covering the eastern portion of the study site, showing distribution of sediment deposited during the storms of January, 1997. View to the northeast (photo was taken in March of 1997).

Figure 14. Close-up photograph of alluvial fan deposits of January, 1997. Note the presence of cobbles and boulders in the background and progressively finer-grained sand in foreground. View to the northeast (photo was taken in March of 1997).

emanating from Arano Creek runs roughly parallel to the fault for a distance of about 30 m between Trenches 2 and 3 (Figs. 9, 11).

Although not conclusive, historical evidence suggests that coseismic surface rupture associated with the 1906 earthquake may have extended through the study site. Prentice and Schwartz (1991) were given a first-hand account of 1906 surface deformation by Tim Arano, a man who lived in the vicinity of the study site during this time. They quoted him as follows: "It (the 1906 surface crack) was really good across there and went out across the dry pond and all the way to Hazel Dell." When he said this, he was standing just to the southeast of the study site, and was pointing to the northwest; Hazel Dell is located several kilometers northwest of the site. The dry pond he referred to is the sag pond (Figs. 9, 11) located at the northwest end of the study site (D. Schwartz, U.S. Geological Survey, personal communication, 1996). Although it is obvious from this account that surface cracks associated with the 1906 earthquake did extend through the site, these cracks could have been of secondary shaking-related origin, and do not in themselves represent unequivocal evidence of primary surface rupture (Prentice and Schwartz, 1991).

GENERALIZED SITE STRATIGRAPHY

Generalized Stratigraphic Descriptions

At the study site, a sequence of about 1.5 to 2.5 m of predominantly fine-grained deposits overlies the weathered siltstone bedrock of the fault zone. These deposits have been divided up into discrete units on the basis of their predominant physical characteristics (Fig. 15). The sequence is thinnest in the region adjacent to the linear ridge and thickens progressively to the southeast, as the depth to bedrock increases (see Appendix A for detailed unit descriptions; see Plates 2-5 for trench logs).

Because most of the units comprising this sequence are correlative between Trenches 1, 3, and 4, these units have been designated with numbers. The units exposed in Trench 2, on the other hand, could not be directly correlated with the others, and have therefore been designated with letters. Larger numbers or letters nearer the end of the alphabet represent older (stratigraphically lower) units than do smaller or earlier ones.

Units 22-110, which comprise the lower portion of the sequence exposed in Trenches 1, 3, and 4 (Fig. 15), as well as the entire sequence exposed in Trench 2, with the exception of Unit I (Plate 3), consist of well-stratified, well-sorted deposits of yellowish-brown fine sand to silty, fine sand alternating with grayish-brown clayey silt to sandy silt. Thin, relatively continuous layers of dark-gray clay are present within the lowermost sand deposits (Units 65, 100, F, and G). Effects of bioturbation and pedogenesis within these units are relatively minor. These deposits exhibit substantial lateral continuity and can commonly be

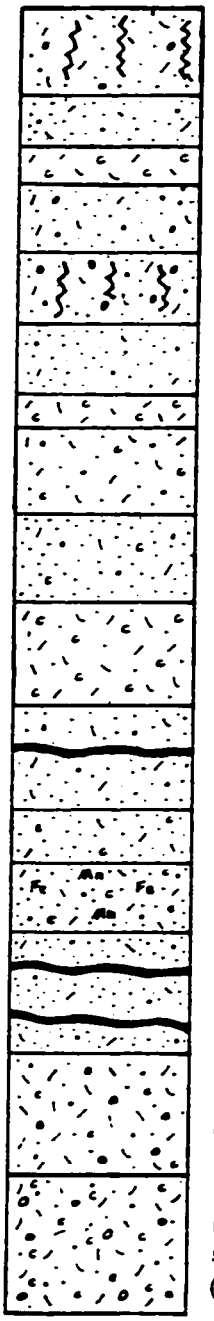

Generalized Stratigraphic Column

Unit Description

Unit 10: Reddish gray, silty, fine sand, some medium to coarse sand and fine to coarse gravel (A horizon).

Unit 17: Pale yellow fine sand, some silt and pebbles, little medium sand.

Unit 17/18: Dusky red silty clay (in-situ burn layer).

Unit 18: Yellowish brown, silty, fine sand, little medium to coarse sand, little fine to medium gravel.

Unit 19: Gray, silty, fine sand, some medium to coarse sand and fine to coarse gravel (buried A horizon).

Unit 22: Yellowish brown and gray mottled fine sand, some medium to coarse sand and pebbles, little silt.

Unit 22/25: Dusky red silty clay (in-situ burn layer).

Unit 25: Grayish brown, fine, sandy silt, some clay, little medium to coarse sand and pebbles.

Unit 40: Yellowish brown and gray mottled fine sand, some silt, little clay, medium to coarse sand, and pebbles.

Unit 50: Grayish brown clayey silt, some fine sand.

Unit 65: Brown and gray mottled, silty, fine sand, little medium to coarse sand, contains thin layer of dark gray clay.

Unit 80: Light brownish gray, silty, fine sand, little clay.

Unit 90: Dusky red, silty, fine sand, some clay, little coarse sand, abundant iron and manganese oxide nodules.

Unit 100: Brown and gray mottled fine sand, some silt, little medium to coarse sand and pebbles, contains thin layers of dark gray clay.

Unit 110: Brown and gray mottled gravelly sandy silt, some clay.

Unit 115: Gray and brown mottled clayey silt, some fine to medium sand and fine to coarse gravel (weathered bedrock).

Figure 15. Generalized stratigraphic column depicting the units exposed in Trenches 1, 3, and 4 (not drawn to scale).

traced horizontally for several tens of meters (Plates 2, 3), despite the fact that precise correlations between the units exposed in Trench 2 and those in the other trenches could not be made. Because of the lateral continuity of these deposits, the lower sequence exposed in Trenches 1, 3, and 4 is very similar on both sides of the fault.

In the eastern portion of the site, deposits consisting of gray silty sand with some gravel, yellowish-brown silty sand, and pale yellow fine sand (Units 19, 18, and 17, respectively) overlap and interfinger with the underlying well-stratified deposits (Fig. 15); these units are found only in Trenches 1, 3, and 4. Although these overlying deposits are mainly limited to the east side of the fault, their distal portions do extend a short distance to the west of it. In general, these deposits are thoroughly bioturbated, with widespread krotovina, burrows, and rootlets; they also show considerable evidence of pedogenesis. Because of its gray color, very heavy bioturbation, and substantial soil development, Unit 19 has been interpreted as a buried A horizon.

A normally-graded, lens-shaped deposit consisting of fine to coarse sand and gravel (Unit I) was exposed near the eastern end of Trench 2, directly below the topographic depression that marks the flood channel (Plate 3). In Trench 4, weathered bedrock consisting of gray and brown mottled clayey silt with variable amounts of sand and gravel (Unit 115) was encountered at a depth of about 1.5 to 2.0 m. A soil horizon with an average thickness of about 0.5 m (Units 10 and A) was revealed in the uppermost portion of all the trenches (Fig. 15, Plate 3, respectively); it consists of heavily-bioturbated, gray silty sand to sandy silt with

abundant krotovina, burrows, rootlets, and locally moderately to well developed granular soil structure.

Depositional Environments of Stratigraphic Units

The fine-grained, well-sorted texture and lateral continuity of the deposits comprising the lower, well-stratified portion of the sedimentary sequence exposed in Trenches 1, 3, and 4 (Units 22-110), and virtually the entire sequence exposed in Trench 2 (Fig. 15, Plate 3, respectively), suggest that they constitute overbank deposits originating from the adjacent Arano Creek. The fine sand layers probably represent larger-magnitude, higher-energy flooding events, whereas the silt and clay layers likely represent smaller-magnitude, lower-energy events.

The higher proportion of gravel clasts, generally poorer sorting, and limited lateral distribution of the deposits comprising the upper portion of the sequence exposed in Trenches 1, 3, and 4 (Units 17, 18, and 19) suggest that they probably were deposited on alluvial fans that originated northeast of Arano Creek. Their coincidence with the geomorphic expression of the alluvial fan that occupies the eastern portion of the site is consistent with this interpretation, and their proximity to its distal end probably accounts for their predominantly fine-grained texture. The occurrence of widespread alluvial fan deposits of fine sand in this area following the heavy rains of January, 1997 lends further support to this interpretation (Figs. 13, 14).

The lens-shaped sand and gravel exposure (Unit I) located near the eastern edge of Trench 2 represents a channel deposit. This conclusion is

reinforced by the fact that it is situated directly beneath the surface expression of the flood channel. This unit contains a piece of broken glass measuring 4-5 cm in diameter, indicating that it was deposited within the recent historic past. Therefore, the stream channel from which it is derived probably emanated from an alluvial fan to the east, rather than from the currently incised Arano Creek during a flooding event.

The thickness and lateral continuity of the overbank deposits attest to the fact that Arano Creek must have flooded frequently in the past, before significant incision of the channel had occurred. The lack of substantial bioturbation and pedogenesis of these deposits further suggests that deposition of these units probably was relatively continuous. After substantial incision had occurred, the creek evidently no longer overflowed its banks, and deposition of the overbank material ceased. Since that time, the alluvial fans to the east appear to have been the only significant source of sedimentation across the fault zone. Therefore, incision of the creek channel to the point at which significant flooding could no longer occur probably took place after the deposition of Unit 22, which represents the most recent overbank deposit, and prior to the deposition of Unit 19, which represents the earliest alluvial fan deposit (Fig. 15).

Deposition of the alluvial fan sediments in the vicinity of the fault zone probably was considerably less continuous than that of the overbank deposits, as evidenced by the fact that the alluvial fan deposits are, in general, thoroughly bioturbated and show considerable evidence of pedogenesis. Because Unit 19 most likely represents a buried A horizon, a minimum time interval of approximately 200 years (Birkeland, 1984) must have elapsed between its

deposition and that of Unit 18, which directly overlies it. The deposition of alluvial fan deposits in the vicinity of Trenches 1, 3, and 4 in January of 1997 and the presence of broken glass within the Trench 2 channel deposit attest to the fact that such episodic sedimentation has continued up to the present.

RADIOCARBON DATING

Overview of Procedures and Limitations

In order to determine the ages of the stratigraphic units exposed in the trenches at the study site, samples of charcoal, wood, and bulk sediment were collected and their locations recorded on the trench logs (Plates 2-5). The sediment in the trenches contains abundant detrital charcoal as well as two prominent in-situ burn layers. Eighty-eight samples were subjected to radiocarbon analysis. Five of these samples were split into two portions, each of which was analyzed separately.

Radiocarbon dating of organic materials is based on the decay of the radioactive isotope ^{14}C. This carbon isotope is manufactured in the earth's upper atmosphere by the interaction of cosmic ray neutrons and nitrogen atoms, and absorbed, along with the stable isotopes ^{12}C and ^{13}C, by living organisms. Once the carbon has become fixed in the organism's tissues, the ^{14}C can only disappear by radioactive decay (to ^{14}N), which occurs at a known rate. Using the half-life of ^{14}C of 5,568 years, the age of the organic material is then determined by measuring the proportion of ^{14}C left in the sample. Although this half-life value is known to be in error by 3 percent, the more accurate value of 5730 years is not used, by convention, in order to avoid confusion with earlier reported dates (Mook and Waterbolk, 1985).

Analysis of the samples collected at the study site was performed at the Center for Accelerator Mass Spectrometry at Lawrence Livermore National Laboratory. Accelerator Mass Spectrometry (AMS) uses a mass spectrometer to

measure the ^{14}C to ^{12}C ratio by counting the individual atoms of these two isotopes within a given sample. This technique represents a significant improvement over conventional radiocarbon analysis, because samples as small as 1 mg can be precisely dated, whereas a minimum of about 1 to 3 g was previously required.

Prior to AMS analysis, rootlets and other foreign materials were removed from the samples. The samples were then pretreated with washes of HCl, NaOH, and de-ionized water in order to remove inorganic contaminants, absorbed humic acids, and other substances. Next, the samples were burned to completion to form CO_2, which was subsequently converted back into purified solid graphite. After completion of these preliminary procedures, the samples were ready for AMS analysis. I performed all of these preliminary procedures on my samples at Lawrence Livermore National Laboratory.

The sample ages derived by the lab represent standard radiocarbon ages reported in radiocarbon years before present (B.P.). The reported ages have been corrected for isotope fractionation, which occurs in plants during photosynthesis, by normalizing to a delta ^{13}C ($^{13}C/^{12}C$) value of –25 per mil. However, because the concentration of ^{14}C in the earth's atmosphere has varied through time, these radiocarbon ages cannot be utilized directly, but must first be converted to standard calendric ages. This is accomplished through the use of tree-ring calibration curves (dendrochronology), which provide a long-term record of temporal variations in atmospheric ^{14}C concentration as measured in the tissues of bristlecone pines and other very old trees. I used the 3.0.3c version of the Calib calibration program (Stuiver and Reimer, 1993) to convert radiocarbon

years to calendar years. This program generates 1 sigma and 2 sigma probability distributions in calendar years for each radiocarbon age, and associated standard deviation, that is entered. These probability distributions are reported as one or a series of age range(s), each with its corresponding percent probability of representing the true age of the sample, within the limits of the 1 sigma or 2 sigma interval. Because of irregularities in the calibration curves, some radiocarbon ages yield more than one possible calendric age (Fig. 16), in which case each has less than a 100 percent probability of representing the true age of the sample within 1 sigma or 2 sigma. Unless otherwise noted, all ages reported herein represent 2 sigma age ranges in calendar years, and their associated probability percentages refer to their likelihood of representing the sample's true age within the constraints of the 2 sigma interval (i.e. at the 95 percent confidence level). In order to eliminate the substantial increase of ^{14}C in the atmosphere resulting from above-ground nuclear testing, sample ages that are reported as years before present are counted relative to the year 1950 A.D., with 0 B.P. equal to 1950 A.D.

The dating of detrital charcoal presents some inherent limitations. Unlike in-situ organic deposits such as peat, detrital charcoal can be significantly older or younger than the deposit in which it is found. Charcoal sample ages that are substantially greater than that of the stratum in which they occur can result from: 1) reworked charcoal that has been eroded away and re-deposited in successive episodes of cut-and-fill; 2) charcoal that has rested in place for long periods of time before being picked up and deposited; and 3) charcoal that is derived from very old trees such as redwoods, which are common in the vicinity of the study

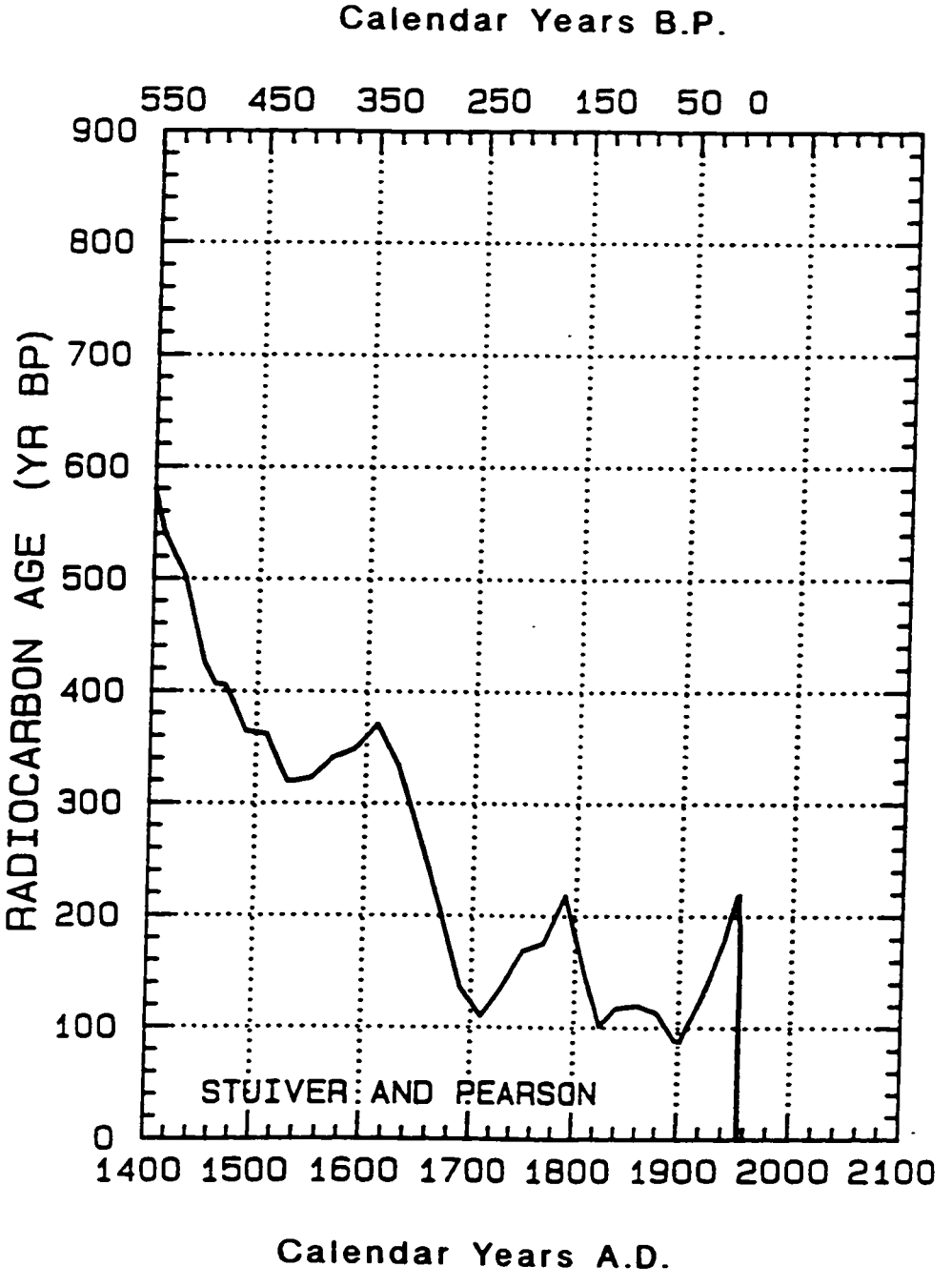

Figure 16. A portion of the dendrochronologically derived calibration curve used to convert radiocarbon ages to calendar ages. The x-axis represents ages in calendar years, with A.D. calendar ages shown at the bottom and calendar years before present (B.P.) shown at the top. The y-axis represents radiocarbon ages in radiocarbon years B.P. Note that a radiocarbon age of between 100 and 200 years yields several possible calendar ages (from Stuiver and Pearson, 1993).

site. On the other hand, burrowing and bioturbation by rodents and other soil organisms can introduce younger detrital charcoal into underlying older deposits, as can roots that have penetrated from above. Contamination by dissolved organic material carried by percolating groundwater can result in sample ages that are either younger or older than that of the deposit in which they occur (Murphy and others, 1979). Because the age of a detrital charcoal sample usually is greater, by some amount, than that of the deposit in which it is incorporated, sample ages normally are considered to represent maximum ages of deposits.

In an attempt to reduce the uncertainties associated with the dating of detrital charcoal, various sampling procedures were employed. Angular samples were given preference over rounded ones, because they are less likely to have been substantially reworked. Heavily bioturbated areas were avoided where possible, although it was sometimes difficult to determine the degree of bioturbation with confidence. In the laboratory, root hairs and other foreign materials were removed with tweezers and a scalpel. The effectiveness of these procedures, however, is limited; they may decrease the degree of uncertainty to some extent, but they can never eliminate it entirely. The charcoal collected from burn layers, which presumably represents in-place organic material, should theoretically provide better age control than other charcoal samples.

For most of the stratigraphic units, multiple samples were analyzed. In such cases, a weighted average of these sample ages was calculated, provided their age differences were found to be statistically insignificant (Long and Rippeteau, 1974). A weighted average upweights dates with smaller standard

deviations and downweights those with larger standard deviations. The statistical significance of age differences between samples was derived by applying the chi-squared test, which determines whether or not the sample ages have a 95 percent probability of being contemporaneous (Stuiver and Reimer, 1993). Sample ages that did not meet these criteria were not included in the weighted average. Weighted averages are reported in radiocarbon years.

Because sample ages are usually considered to represent maximum ages of deposits, the youngest date obtained for a given unit is sometimes taken to represent the closest approximation of the actual age of that unit. Weighted averages are usually preferable, however, for two reasons: 1) the magnitude of the standard deviation decreases as the number of samples averaged together increases; and 2) uncertainties inherent in the radiocarbon dating process itself can result in ages that are somewhat younger (or older) than the actual age of the sample (J. Southon, Lawrence Livermore National Laboratory, personal communication, November, 1996).

Results: Age Constraints of Stratigraphic Units

Because they are largely correlative, the units exposed in Trenches 1, 3, and 4 have been grouped together in the following discussion. The units revealed in Trench 2, the only logged trench that did not exhibit any evidence of faulting, do not correlate precisely with the others, and are therefore treated separately. The units are discussed from youngest to oldest, beginning at the top of the section, because the preferred ages of a number of the units are chosen on the basis of stratigraphic relationships with overlying units. As

previously noted, unit numbers (or letters) become larger with increasing depth (and age) in the stratigraphic section. Only units from which charcoal samples were obtained are discussed in this section. Appendix B lists raw laboratory data; Appendix C shows ages of individual samples; Plates 2-5 show locations of samples; Table 1 presents a summary of the various age possibilities for the units in Trenches 1, 3, and 4; Fig. 15 presents a depiction of the stratigraphic relationships between the units in Trenches 1, 3, and 4; and Table 2 presents a summary of the ages for the units in Trench 2.

Units Exposed in Trenches 1, 3, and 4

Unit 10: This unit consists of silty sand that is heavily bioturbated and is interpreted as an A horizon. Four samples were analyzed from this unit, all of which were collected from Trench 1. Their radiocarbon ages are: 120±60, 150±60, 180±60, and 370±60. The anomalously old sample, which consisted of redwood, was discarded. A weighted average of 150±35 radiocarbon years was obtained for the three younger samples, all of which consisted of charcoal. The weighted average yields a 48 percent probability that the age of this unit lies within the range 1671-1783 A.D., a 34 percent probability that it lies within 1795-1891 A.D., and a 17 percent probability that it lies within the range 1906-1947 A.D. However, it is highly unlikely that the most recent age range represents the true age of the deposit.

Unit 17: This unit consists of a fine sand of alluvial fan origin. Four samples, all of them charcoal, were analyzed from this unit. All of the samples

TABLE 1. SUMMARY OF AGES FOR STRATIGRAPHIC UNITS IN TRENCHES 1, 3, AND 4

Unit[1]	# Samples Tested[2]	# Samples Discarded[3]		Weighted Averages (^{14}C Yrs. B.P.)[4]		Highest Probability Calendar Age Range A.D. (2 σ limits)[5]		% Probability (within 2 σ)[6]	
		Too Young	Too Old	Most Likely Population	Less Likely Population	Most Likely Population	Less Likely Population	M.L. Pop.	L.L. Pop.
10	4	———	1	150±35	———	1671-1891	———	82	—
17	4	———	2	204±39	———	1645-1819	———	80	—
17/18	4	———	———	238±27	———	1641-1803	———	84	—
18	13	2	3	268±19	———	1635-1667	———	100	—
19	17	1	3	404±43	158±18	1434-1634	1673-1865	100	80
22	6	———	———	481±33	348±27	1407-1467	1480-1637	100	100
22/25	6	1	———	439±35	317±35	1417-1514	1487-1652	94	100
25	10	———	4	599±31	391±38	1304-1409	1440-1634	100	100
40	3	———	———	690±60	462±49	1242-1403	1400-1519	100	91
50	2	1	———	910±60	———	1020-1246	———	100	—
100	3	———	———	997±33	———	987-1159	———	100	—

Table 1 (continued).

[1] Number designation of the stratigraphic unit from which the radiocarbon samples were obtained.

[2] Number of radiocarbon samples that were analyzed from the corresponding unit.

[3] Number of radiocarbon samples that were discarded as a result of being either too young or too old -- i.e. the differences between their ages and those of the other samples were statistically significant at the 95 percent level.

[4] Weighted average of the samples that were not discarded in radiocarbon years before present. For units displaying two age populations, both corresponding weighted averages are shown, one of which is judged to be more viable ("Most Likely Population") than the other ("Less Likely Population") on the basis of stratigraphic relationships with other units. The expressed errors represent one standard deviation.

[5] Highest probability 2 sigma age range in calendar years A.D. that corresponds with each weighted average. For units displaying dual age populations, calendric age ranges are shown for both the population that is judged to be more viable ("Most Likely Population") and the one judged to be less viable ("Less Likely Population"). Samples were calibrated by using the 3.0.3c version of the Calib calibration program (Stuiver and Reimer, 1993).

[6] Percent probability of each calendric age range corresponding to its respective weighted average in radiocarbon years, within the limits of the 2 sigma interval (i.e. at the 95 percent confidence level). For units displaying dual age populations, probability percentages are shown for both the population that is judged to be most likely ("M.L. Pop.") and the one judged to be less likely ("L.L. Pop.").

TABLE 2. SUMMARY OF AGES FOR STRATIGRAPHIC UNITS IN TRENCH 2

Unit[1]	# Samples Tested[2]	# Samples Discarded[3]		Weighted Average (^{14}C Yrs. B.P.)[4]	Highest Probability Calendar Age Range (2 σ limits)[5]	% Probability (within 2 σ)[6]
		Too Young	Too Old			
A	2	———	1	230±60	1620-1823 A.D.	68
C	3	———	———	139±33	1675-1943 A.D.	100
E1	3	1	———	265±43	1497-1681 A.D.	77
F	1	———	———	840±70	1042-1286 A.D.	100
G	2	———	———	882±39	1041-1244 A.D.	100

Table 2 (continued).

[1] Letter designation of the stratigraphic unit from which the radiocarbon samples were obtained.

[2] Number of radiocarbon samples that were analyzed from the corresponding unit.

[3] Number of radiocarbon samples that were discarded as a result of being either too young or too old, i.e. the differences between their ages and those of the other samples were statistically significant at the 95 percent level.

[4] Weighted average of the samples that were not discarded in radiocarbon years before present. The expressed errors represent one standard deviation.

[5] Highest probability 2 sigma age range in calendar years that corresponds with the weighted average. Samples were calibrated by using the 3.0.3c version of the Calib calibration program (Stuiver and Reimer, 1993).

[6] Percent probability of the calendric age range corresponding to its respective weighted average in radiocarbon years, within the limits of the 2 sigma interval (i.e. at the 95 percent confidence level).

were obtained from Trench 1. Their radiocarbon ages are: 170±50, 250±60, 370±40, and 430±60. A weighted average of 204±39 radiocarbon years was obtained for the two younger dates; the two older dates were discarded, because the age difference between the older and younger groups was found to be statistically significant at the 95 percent level. The younger dates are considered to be more viable than the older ones because they are consistent with the preferred ages of all the underlying units (Table 1), whereas the older ones are not. The older dates probably represent reworked charcoal or anomalously old redwood samples. The weighted average of the two younger dates yields a 54 percent probability that the age of the unit lies within the range 1717-1819 A.D., a 26 percent probability that it lies within 1645-1703 A.D., a one percent probability that it lies within 1848-1863 A.D., and a 20 percent probability that it lies within 1916-1955 A.D. However, as with Unit 10, it is highly unlikely that the youngest age range represents the true age of the deposit.

Unit 17/18: This unit consists of a reddish-brown, in-situ burn layer that is 1-2 cm thick. Four charcoal samples, all of them from Trench 1, were analyzed from this unit. Their radiocarbon ages are: 180±60, 190±50, 270±60, and 300±50. Because the differences between these ages were found to be statistically insignificant at the 95 percent level, they were all included in the calculation of the weighted average for this unit, which is 238±27 radiocarbon years. This weighted average yields a 53 percent probability that the age of the unit lies within the range 1641-1679 A.D., a 31 percent probability that the age lies within 1765-1803 A.D., and a 16 percent probability that it lies within 1939-

1955 A.D. Again, the most recent age range is highly unlikely. Because this unit is composed of in-place, rather than detrital, charcoal, the age of the material should more closely reflect the time of formation of Unit 17/18.

Unit 18: This unit consists of silty sand of alluvial fan origin. Thirteen samples, which consisted of either charcoal, bulk sediment, or a charcoal/sediment mixture, were analyzed from this unit. The samples were collected from Trenches 1 and 3, and have the following radiocarbon ages: 2520±70, 1220±50, 380±60, 120±60, 80±60, 340±60, 310±60, 290±60, 280±50 (2 samples), 230±50, 220±60, and 220±50. The last eight of these dates were used to calculate a weighted average of 268±19 radiocarbon years for the unit. The first five of these dates were discarded because they were either too old (3) or too young (2) to be included in the weighted average. The weighted average yields a 100 percent probability that the age of the unit lies within the range 1635-1667 A.D. Because the unit is heavily bioturbated, it is likely that the two anomalously young dates represent material that was transported down from above by burrowing.

Unit 19: This unit consists of silty sand with some gravel and is likewise of alluvial fan origin; it has also been interpreted as a buried A horizon. This unit represents the earliest of the alluvial fan deposits post-dating the incision of Arano Creek. Seventeen samples, collected from Trenches 1, 3, and 4, were analyzed from this unit. Most of these samples consisted of charcoal, but a few were either bulk sediment or charcoal/sediment mixtures. Their radiocarbon

ages are as follows: 3450±70, 2500±60, 1870±60, 460±60, 350±60, 210±60, 200±60, 180±50, 170±60, 160±60 (2 samples), 150±60 (2 samples), 130±60, 130±50, 100±60, and 50±50. This suite of dates includes two distinct populations -- a younger one that includes 11 dates ranging from 100±60 years to 210±60 years and an older one consisting of two dates -- 460±60 years and 350±60 years. Four dates were discarded because they were either too old (3) or too young (1) to be included in either age population.

A weighted average of 404±43 radiocarbon years was obtained for the two older dates, which yields a 64 percent probability that the age of the unit lies within the range 1434-1529 A.D. and a 36 percent probability that it lies within 1547-1634 A.D. These age ranges are consistent with the calculated age of the overlying Unit 18, which is 1635-1667 A.D. Because the formation of an A horizon requires a considerable amount of time, this proposed time span of approximately 150 to 200 years between the deposition of units 19 and 18 -- assuming the 64 percent probability age range for Unit 19 is correct -- is reasonable.

On the other hand, the weighted average obtained for the younger population of dates is 158±18 radiocarbon years, which yields a 45 percent probability of the unit's age lying within the range 1717-1780 A.D., a 17 percent probability within 1673-1703 A.D., a 15 percent probability within 1796-1820 A.D., a 3 percent probability within 1842-1865 A.D., and a 20 percent probability within 1916-1946 A.D. Because this entire range of ages is younger than the age obtained for Unit 18, this age of Unit 19 or the age of Unit 18 must be incorrect.

If this younger age population for Unit 19 does, in fact, represent the true age of the deposit, then the bulk of the samples from all of the overlying units must represent charcoal that is much older than the age of the respective deposits in which they are incorporated, which is unlikely. If this were the case, the ages of the overlying units would likely be more randomly distributed, and would probably not be in correct stratigraphic order, as in fact they are. In addition, the time interval between the deposition of Units 19 and 18 -- assuming the two anomalously young dates from Unit 18 represent the true age of the deposit -- would not be sufficient to allow for the formation of an A horizon. For these reasons, it is much more likely that the older population of dates for Unit 19, although substantially smaller, represents a closer approximation of the true age of the deposit. As previously noted, Unit 19 is heavily bioturbated, so it is possible that the younger population of dates represents material brought down from above by burrowing. If this unit contained very little charcoal to begin with, it is not surprising that the great majority of samples are not representative of the unit's true age, because they would have been introduced into the deposit later as a result of burrowing action.

Unit 22: This unit consists of fine sand, and represents the most recent overbank deposit in the section. Following the deposition of this unit, incision of Arano Creek took place to the point at which significant flooding could no longer occur. Six samples, all of them charcoal, were analyzed from this unit. The samples were collected from Trenches 1 and 3. To check for consistency, two of these samples were split into two portions and analyzed separately. The

radiocarbon ages obtained for these samples are: 500±60, 330±60, 310±50, 350±50, 420±60, 800±50 (re-run of previous sample), 510±50, and 700±50 (re-run of previous sample). As with Unit 19, there are two fairly distinct populations of dates. The older population includes the dates 500±60, 510±50, and 420±60, while the younger population includes the dates 330±60, 310±50, 350±50, and 420±60. Note that the date 420±60 is included in both populations, because it was found to be statistically consistent with both of them. The two re-runs, both of which were substantially older than either population of dates, were discarded. A weighted average of 481±33 radiocarbon years was obtained for the older population, which yields a 100 percent probability that the age of the unit lies within 1407-1467 A.D. The younger population has a weighted average of 348±27 radiocarbon years, which yields a 100 percent probability that the age of the unit lies within 1480-1637 A.D.

The reason for this discordance in sample ages is not clear. For the most part, Unit 22 does not appear to be intensely bioturbated, so it is unlikely that the younger dates represent material introduced from above by burrowing or root growth. It is possible that the older dates represent reworked charcoal or pieces of very old wood. However, I suspect that these age differences are caused by variations in the amount of absorbed organic materials within the charcoal samples, despite the fact that the sample pretreatment process is supposed to eliminate such contaminants. These organic substances can be introduced into the samples by percolating groundwater, and can result in sample ages being either too young or too old. The fact that large age discrepancies exist between the two dates comprising one of the split samples (420±60 and 800±50) lends

support to this proposition, because this sample was pretreated separately for each analysis, which allows for variability in the amount of organic contaminants removed. The other split sample was only pretreated once, so the cause of the age differences within it is not known.

There is little independent evidence favoring either of the two age populations within Unit 22. If, however, the older population of dates within Unit 19 represents the true age of that deposit, which, as discussed above, is a reasonable interpretation, then the older age range for unit 22 is probably more viable than the younger one, because the former is in the correct stratigraphic order, whereas the latter is not.

Unit 22/25: Like Unit 17/18, this unit consists of a reddish brown in-situ burn layer and is about 1-2 cm thick. Six charcoal samples, including one split, were analyzed from this unit. The samples were obtained from Trenches 3 and 4, and have the following radiocarbon ages: 320±60, 270±60 (re-run of previous sample), 360±60, 490±60, 470±60, and 170±50. Two age populations are again exhibited: an older one consisting of the dates 490±60, 470±60, and 360±60, and a younger one consisting of the dates 320±60, 270±60, and 360±60. The last date was discarded, as it was too young to be included within either population. The radiocarbon age 360±60 is included in the older and younger populations, because it is statistically consistent with both of them. A weighted average of 439±35 radiocarbon years was obtained for the older population, which yields a 94 percent probability that the age of the unit lies within 1417-1514 A.D. and a 6 percent probability that is lies within 1595-1619 A.D. The younger

population has a weighted average of 317±35 radiocarbon years, which yields a 75 percent probability that the age of the unit lies within 1487-1609 A.D. and a 25 percent probability that it lies within 1611-1652 A.D.

Because this unit also does not show evidence of intense bioturbation, the discordance in ages may again be due to variable amounts of absorbed organic material that survived the pretreatment process. As with the previous unit, there is little independent evidence for favoring either population of dates. Because it is more consistent with the preferred age of Unit 19, I would again tend to favor the older population for Unit 22/25. However, this older population is younger than the older population for the overlying Unit 22, so I suspect that either the age of the older Unit 22 population is too great or the ages of both Units 22 and 22/25 are incorrect. Alternatively, it is possible that neither population of dates for Unit 22/25 is very credible, despite the fact that the charcoal obtained from this unit represents in-situ material.

Unit 25: This unit consists of sandy silt and is of overbank origin as well. Ten samples, including one split, were analyzed from this unit. The samples consisted of charcoal, bulk sediment, and charcoal/sediment mixtures and were obtained from Trenches 1 and 3. The radiocarbon ages of the samples are: 3120±60, 2300±80, 1110±60, 770±40, 410±80, 380±60, 390±60, 630±50 (re-run of previous sample), 610±60, and 560±50. As with the three previous units, there are two populations of ages -- an older one that includes the dates 630±50, 610±60, and 560±50 and a younger one that includes the dates 410±80, 380±60, and 390±60. The first four dates, which are anomalously old, were discarded.

The weighted average for the older population is 599±31 radiocarbon years, which yields a 67 percent probability that the age of the unit lies within 1304-1369 A.D. and a 33 percent probability that it lies within 1371-1409 A.D. The younger population has a weighted average of 391±38 radiocarbon years, yielding a 59 percent probability that the age of the unit lies within 1440-1529 A.D. and a 41 percent probability that it lies within 1546-1634 A.D.

As with the preceding two units, I suspect that these age discrepancies result from the presence of absorbed organic material within the samples, because this unit also does not exhibit evidence of intense bioturbation. Apparently, a portion of this absorbed organic material sometimes survived the pretreatment process. The fact that the split sample -- each portion of which was pretreated separately -- yielded one date within each of the two populations strongly supports this assertion. Again, little independent evidence favors either one population or the other. However, as before, the older population is more consistent with the preferred age of Unit 19, so it is probably more likely.

Unit 40: This unit consists of fine sand and is also of overbank origin. Three charcoal samples were analyzed from this unit, all of which were collected from Trench 1. The radiocarbon ages of these samples are as follows: 690±60, 480±60, and 430±80. Again, there are two populations of ages, although the older one consists of only a single date -- 690±60. The other two dates comprise the younger population. The older date yields a 100 percent probability that the age of the unit lies within 1242-1403 A.D. The weighted average of the younger population is 462±49 radiocarbon years, yielding a 91 percent probability that the

age of the unit lies within 1400-1519 A.D. and a 9 percent probability that it lies within 1575-1625 A.D.

As with the previous units, the age disparity between the two populations may result from variations in the amount of absorbed organic material within the samples, as this unit also does not appear to be intensely bioturbated. Because, as before, the older population is more consistent with the preferred age of Unit 19, it is again more likely than the younger population.

Unit 50: This unit consists of clayey silt and is also an overbank deposit. Two samples were analyzed from this unit -- one consisting of charcoal, and the other a charcoal/bulk sediment mixture. Both were collected from Trench 1. Their radiocarbon ages are: 910±60 and 160±60. Because the latter date is clearly too young, it was discarded, leaving only the single older date. This date yields a 100 percent probability that the age of the unit lies within 1020-1246 A.D., which places it in proper stratigraphic order.

Unit 100: This unit consists of fine sand with some clay stringers. Like the previous several units, it represents an overbank deposit. Three charcoal samples, all of them from Trench 1, were analyzed from this unit. The radiocarbon ages of the samples are: 1060±60, 1000±60, and 950±50. Because the age differences between these samples were found to be statistically insignificant at the 95 percent level, they were all included in the calculation of the weighted average, which is 997±33 radiocarbon years. This weighted average yields a 67 percent probability that the age of the unit lies within 987-

1063 A.D., a 22 percent probability that it lies within 1076-1126 A.D., and an 11 percent probability within 1133-1159 A.D. Summation of all three age ranges gives a combined range of 987-1159 A.D. (100 percent probability), which places it in correct stratigraphic order.

Units Exposed in Trench 2

Unit A: This unit consists of gravelly sandy silt to silty sand that is heavily bioturbated and is interpreted as an A horizon. Two samples -- one charcoal and one wood -- were analyzed from this unit. Their radiocarbon ages are 230±60 and 1220±60. The latter date, which probably represents charcoal that has been reworked or derived from a very old tree, is most likely too old, because its age is greater than that of all the samples included in the age calculations of all units exposed in Trenches 1, 3, and 4. Therefore, it was discarded. The younger date yields a 68 percent probability that the age of the unit lies within 1620-1823 A.D., a 15 percent probability that it lies within 1911-1955 A.D., a 12 percent probability within 1514-1594 A.D., and a 6 percent probability within 1830-1885 A.D.

Unit C: This unit consists of silty sand and is of overbank origin. Three charcoal samples were analyzed from this unit, with radiocarbon ages of 160±60, 150±50, and 100±60. Because their age differences are not statistically significant at the 95 percent level, all three dates were included in the calculation of the weighted average, which is 139±33 radiocarbon years. This weighted average yields a 43 percent probability that the age of the unit lies within 1675-

1776 A.D., a 40 percent probability that it lies within 1799-1897 A.D., and a 17 percent probability that it lies within 1902-1943 A.D.

Unit E1: This unit consists of sandy silt. It represents an overbank deposit and has also been interpreted as a buried A horizon. Three charcoal samples were analyzed from this unit, with radiocarbon ages of 290±60, 240±60, and 120±50. The latter date, which is anomalously young and may represent material introduced from above by burrowing action, was discarded. A weighted average of 265±43 radiocarbon years was obtained for the two older dates, yielding a 44 percent probability that the age of the unit lies within 1614-1681 A.D., a 33 percent probability that it lies within 1497-1603 A.D., a 16 percent probability that it lies within 1749-1805 A.D., and a 7 percent probability that it lies within 1936-1955 A.D.

Unit F: This unit consists of fine sand and is also an overbank deposit. One charcoal sample was analyzed from this unit, with a radiocarbon age of 840±70, which yields a 70 percent probability that the age of the unit lies within 1150-1286 A.D. and a 30 percent probability that it lies within 1042-1150 A.D.

Unit G: This unit consists of fine to medium sand with variable amounts of gravel, and it also represents an overbank deposit. Two charcoal samples were analyzed from this unit, with radiocarbon ages of 840±50 and 940±60. A weighted average of 882±39 radiocarbon years was obtained for these two

samples, yielding a 100 percent probability that the age of this unit lies within 1041-1244 A.D.

A depiction of the stratigraphic relationships between the units exposed in Trenches 1, 3, and 4, along with their highest probability ages, is presented on Figure 17. A more detailed summary of the various age possibilities for these units is shown on Table 1. Table 2 summarizes the ages of the units exposed in Trench 2.

Discussion

As noted above, considerable uncertainties exist in the Arano Flat radiocarbon data set, particularly as seen in Trenches 1, 3, and 4. Of special concern are the following factors: 1) the inability to consistently replicate results; and 2) the widespread occurrence of dual age populations -- some of which are not in proper stratigraphic order -- within stratigraphic units.

Of the five split samples that were analyzed, only two yielded repeatable results; the age differences between the other three pairs were found to be statistically significant. Three of the five split samples were pretreated separately for each analysis, so age differences among these samples could be the result of variability in their absorbed organic material content. Of the two that were not pretreated separately, one was repeated and the other was not. The age discordance between the two portions of the non-repeatable split sample is problematic, and its cause unknown, although the possibility of laboratory contamination cannot be completely ruled out.

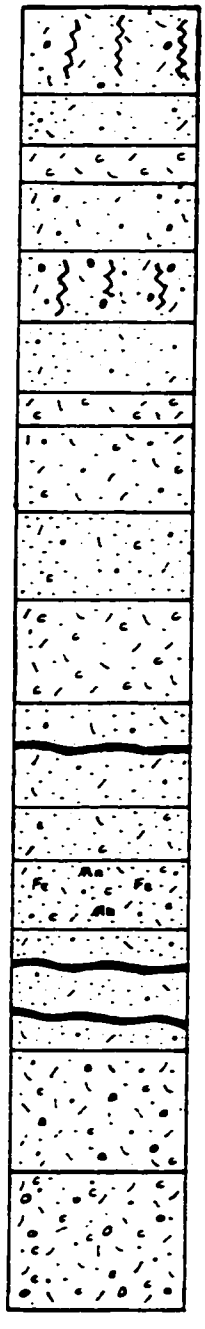

Generalized Stratigraphic Column	Unit Description	Highest Probability Calendar Age Range (2 σ limits)
	Unit 10: Reddish gray, silty, fine sand, some medium to coarse sand and fine to coarse gravel (A horizon).	**1671-1891 AD**
	Unit 17: Pale yellow fine sand, some silt and pebbles, little medium sand.	**1645-1819 AD**
	Unit 17/18: Dusky red silty clay (in-situ burn layer).	**1641-1803 AD**
	Unit 18: Yellowish brown, silty, fine sand, little medium to coarse sand, little fine to medium gravel.	**1635-1667 AD**
	Unit 19: Gray, silty, fine sand, some medium to coarse sand and fine to coarse gravel (buried A horizon).	**1434-1634 AD**
	Unit 22: Yellowish brown and gray mottled fine sand, some medium to coarse sand and pebbles, little silt.	**1407-1467 AD**
	Unit 22/25: Dusky red silty clay (in-situ burn layer).	**1417-1514 AD**
	Unit 25: Grayish brown, fine, sandy silt, some clay, little medium to coarse sand and pebbles.	**1304-1409 AD**
	Unit 40: Yellowish brown and gray mottled fine sand, some silt, little clay, medium to coarse sand, and pebbles.	**1242-1403 AD**
	Unit 50: Grayish brown clayey silt, some fine sand.	**1020-1246 AD**
	Unit 65: Brown and gray mottled, silty, fine sand, little medium to coarse sand, contains thin layer of dark gray clay .	———
	Unit 80: Light brownish gray, silty, fine sand, little clay	———
	Unit 90: Dusky red, silty, fine sand, some clay, little coarse sand, abundant iron and manganese oxide nodules.	———
	Unit 100: Brown and gray mottled fine sand, some silt, little medium to coarse sand and pebbles, contains thin layers of dark gray clay.	**987-1159 AD**
	Unit 110: Brown and gray mottled gravelly sandy silt, some clay.	———
	Unit 115: Gray and brown mottled clayey silt, some fine to medium sand and fine to coarse gravel (weathered bedrock).	———

Figure 17. Generalized stratigraphic column -- with ages shown -- of Units exposed in Trenches 1, 3, and 4. Ages are shown only for units from which radiocarbon samples were obtained (not drawn to scale).

The dual population and age reversal problems are undoubtedly due in part to bioturbation, which is pervasive in the upper meter or so of material exposed in the trenches (Units 10-19). The presence of reworked charcoal, or charcoal derived from very old trees, also most likely contributes to the uncertainties. However, because these upper units were sampled extensively, these potential sources of error were likely minimized, and the preferred age constraints obtained for them probably are reasonably accurate.

Dual age populations were especially prevalent in the lower portion of the section (Units 22-100), where every unit except Units 50 and 100 exhibited two populations of dates. The accuracy of the age constraints obtained for these units is more questionable, however, for the following reasons: 1) they were not sampled as extensively as those comprising the upper portion of the section; and 2) the younger populations are probably not a result of bioturbation, because the effects of bioturbation within these units appear to be relatively minor.

As mentioned above, I suspect that the age disparities within these units result from variability in the amount of absorbed organic materials within the charcoal samples, even though the sample pretreatment process is supposed to eliminate such contaminants. These organic materials can be introduced into the samples by percolating groundwater, resulting in sample ages that may be either too young or too old. It also is possible, although not very likely, that contaminants were inadvertently introduced into some of the samples in the laboratory.

Because they are more consistent with the preferred age of Unit 19, I favored the older populations throughout the lower portion of the section.

However, it is possible that none of the populations within these units is very accurate, because it is not known for certain whether or not some amount of residual absorbed organic contaminants remained in all of the samples. Both age populations within Unit 22/25, for example, are out of stratigraphic order, which means that either they are incorrect, the Unit 22 populations are incorrect, or both. Although these uncertainties are troubling, the accuracy of the age constraints of the units comprising the lower portion of the section is not as critical to the paleoearthquake history of the site as that of the upper portion.

Inconsistencies in radiocarbon ages such as those discussed above highlight the inherent limitations associated with the dating of detrital charcoal and are common in investigations in which large numbers of samples are analyzed (e.g. Niemi, 1992; Clahan, 1996; Baldwin, 1996). Although these inconsistencies may be less apparent when smaller numbers of samples are used, their effects are likely to be magnified. Earthquake chronologies that are based on very small numbers of dates, although relatively common, can lead to serious misinterpretations. Larger data sets are preferable, because they provide a clearer picture of both the age constraints and the inherent uncertainties involved.

FAULT ZONE EXPOSURES

The trenches in which the fault is exposed (Trenches 1, 3, and 4) are situated near the southeast end of a prominent fault trace and directly northwest of a releasing (right) stepover in the fault. Although at least one additional trace was mapped in this area by Sarna-Wojcicki and others (1975), no others were encountered in the trenching excavations.

The fault zone is narrow and well-defined, ranging in width from about 1.5 to 3.0 m. It is expressed in the trenches in the following ways: 1) displacement or truncation of stratigraphic units across shear planes; 2) warping of stratigraphic units; 3) discontinuous fractures; and 4) discoloration along shear planes. The stratigraphic displacements observed in the trenches represent the relatively minor vertical components of larger strike-slip offsets, the magnitudes of which are unknown. Detailed logs of the trenches are shown on Plates 2-5; Plates 2, 4, and 5 (Trenches 1, 3, and 4) include fault zone exposures. Figure 18 shows a detailed log of the fault zone exposure on the south wall of Trench 1.

Trench 1 exhibited by far the clearest expression of both fault strands and stratigraphy. The fault zone in Trench 1 (Plate 2) is about 2.5-3.0 m wide and is characterized by pronounced warping of much of the sequence as well as numerous shear planes and fractures. On the south wall (Figs. 18, 19), the two principal shear planes have near-vertical dips near the base of the trench, but bend to the northeast and converge higher up in the section. The westernmost shear plane extends upward to within about 60 cm of the ground surface and cuts Unit 17, whereas the easternmost shear plane extends to within 40 cm or

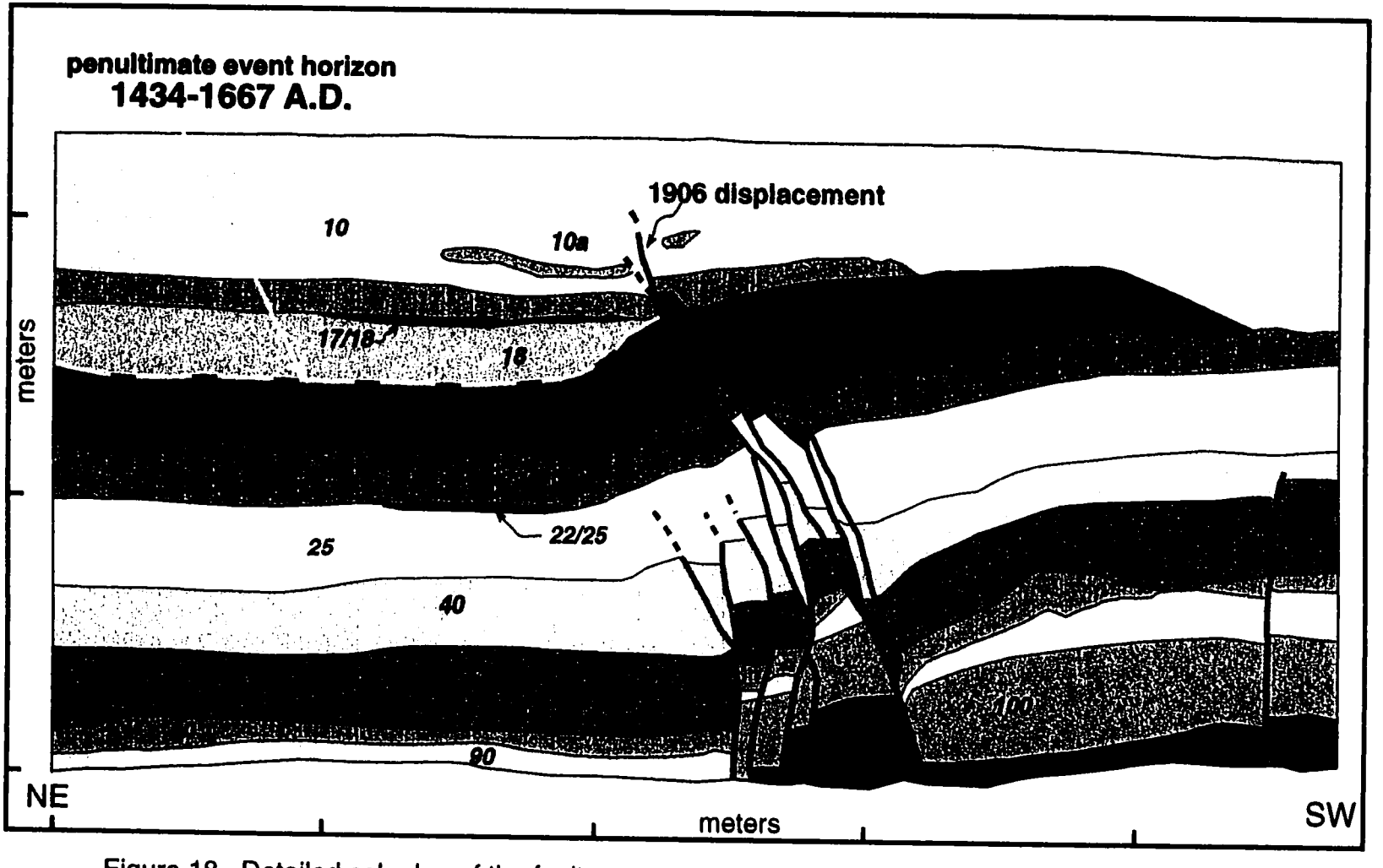

Figure 18. Detailed color log of the fault zone exposure on the south wall of Trench 1, showing vertical displacement associated with the 1906 earthquake and the location of the penultimate event horizon. Number designations are shown for principal stratigraphic units.

Figure 19. Photograph of the fault zone exposure on the south wall of Trench 1. Grid spacing on trench wall is 1 m horizontally and 0.5 m vertically (view to the southwest).

less and cuts Units 10 and 10a. The western strand displaces adjacent strata about 36 cm in a down-to-the-west, normal sense near the base of the section (Unit 90) and about 16 cm in the upper central portion (Unit 22). The eastern strand, on the other hand, displaces adjacent strata about 22 cm in an up-to-the-west, reverse sense in the lower portion of the section (Unit 90), about 10 cm in the upper central portion (Unit 22), and 7-8 cm near the top (Unit 10a). Numerous subsidiary strands exhibit smaller amounts of displacement and do not extend as far upward in the section. Warping of strata on the south wall of Trench 1 is on the order of about 50 to 55 cm in an up-to-the-west sense for all units up through Unit 19. Units 10a, 17, and 18, which overlie Unit 19, do not appear to be warped. Unit 18 pinches out along the steeply inclined upper surface of Unit 19 directly east of the two principal fault traces, whereas Units 10a and 17 extend across these principal traces (Fig. 18).

The north wall of Trench 1 (Plate 2) also displays two principal fault strands and a number of subsidiary strands. As with the south wall, both principal strands dip very steeply in the lower portion of the trench and converge in the upper portion. However, unlike the south wall, they bend in opposite directions as they converge, with the westernmost strand bending to the northeast and the easternmost strand bending to the southwest. The former strand exhibits normal, down-to-the-west displacement, can be traced to within about 55 cm of the ground surface, and cuts Unit 20, whereas the latter exhibits normal, up-to-the-west displacement, can be traced to within about 65 cm of the surface, and cuts Unit 22. Both exhibit displacements of about 6-10 cm throughout their lengths. Warping of strata on the north wall is on the order of

about 65-70 cm in an up-to-the-west sense for all units up through Unit 19. As with the south wall, none of the overlying units appears to be warped, and Unit 18 pinches out along the steeply inclined upper surface of Unit 19. Unlike the south wall, however, Unit 17 does not extend across the fault zone, but instead also pinches out along the upper surface of Unit 19. Unit 10a is absent on the north wall of Trench 1 (Plate 2).

Trenches 3 and 4 also show evidence of faulting, but neither the stratigraphy nor the faults themselves are as clear and well-defined as in Trench 1. In Trench 3 (Plate 4), the fault zone is about 2.0 m wide and includes only one principal shear plane. As with the south wall of Trench 1, this principal shear plane is nearly vertical in the lower portion of the trench and bends northeastward higher in the section. It can be traced to within about 60 cm of the ground surface on the south wall, where it cuts Unit 10, and to within about 42 cm of the surface on the north wall, where it also cuts Unit 10. Although displacement values are more difficult to measure in this trench as a result of the gradational transitions between many of the strata, the principal fault strand exhibits about 15 cm of displacement in the central portion of the trench (Unit 22) and about 4-6 cm of displacement in the upper portion (Unit 17). Other shear planes do not extend as high upward in the section and exhibit lesser amounts of displacement. Discontinuous fractures are common. Warping of some of the stratigraphic units is noticeable, but is much less pronounced than in Trench 1. Unit 22, which exhibits relatively sharp contacts, displays up-to-the-west warping of about 24 cm. Because of the gradational nature of the boundaries, it is difficult to determine the degree of warping, if any, in Units 18 and 19. The relationship

observed in Trench 1 between these two units, in which Unit 18 pinches out along the upper surface of Unit 19, is likewise much less evident in Trench 3. Unit 17 does not appear to be appreciably warped. Both Units 17 and 18 appear to extend across the fault zone on both walls of Trench 3, whereas Unit 10a is again absent (Plate 4).

In Trench 4 (Plate 5), the fault zone is about 2.0 to 2.5 m wide. As with Trench 1, all units up through Unit 19 appear to be warped in a west-side-up fashion, although the relatively indistinct stratigraphy makes these relationships less clear. The amount of discernable warping among units varies from about 30 to 50 cm. Two principal fault strands occur on each wall of the trench, and both extend up to about the same level. On the north wall, these two strands converge into a single strand in the upper portion of the section, whereas on the south wall, a single strand near the base of the trench diverges into two strands higher up in the section. As in the other trenches, the principal strands bend to the northeast and flatten in the upper portion of the section, with the exception of the westernmost divergent strand on the south wall, which steepens as it propagates upward. However, these fault strands cannot be traced as far upward as in the other trenches. On the north wall, the primary strand can be traced to within about 96 cm of the ground surface and cuts Unit 25, whereas on the south wall, the two divergent strands can be traced to within about 104-106 cm of the surface and also cut Unit 25. Discontinuous fractures, which are in general alignment with the primary strands, extend up into Unit 19 on both walls of the trench. Displacement magnitudes along the principal fault strands range from about 4 to 12 cm. As in Trench 1, Unit 18 does not appear to be warped,

but instead pinches out along the upper surface of Unit 19 directly east of the fault zone on both walls of Trench 4. However, the gradational boundaries between units make this relationship less clear than in Trench 1. Units 10a and 17 are both absent in Trench 4 (Plate 5).

The up-to-the-west warping exhibited in Trenches 1, 3, and 4 is consistent with the vertical displacement of the northeast-facing linear ridge located directly to the northwest. The ridge displays west-side-up displacement of about 1.0 to 1.5 m, with the principal fault trace traversing its northeastern edge (Fig. 9). This appreciable relief implies that up-to-the-west coseismic displacements have repeatedly occurred along this section of the fault.

PALEOSEISMIC EVENTS AND THEIR IMPLICATIONS

The predominantly fine-grained texture, well-defined stratigraphy, relatively continuous sedimentation, and lack of significant erosion that characterize the sedimentary sequence at Arano Flat make it a favorable site for recording paleoearthquakes. Although paleoseismic events are most clearly expressed in Trench 1, their age constraints were derived by dating stratigraphic units in Trenches 3 and 4 as well as Trench 1, because strata are correlative in all three trenches.

Evidence for two paleoseismic events is revealed in these trenches. The most recent event is characterized by faulting of all stratigraphic units up through Unit 10a. The previous (penultimate) event is expressed as both warping and brittle faulting of strata up through Unit 19 (Fig. 18, Plate 2).

Timing of Paleoseismic Events

Most Recent Event

The clearest evidence for the most recent event is found on the south wall of Trench 1, where Unit 10a, which is a 3- to 4-cm-thick layer of fine sand situated in the lower portion of Unit 10, shows a vertical stratigraphic separation of 7-8 cm (Fig. 18, Plate 2). Above this layer, which is about 35-40 cm below the ground surface, the fault is obscured by heavy bioturbation. The zone of faulting associated with this most recent event is relatively simple in structure, consisting of only one or two strands in the upper portion of the section, and is confined to a narrow zone no more than 20 cm wide in the vicinity of Unit 10a. In Trench 3

(Plate 4), which does not contain Unit 10a, this event displaced Unit 17 about 4-6 cm, and the causative fault strand can be traced to within about 42 cm of the ground surface on the north wall. There is no evidence for this event in Trench 4.

The highest probability age range (82%) for Unit 10 is 1671-1891 A.D. (59-279 yrs. B.P.), indicating that the most recent event probably occurred some time after 1671 A.D. Radiocarbon dating, therefore, does not provide tight age constraints for the timing of this event. However, considering the fact that 1906 surface rupture most likely extended throughout the entire length of the southern Santa Cruz Mountains (Prentice and Schwartz, 1991), as well as the supporting evidence for very recent faulting revealed at the Grizzly Flat site 15 km to the northwest (Schwartz and others, in press), this most recent event most likely represents the 1906 earthquake. Although it is possible that the 7-8 cm vertical separation of Unit 10a is the result of other earthquakes in addition to 1906, the small amount of displacement and structural simplicity of this portion of the fault zone make it unlikely that any other large lateral displacements equal to or greater than approximately 1-2 m were involved.

Penultimate Event

The penultimate event, like the 1906 earthquake, is most clearly expressed in Trench 1, where all units up through Unit 19 are markedly warped in an up-to-the-west fashion (Fig. 18, Plate 2). The same units appear to be affected in Trench 4 (Plate 5), although the gradational nature of many of the unit boundaries makes this considerably more difficult to discern. Trench 3 does not contain conclusive evidence for this event. In Trench 1, substantial brittle

displacement also is associated with the penultimate event, but because some of the same shear planes also were activated in 1906, the brittle faulting cannot be used to constrain the timing of the event. The amount of total vertical separation among units, including both warping and brittle displacement, is quite consistent in Trench 1, about 50-55 cm on the south wall and about 65-70 cm on the north wall, which suggests that this deformation is the result of a single event (Fig. 18, Plate 2).

The warping associated with this event evidently resulted in the formation of an east-facing scarp at the ground surface, which is represented by the upper contact of Unit 19. Unit 18, which directly overlies Unit 19, does not appear to have been involved in the deformation, but rather pinches out along the upper surface of Unit 19 (Fig. 18, Plates 2, 5). Thus it appears that Unit 18, which consists of silty, fine sand, ponded up against the scarp formed by the penultimate event. The penultimate event horizon, therefore, appears to coincide with the Unit 18/19 contact (Fig. 18).

The radiometric age obtained for Unit 18 is 1635-1667 A.D., or 283-315 yrs. B.P. (100% probability). Unit 19 has two disparate populations of dates, the younger of which is probably incorrect. The older population, which appears to be much more viable, yields an age of 1434-1634 A.D., or 316-516 yrs. B.P. (100% probability). Thus the penultimate event most likely occurred prior to 1667 A.D. and after 1434 A.D.

Discussion

Comparison of Penultimate Age Constraints with other Sites to the North

Age constraints for a penultimate event have been obtained previously at five sites along the North Coast segment and at one additional site on the Santa Cruz Mountains segment (Figs. 2, 20). At Grizzly Flat, 15 km northwest of the study site, Schwartz and others (in press) determined that a pre-1906 event occurred prior to 1655 A.D. and after 1016 A.D. At Dogtown, Niemi (1992) re-interpreted the data of Cotton and others (1982), thereby constraining the timing of the penultimate event to be after 1521 A.D. At the Vedanta site, Niemi (1992) found that the penultimate event most likely occurred after 1591 A.D. At Bodega Harbor, Knudsen and others (1997) constrained the timing of the penultimate event to be prior to 1648 A.D. and after 1453 A.D. At Fort Ross, Simpson and others (1996) determined that the penultimate event occurred between 1170 A.D. and 1650 A.D. At Point Arena, Prentice (1989) constrained the timing of the penultimate event to be after 1531 A.D., and most likely after 1636 A.D. (Fig. 20).

Although there is considerable uncertainty in the age constraints of these events, they all overlap -- an observation that led Schwartz and others (in press) to suggest the occurrence of either of the following alternatives: 1) a large magnitude event took place in the mid-1600's that ruptured all the way from near San Juan Bautista to near Point Arena; or 2) a sequence of closely-timed but discrete events affected each of the aforementioned sites along the northern SAF. The single-event scenario is based principally on the fact that the same portion of the fault ruptured in 1906.

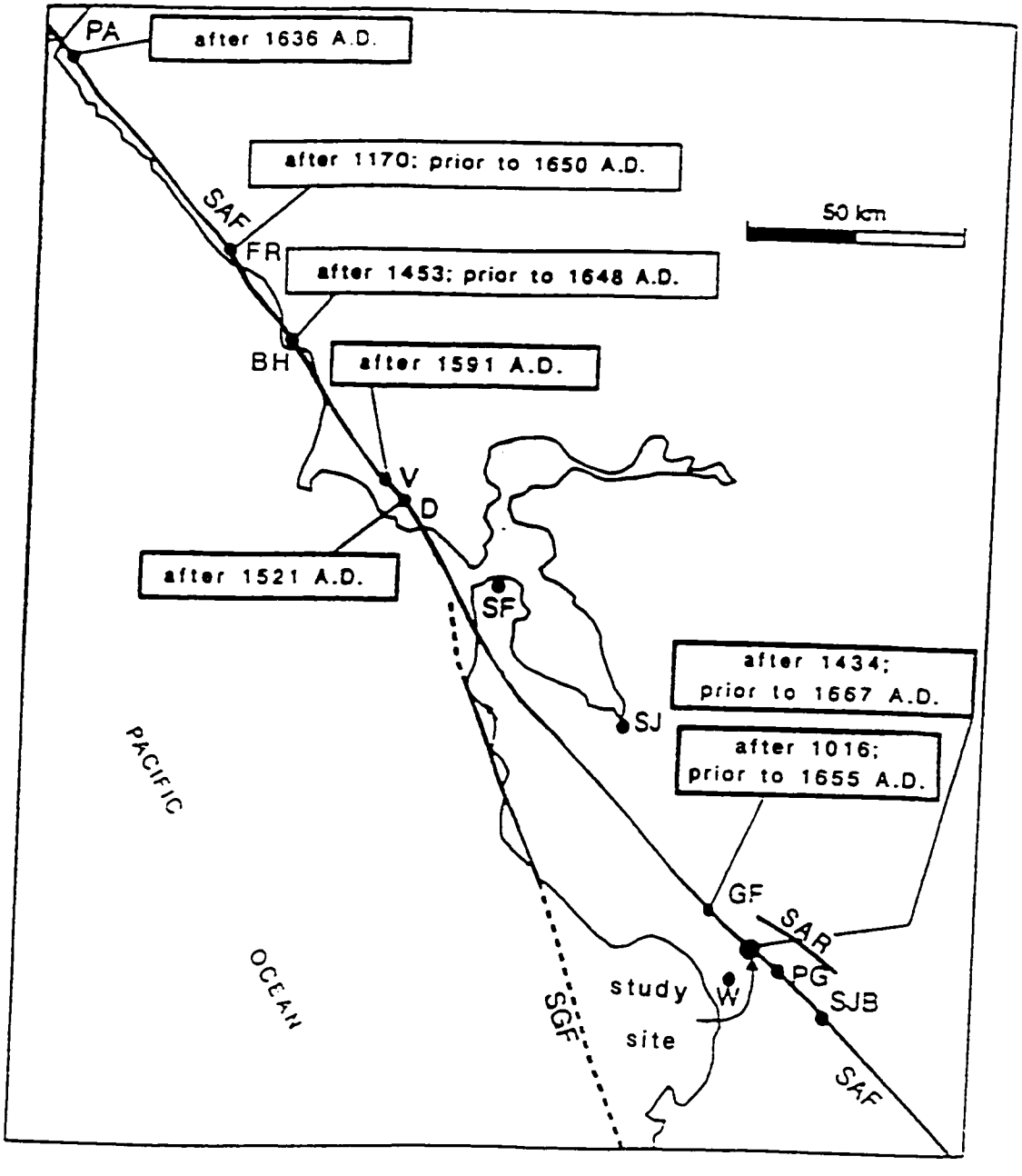

Figure 20. Map of the northern San Andreas fault (SAF) showing location of the study site and other paleoseismic sites along with their respective age constraints for the penultimate event. PA=Point Arena; FR=Fort Ross; BH=Bodega Harbor; V=Vedanta Wind Gap site; D=Dogtown; SF=San Francisco; SJ=San Jose; GF=Grizzly Flat; W=Watsonville; PG=Pajaro Gap; SJB=San Juan Bautista; SAR=Sargent fault; SGF=San Gregorio fault (modified from Schwartz and others, in press).

Implications of Earthquake Timing on Segmentation of the San Andreas Fault

Based on the age constraints of the earthquakes identified at Arano Flat, the minimum elapsed time between the 1906 and penultimate events is 239-271 years, which closely matches the 251-273-year minimum time interval obtained at Grizzly Flat (Schwartz and others, in press). It appears unlikely that any additional large-displacement events equal to or greater than approximately 1-2 m affected the study site during this period -- whether in 1836, 1838, or 1865. If they had, the uppermost portion of the fault zone would likely exhibit greater complexity, and the youngest units would probably display more than 7-8 cm of vertical displacement. There is a similar lack of evidence for large-displacement events at Grizzly Flat (Schwartz and others, in press). Nevertheless, the possibility that these or other earthquakes produced relatively small lateral displacements of less than about 1-2 m, with a minor vertical component, cannot be ruled out, because it is conceivable that one or more such potential displacements could have been subsequently overprinted by the 1906 earthquake. However, no direct evidence for this was found at either site.

If this minimum recurrence time of ~250-270 years between the two most recent events identified at these sites is representative of the long-term recurrence interval of the SCMS, it is somewhat surprising that no older events were found at Arano Flat. Unit 100, which is one of the oldest units revealed in the trenches, has a radiometrically-derived age of 987-1159 A.D. (100% probability), which leaves sufficient time for at least one, and probably two, additional event(s). Perhaps the pronounced warping of strata associated with the penultimate event overprinted evidence of these earlier events, particularly if

they involved relatively small amounts of vertical displacement, similar to that resulting from the 1906 earthquake.

This proposed minimum recurrence interval of ~250-270 years is much longer than most previous estimates for this segment of the fault. Because it is comparable to recurrence estimates obtained at various sites along the NCS, this also raises the possibility that the SCMS may rupture primarily in conjunction with the NCS and SFPS, as in 1906 (Schwartz and others, in press). Most previous workers have assumed that the SCMS ruptures independently, with average recurrence estimates for events exhibiting ~2.5 meters of slip ranging from 96±16 years (Working Group on California Earthquake Probabilities, 1990) to 100±24 years (Working Group on California Earthquake Probabilities, 1988).

These findings also open to question some basic premises regarding fault segmentation and slip distribution along the northern SAF. The uniform slip model of slip distribution (Sieh, 1981), upon which the earlier recurrence estimates are predicated, is based upon a constant slip rate along the length of the fault. Segments displaying lower amounts of slip per event must therefore experience more frequent earthquakes of smaller magnitude in order to "catch up" with segments exhibiting higher magnitudes of slip per event (Fig. 21). Thus the Working Group on California Earthquake Probabilities (1988, 1990) theorized that the SCMS must rupture more frequently than other segments of the northern SAF, because 1906 coseismic slip values were significantly smaller for this segment.

The longer recurrence intervals derived for large-displacement events on the SCMS at Grizzly Flat and Arano Flat suggest that the uniform slip model may

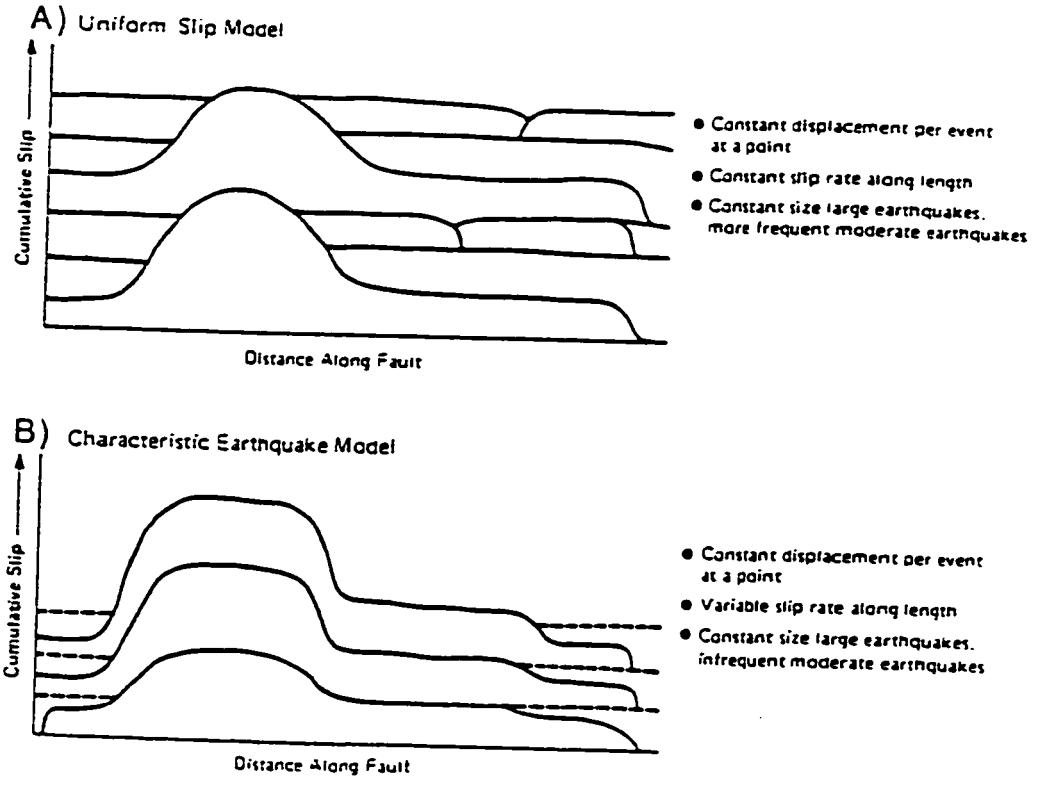

Figure 21. Conceptual models of coseismic slip distribution. Cumulative slip distribution is shown for each model. Dashed lines represent ruptures from adjacent segments (modified from Schwartz and Coppersmith, 1984).

not adequately explain the behavior of the northern San Andreas fault. Instead, the characteristic earthquake model (Schwartz and Coppersmith, 1984), in which both coseismic slip magnitude and slip rate vary along the length of the fault, may be more appropriate. This model does not require that low-slip segments rupture more often than those displaying higher amounts of slip per event and allows for long-term differences in cumulative slip among segments (Fig. 21). For segments exhibiting lower amounts of slip per event, the excess slip is transferred to other nearby faults.

As noted by Schwartz and others (in press), the parallels between variations in late Holocene slip rate and 1906 coseismic slip magnitude among the segments comprising the northern SAF are consistent with this model: the 2000-year slip rate of 14.9±2.6 mm/yr obtained for the SFPS by Clahan (1996) is about 62 percent of the 1800-year value of 24±3 mm/yr assigned to the NCS by Niemi and Hall (1992), and the average geodetically-derived 1906 coseismic slip value of ~3.5 m for the SFPS (Thatcher and others, 1997) is about 67 percent of the ~5.2 m average for the NCS (Thatcher and others, 1997). Likewise, the estimated slip rate for the SCMS of approximately 13-14 mm/yr is about 56 percent of that of the NCS, and the average 1906 geodetic slip magnitude obtained for the SCMS, about 2.6 m (Segall and Lisowski, 1990; Thatcher and others, 1997), is about 50 percent of that of the NCS. These roughly proportional relationships give credence to the proposition that the considerable "slip deficit" on the SCMS resulting from the 1906 earthquake may be a relatively long-term phenomenon, and one that increases with each 1906-type event (Schwartz and others, in press).

Although the characteristic earthquake model is consistent with much of the data relating to the behavior of the northern SAF, it may be somewhat too simplistic, because one or more of the three constituent segments may also have the capacity to rupture independently. The 1838 event, if on the SAF, is an example of such a segment-specific rupture. Schwartz and others (in press) have suggested that the northern SAF may represent a master rupture segment, which they define as a "large displacement rupture that repeats itself in both length and slip distribution." These master segments, they assert, can also contain shorter segments that are capable of generating their own earthquakes. A somewhat modified version of the characteristic earthquake model, whereby one or more of the constituent segments has the capability of rupturing independently, may thus approximate the behavior of the northern SAF most closely.

Implications for Seismic Hazards

The earthquake chronologies obtained at Grizzly Flat and Arano Flat provide insight into the seismic hazards posed by the SCMS, although a considerable amount of ambiguity still remains. If, as the evidence suggests, large coseismic displacements equal to or greater than approximately 1-2 m along the SCMS are primarily associated with long, multiple-segment ruptures, and the minimum recurrence interval for such 1906-type events is on the order of about 250-270 years, then the short-term probability of a large-displacement event affecting the SCMS is very low.

However, the possibility that the SCMS also ruptures independently in relatively small-displacement events of less than about 1-2 m cannot be ruled out on the basis of the paleoseismological record. In addition, if the estimated slip rate of about 13-14 mm/yr for the SCMS is close to the actual value, then 1906-type events that are characterized by 2.5-2.7 m of displacement and recurrence times of 250-270 years would fail to account for all of the strain. Additional smaller-displacement events would be required, although the current lack of geologic slip rate data and other uncertainties make this conclusion somewhat tentative. If the SCMS does indeed rupture independently, then there are at least two alternative short-term assessment scenarios, based upon whether or not the Loma Prieta earthquake relieved most of the shear stress along the SCMS. Because this event most likely did not occur on the SAF, but rather on a closely associated oblique-slip blind thrust fault, its effect on the stress state of the SAF is not entirely clear. The 1990 Working Group on California Earthquake Probabilities reasoned that because the two faults are in such close proximity, the 1989 event must have relieved most of the shear stress along the SAF. Therefore, they reduced their estimated short-term probability of a M_w7 or greater earthquake occurring along the SCMS in the next 30 years to near zero.

Segall and Lisowski (1990) and Thatcher and others (1997), on the other hand, pointed out that although the Loma Prieta earthquake must have decreased the shear stress along the SAF at depth, it probably increased the stress at shallow to intermediate levels, because the event ruptured only to within several kilometers of the ground surface. They suggested that the 1989 event may therefore have actually pushed forward the occurrence time of the next

earthquake along the SCMS of the SAF. Because this latter explanation takes into account some aspects of fault geometry and slip distribution along the Loma Prieta rupture zone, it appears to be somewhat more likely than the previous alternative.

In summary, a considerable amount of uncertainty exists regarding the seismic hazards posed by the SCMS of the SAF. The short-term probability of a large-displacement event equal to or greater than approximately 1-2 m affecting this segment is probably quite low, because no evidence for such events occurring between the penultimate and 1906 earthquakes was found either at Grizzly Flat or Arano Flat. However, the prospect of it also rupturing independently in relatively small-displacement events of less than about 1-2 m remains a possibility, in which case the short-term probability would likely be considerably higher. Although the resulting damage from such an event would presumably be substantially less than that caused by a 1906-type event, its effects could still be quite serious, as demonstrated by the 1989 Loma Prieta earthquake, which did not involve any surface rupture at all.

SUMMARY AND CONCLUSIONS

Summary of Findings

Timing of Paleoseismic Events

Evidence for two paleoseismic events was revealed within the trenches at Arano Flat. The most recent event occurred after 1671 A.D. and most likely represents the 1906 earthquake, and the penultimate event appears to have occurred prior to 1667 A.D. and after 1434 A.D. Although no direct evidence was found for large displacements equal to or greater than approximately 1-2 m associated with the 1836, 1838, or 1865 earthquakes, small displacements of less than about 1-2 m attributable to these or other events cannot be ruled out.

Implications of Earthquake Timing on Fault Segmentation

The age constraints for the penultimate event match closely with others obtained to the north along the SCMS and NCS. These overlapping dates are consistent with the suggestion that either a large-magnitude event occurred in the mid-1600's that, like the 1906 earthquake, ruptured all the way from near San Juan Bautista to near Point Arena, or a sequence of closely-timed but discrete events ruptured adjacent segments of the northern SAF.

The minimum recurrence time between the 1906 and penultimate events derived at Arano Flat (239-271 years) is similar to that obtained by Schwartz and others (in press) at Grizzly Flat (251-273 years), 15 km to the northwest. These values are substantially longer than previous recurrence estimates for the SCMS of 96 to 100 years (Working Group on California Earthquake Probabilities, 1988,

1990) and are comparable to recurrence estimates obtained along the NCS, which suggests that the SCMS may rupture primarily in conjunction with other segments, as in 1906.

Because of systematic variations in slip rate and 1906 coseismic slip among the segments comprising the northern SAF, as well as the observation that the SCMS may rupture mainly in association with other segments, the behavior of the northern SAF probably is more closely approximated by the characteristic earthquake model -- in which both slip rate and coseismic displacement vary along the length of the fault -- than by the uniform slip model, in which coseismic displacement varies, but slip rate remains constant. A somewhat modified version of the characteristic earthquake model, whereby individual segments can also rupture independently, as may have been the case with the SFPS in 1838, appears to fit the data even better.

Radiocarbon Dating

Eighty-eight radiocarbon samples were analyzed from the study site; the great majority of these consisted of detrital charcoal. This large data set allowed for the derivation of reasonably tight age constraints for the penultimate event. However, it also revealed considerable uncertainties in the ages of stratigraphic units, accentuating the inherent limitations associated with the dating of detrital charcoal and the importance of using large data sets.

Implications for Seismic Hazards

The short-term probability of a large-displacement event occurring on the SCMS is probably very low, because large coseismic displacements along the SCMS appear to be associated primarily with long, multiple-segment ruptures, and the minimum recurrence interval for such 1906-type events at the study site is on the order of about 250-270 years. Nevertheless, the possibility that the SCMS also ruptures independently in relatively small-displacement events cannot be ruled out, in which case the short-term probability of an earthquake occurring on this segment is likely to be considerably higher, because the 1989 Loma Prieta event may actually have increased the shear stress along the SCMS of the SAF at shallow to intermediate depths. However, the damage caused by such an event would probably be substantially less than damage that would result from a 1906-type earthquake.

Conclusions

The most important independent contribution resulting from this investigation is the considerable tightening of the age constraints for the timing of the penultimate event along the SCMS to between 1434 A.D. and 1667 A.D. Unlike at Grizzly Flat, where only the upper age limit is tightly bracketed, both the upper and lower age limits for this event are relatively well-constrained at Arano Flat, which contributes to the ongoing effort to accurately characterize the seismic hazards affecting this region.

REFERENCES CITED

Argus, D.F., and Gordon, R.G., 1991, Current Sierra Nevada-North America motion from very long baseline interferometry: implications for the kinematics of the western United States: Geology, v. 19, p. 1085-1088.

Atwater, T., 1970, Implications of plate tectonics for the Cenozoic tectonic evolution of western North America: Geological Society of America Bulletin, v. 81, p. 3513-3536.

Aydin, A., and Page, B.M., 1984, Diverse Pliocene-Quaternary tectonics in a transform environment, San Francisco Bay region, California: Geological Society of America Bulletin, v. 95, p. 1303-1317.

Baldwin, J.N., 1996, Paleoseismic investigation of the San Andreas fault on the North Coast segment, near Manchester, California: M.S. thesis, San Jose State University, San Jose, California, 127 pp.

Behr, J., Bilham, R., Bodin, P., Burford, R.O., and Burgmann, R., 1990, Aseismic slip on the San Andreas fault south of Loma Prieta: Geophysical Research Letters, v. 17, no. 9, p. 1445-1448.

Birkeland, P.W., 1984, Soils and Geomorphology: Oxford University Press, New York, New York, 372 p.

Borchardt, G. and Toppozada, T.R., 1996, Relocation of the "1836 Hayward fault earthquake" to the San Andreas fault (abs): EOS, v. 77, no. 46, p. F511.

Brabb, E.E., 1989, Geologic map of Santa Cruz County, California: U.S. Geological Survey Miscellaneous Investigation Map I-1905, scale 1:62500.

Brown, R.D., and Wolfe, E., 1972, Map showing recently active breaks along the San Andreas fault between Point Delgada and Bolinas Bay, California:

U.S. Geological Survey Miscellaneous Investigation Map I-692, scale 1:24000.

Clahan, K.B., 1996, Paleoseismic characteristics of the San Andreas fault, Woodside, California: M.S. thesis, San Jose State University, San Jose, California, 96 pp.

Cotton, W.R., Hall, N.T., Hay, E.A., 1982, Holocene behavior of the San Andreas fault at Dogtown, Point Reyes National Seashore, California: U.S. Geological Survey National Earthquake Hazards Reduction Program Final Technical Report, Contract No. 14-008-0001-19841, 33 pp.

DeMets, C., Gordon, R.G., Argus, D.F., and Stein, S., 1990, Current plate motions: Geophysical Journal International, v. 101, p. 425-478.

DeMets, C., Gordon, R.G., Argus, D.F., and Stein, S., 1994, Effect of recent revisions to the geomagnetic reversal time scale on estimates of current plate motions: Geophysical Research Letters, v. 21, no. 20, p. 2191-2194.

Dibblee, T.W., and Brabb, E.E., 1978, Preliminary geologic map of the Watsonville East quadrangle, Santa Cruz, Santa Clara, and Monterey Counties, California: U.S. Geological Survey Open-File Report 78-453, scale 1:24000.

Dietz, L.D., and Ellsworth, W.L., 1990, The October 17, 1989, Loma Prieta, California, earthquake and its aftershocks: Geometry of the sequence from high-resolution locations: Geophysical Research Letters, v. 17, no. 9, p. 1417-1420.

Ellsworth, W.L., 1990, Earthquake history, 1769-1989, *in* Wallace, R.E., ed., The San Andreas fault system, California: U.S. Geological Survey Professional Paper 1515, p. 153-187.

Greene, H.G., 1977, Geology of the Monterey Bay region: U.S. Geological Survey Open-File Report 77-718, 347 pp.

Hall, N.T., and Wright, R.H., 1993, Paleoseismic investigations of the San Andreas fault on the San Francisco peninsula, California: Final Technical Report, Phase 1, U.S. Geological Survey Award No. 14-09-0001-G2081.

Hill, D.P., Eaton, J.P., and Jones, L.M., 1990, Seismicity, 1980-86, *in* Wallace, R.E., ed., The San Andreas fault system, California: U.S. Geological Survey Professional Paper 1515, p. 115-151.

Irwin, W.P., 1990, Geology and plate-tectonic development, *in* Wallace, R.E., ed., The San Andreas fault system, California: U.S. Geological Survey Professional Paper 1515, p. 61-80.

Kelson, K.I., Lettis, W.R., and Lisowski, M., 1992, Distribution of geologic slip and creep along faults in the San Francisco Bay region, *in* Borchardt, G., Hirschfeld, S.E., Lienkaemper, J.J., McClellan, P., Williams, P.L., and Wong, I.G., eds., Proceedings of the second conference on earthquake hazards in the eastern San Francisco Bay area: California Division of Mines and Geology Special Publication 113, p. 31-38.

King, G.C.P., Lindh, A.G., and Oppenheimer, D.H., 1990, Seismic slip, segmentation, and the Loma Prieta earthquake: Geophysical Research Letters, v. 17, no. 9, p. 1449-1452.

Knudsen, K.L., Garrison, C.E., Baldwin, J.N., Carver, G.A., and Lettis, W.R., 1997, Evidence for earthquake-induced, rapid subsidence preserved in estuarine sediment along the North Coast segment of the San Andreas fault (abs): Geological Society of America Abstracts with Programs, 1997 Annual Meeting.

Lawson, A.C., Chairman, 1908, The California earthquake of April 18, 1906: Report of the State Earthquake Investigation Commission: Carnegie Institute of Washington Publication 87, 451 pp.

Lienkaemper, J.J., Williams, P.L., Taylor, P., and Williams, K., 1995, New evidence of large surface-rupturing earthquakes along the northern Hayward fault (abs): AAPG Bulletin, v. 79, no. 4, p. 591.

Lindh, A.G., 1983, Preliminary assessment of long-term probabilities for large earthquakes along selected fault segments of the San Andreas fault system in California: U.S. Geological Survey Open-File Report 83-63, 15 pp.

Lisowski, M., Prescott, W.H., Savage, J.C., and Johnston, M.J., 1990, Geodetic estimate of coseismic slip during the 1989 Loma Prieta, California, earthquake: Geophysical Research Letters, v. 17, no. 9, p. 1437-1440.

Long, A., and Rippeteau, B., 1974, Testing contemporaneity and averaging radiocarbon dates: American Antiquity, v. 39, no. 2, p. 205-215.

Louderback, G.D., 1947, Central California earthquakes of the 1830's: Bulletin of the Seismological Society of America, v. 37, no. 1, p. 33-74.

Marshall, G.A., Stein, R.S., and Thatcher, W., 1991, Faulting geometry and slip from co-seismic elevation changes: The 18 October 1989, Loma Prieta, California, earthquake: Bulletin of the Seismological Society of America, v. 81, no. 5, p. 1660-1693.

Marshall, G.A., Thatcher, W., and Lisowski, M., 1994, Resolution of fault slip along the 450-km-long rupture of the great 1906 San Francisco earthquake (abs): EOS, v. 75, no. 44, p. 180.

McLaughlin, R.J., Clark, J.C., and Brabb, E.E., 1988, Geologic map and structure sections of the Loma Prieta 7 1/2' quadrangle, Santa Clara and Santa Cruz Counties, California: U.S. Geological Survey Open-File Report 88-752, 31 pp.

McNutt, S.R., and Toppozada, T.R., 1990, Seismological aspects of the 17 October 1989 earthquake, *in* McNutt, S.R., and Sydnor, R.H., eds., The

Loma Prieta (Santa Cruz Mountains), California, earthquake of 17 October 1989: California Division of Mines and Geology Special Publication 104, p. 11-27.

Mook, W.G., and Waterbolk, H.T., 1985, Handbooks for Archaeologists, No. 3: Radiocarbon Dating: European Science Foundation - ISBN 2-903148-44-9, 65 pp.

Murphy, P.J., Briedis, J., and Peck, J.H., 1979, Dating techniques in fault investigations, *in* Hatheway, A.W., and McClure, C.R., eds., Geology in the siting of nuclear power plants: Geological Society of America Reviews in Engineering Geology, v. 4, p. 153-168.

Niemi, T.M., 1992, Late Holocene slip rate, prehistoric earthquakes, and Quaternary neotectonics of the northern San Andreas fault, Marin County, California: Ph. D. thesis, Stanford University, Stanford, California, 199 pp.

Niemi, T.M., and Hall, N.T., 1992, Late Holocene slip rate and recurrence of great earthquakes on the San Andreas fault in northern California: Geology, v. 20, p. 195-198.

Niemi, T.M., and Hall, N.T., in review, 1998, Paleoseismic study of the northern San Andreas fault at the Vedanta site, Marin County, California, *submitted to* Bulletin of the Seismological Society of America.

Noller, J.S., Lettis, W.R., and Simpson, G.D., 1994, Seismic Archaeology: Using human prehistory to date paleoearthquakes and assess deformation rates of active fault zones, *in* Proceedings of the Workshop on Paleoseismology, Marshall, California, 18-22 September, 1994: U.S. Geological Survey Open-File Report 94-568, p. 138-140.

Oakeshott, G.B., 1966, San Andreas fault in the California Coast Ranges province, *in* Bailey, E.H., ed., Geology of northern California: California Division of Mines and Geology Bulletin 190, p. 357-383.

Oppenheimer, D.H., 1990, Aftershock slip behavior of the 1989 Loma Prieta, California earthquake: Geophysical Research Letters, v. 17, no. 8, p. 1199-1202.

Prentice, C.S., 1989, Earthquake geology of the northern San Andreas fault near Point Arena, California: Ph. D. thesis, California Institute of Technology, Pasadena, California, 252 pp.

Prentice, C.S., and Ponti, D.J., 1997, Coseismic deformation of the Wrights tunnel during the 1906 San Francisco earthquake: A key to understanding 1906 fault slip and 1989 surface ruptures in the southern Santa Cruz Mountains, California: Journal of Geophysical Research, v. 102, no. B1, p. 635-648.

Prentice, C.S., and Schwartz, D.P., 1991, Re-evaluation of 1906 surface faulting, geomorphic expression, and seismic hazard along the San Andreas fault in the southern Santa Cruz Mountains: Bulletin of the Seismological Society of America, v. 81, no. 5, p. 1424-1479.

Sarna-Wojcicki, A.M., Pampeyan, E.H., and Hall, N.T., 1975, Map showing recently active breaks along the San Andreas fault between the central Santa Cruz Mountains and the northern Gabilan Range, California: U.S. Geological Survey Miscellaneous Field Studies Map MF-650, scale 1:24000.

Savage, J.C., Prescott, W.H., Lisowski, M., and King, N., 1979, Geodolite measurements of deformation near Hollister, California, 1971-1978: Journal of Geophysical Research, v. 84, no. B13, p. 7599-7615.

Schwartz, D.P., 1990, Introduction, *in* Schwartz, D.P., and Ponti, D.J., eds., Field guide to neotectonics of the San Andreas fault system, Santa Cruz Mountains, in light of the 1989 Loma Prieta earthquake: U.S. Geological Survey Open-File Report 90-274, 38 pp.

Schwartz, D.P., and Coppersmith, K.J., 1984, Fault behavior and characteristic earthquakes: Examples from the Wasatch and San Andreas fault zones: Journal of Geophysical Research, v. 89, no. B7, p. 5681-5698.

Schwartz, S.Y., Orange, D.L., and Anderson, R.S., 1990, Complex fault interactions in a restraining bend on the San Andreas fault, southern Santa Cruz Mountains, California: Geophysical Research Letters, v. 17, no. 8, p. 1207-1210.

Schwartz, D.P., Pantosti, D., Okumura, K., Powers, T.J., and Hamilton, J., in press, 1998, Paleoseismic investigations in the Santa Cruz Mountains, CA: Implications for recurrence of large magnitude earthquakes on the San Andreas fault, *submitted to* Journal of Geophysical Research.

Sedlock, R.L., and Hamilton, D.H., 1991, Late Cenozoic tectonic evolution of southwestern California: Journal of Geophysical Research, v. 96, no. B2, p. 2325-2351.

Segall, P., and Lisowski, M., 1990, Surface displacements in the 1906 San Francisco and 1989 Loma Prieta earthquakes: Science, v. 250, p. 1241-1244.

Sieh, K.E., 1981, A review of geological evidence for recurrence times of large earthquakes, *in* Simpson, D.W., and Richards, P.G., eds., Earthquake Prediction, An International Review: Maurice Ewing Ser., v. 4, p. 181-207, American Geophysical Union, Washington, D.C.

Simpson, G.D., Noller, J.S., Kelson, K.I., and Lettis, W.R., 1996, Logs of trenches across the San Andreas fault, Archae Camp, Fort Ross Historical Park, northern California: NEHRP Final Technical Report, U.S. Geological Survey Award No. 1434-94-G-2474.

Sims, J.D., 1991, Distribution and rate of slip across the San Andreas transform boundary, Hollister area, central California (abs): Geological Society of America Abstracts with Programs, v. 23, no. 2, p. 98.

Stuiver, M., and Pearson, G.W., 1993, High-precision bidecadal calibration of the radiocarbon time scale, A.D. 1950-500 B.C. and 2500 B.C.-6000 B.C.: Radiocarbon, v. 35, no. 1, p. 1-23.

Stuiver, M., and Polach, H.A., 1977, Discussion: Reporting of ^{14}C data: Radiocarbon, v. 19, no. 3, p. 355-363.

Stuiver, M., and Reimer, P.J., 1993, Calib calibration program, version 3.0.3c (Test #10): Quaternary Isotope Lab, University of Washington, Seattle.

Sykes, L.R., and Nishenko, S.P., 1984, Probabilities of occurrence of large plate rupturing earthquakes for the San Andreas, San Jacinto, and Imperial faults, California, 1983-2003: Journal of Geophysical Research, v. 89, no. B7, p. 5905-5927.

Thatcher, W., and Lisowski, M., 1987, Long-term seismic potential of the San Andreas fault southeast of San Francisco, California: Journal of Geophysical Research, v. 92, no. B6, p. 4771-4784.

Thatcher, W., Marshall, G., and Lisowski, M., 1997, Resolution of fault slip along the 470-km-long rupture of the great 1906 San Francisco earthquake and its implications: Journal of Geophysical Research, v. 102, no. B3, p. 5353-5367.

Toppozada, T.R., and Borchardt, G., 1996, Implications for the 1838 San Andreas fault earthquake, of relocating the 1836 earthquake to San Juan Bautista (abs): EOS, v. 77, no.46, p. F511.

Toppozada, T.R., and Real, C.R., 1981, Preparation of isoseismal maps and summaries of reported effects for pre-1900 California earthquakes: U.S. Geological Survey Open-File Report 81-262, 78 pp.

Tuttle, M.P., and Sykes, L.R., 1992, Re-evaluation of several large historic earthquakes in the vicinity of the Loma Prieta and Peninsular segments of

the San Andreas fault, California: Bulletin of the Seismological Society of America, v. 82, no. 4, p. 1802-1820.

U.S. Geological Survey Staff, 1990, The Loma Prieta, California, earthquake: An anticipated event: Science, v. 247, p. 286-293.

Wallace, R.E., 1990, General features, *in* Wallace, R.E., ed., The San Andreas fault system, California: U.S. Geological Survey Professional Paper 1515, p. 3-12.

Working Group on California Earthquake Probabilities, 1988, Probabilities of large earthquakes occurring in California on the San Andreas fault: U.S. Geological Survey Open-File Report 88-398, 62 pp.

Working Group on California Earthquake Probabilities, 1990, Probabilities of large earthquakes in the San Francisco Bay Region, California: U.S. Geological Survey Circular 1053, 52 pp.

Working Group on Northern California Earthquake Potential, 1996, Database of potential sources for earthquakes larger than magnitude 6 in northern California: U.S. Geological Survey Open-File Report 96-705, 40 pp.

APPENDIX A:

UNIT DESCRIPTIONS

Explanation of Unit Descriptions

The units exposed in the trenches are divided into two groups: those exposed in Trenches 1, 3, and 4, which are largely correlative, and those exposed in Trench 2, which cannot be precisely matched with the others. The former are designated with numbers, and the latter with letters. For the first group of units, the trench(es) in which each of the units is revealed is/are listed in parentheses directly after the unit designation. The units are discussed below from oldest to youngest, beginning at the bottom of the section. Larger numbers or letters near the end of the alphabet represent older (stratigraphically lower) units than do smaller or earlier ones. In the following descriptions, granules are defined as having median diameters of 2-4 mm, pebbles are defined as having median diameters of 4-64 mm, and cobbles are defined as having median diameters of 64-256 mm. The extent and distribution of the units are shown on the trench logs (Plates 2-5).

Units Exposed in Trenches 1, 3, and 4

Unit 115 (Trench 4): Very dark-gray (N2.5), strong-brown (7.5YR4/6), and bluish-gray (5B5/1) mottled clayey silt; some sand and pebbles (sand fine to medium, ~15-20%; pebbles fine to coarse, ~20-25%); trace cobbles (~1-5%); moist; locally very hard and well-indurated; little bioturbation; localized occurrence of dark, elongate, subvertical mineral stains; charcoal very rare (weathered bedrock).

Unit 110 (Trench 1): Strong-brown (7.5YR4/6) and bluish-gray (5B5/1) mottled pebbly sandy silt (sand fine to medium; pebbles fine to medium); some clay (~15-20%); little coarse sand (~10-15%); slightly moist to moist; very stiff; little bioturbation; charcoal relatively rare.

Unit 100 (Trenches 1 and 3): Strong-brown (7.5YR5/8) and bluish-gray (5B5/1) mottled fine to very fine sand; some silt (~20-25%); little medium to coarse sand, granules, and fine pebbles (combined total of ~5-10%); several thin (1.5-3.0 cm), relatively continuous, dark-bluish-gray (5B4/1) clay layers within unit; relatively homogeneous and uniform; slightly moist to moist; little bioturbation; charcoal relatively rare.

Unit 90 (Trenches 1 and 3): Very dusky-red (2.5YR2.5/3) silty sand (sand fine to medium); some clay (~15-20%); little coarse sand (~10-15%); abundant subrounded reddish-brown (iron oxide) and black (manganese oxide) nodules, ranging in size from coarse sand to fine pebbles; moist; porous; crumbly; little bioturbation; charcoal rare.

Unit 80 (Trenches 1 and 4): Light-brownish-gray (2.5Y6/2), silty, fine sand with some yellowish-brown (10YR5/8) mottling; little clay (~5-10%); homogeneous and uniform; moist; slightly bioturbated, with some krotovina; charcoal rare.

Unit 65 (Trench 3): Strong-brown (7.5YR5/8) and bluish-gray (5B5/1) mottled, silty, fine sand; little medium to coarse sand (~5-10%); trace fine pebbles (~1-5%); homogeneous and well-sorted; moist; reddish-brown iron oxide nodules and black manganese staining common; thin (2-4 cm), relatively continuous dark-gray clay layer in middle portion of unit; little bioturbation; charcoal rare.

Unit 50 (Trenches 1, 3, and 4): Grayish-brown (2.5Y5/2) clayey silt; some fine sand (~15-20%); trace medium to coarse sand (~1-5%); homogeneous and uniform; slightly moist to moist; moderately stiff; slightly bioturbated, with some krotovina; localized development of weak to moderately-developed granular soil structure; localized occurrence of dark reddish-brown coarse sand- to fine pebble-sized iron oxide nodules; charcoal relatively uncommon.

Unit 40 (Trenches 1, 3, and 4): Yellowish-brown (10YR5/8) and bluish-gray (5B6/1) mottled very fine to fine sand; some silt (~15-20%); little clay, medium to coarse sand, granules, and fine pebbles (combined total of ~10-15%); relatively homogeneous and well-sorted; widespread black (manganese) and reddish-brown (iron) staining; moist; slightly to moderately bioturbated, with some rootlets and krotovina; charcoal relatively uncommon.

Unit 30 (Trench 1): Grayish-brown (2.5Y5/2), silty, fine sand; some granules, coarse sand, and clay (combined total of ~15-20%); few fine to medium pebbles (~10-15%); dry; hard; slightly to moderately bioturbated, with some

rootlets and krotovina; weakly developed granular soil structure; charcoal relatively uncommon.

Unit 25 (Trenches 1, 3, and 4): Dark-grayish-brown (2.5Y4/2) fine sandy silt to silty sand; some clay (~10-15%); little medium to coarse sand, granules, and fine pebbles (combined total of ~5-10%); relatively homogeneous and well-sorted; slightly moist to moist; moderately stiff; slightly to moderately bioturbated, with some rootlets and krotovina; charcoal relatively uncommon.

Unit 22/25 (Trenches 3 and 4): Thin (1-2 cm), relatively continuous layer of very dusky-red (2.5YR2.5/4) silty clay; slightly moist to moist; charcoal common (in-situ burn).

Unit 22 (Trenches 1, 3, and 4): Yellowish-brown (10YR5.5/8) and greenish-gray (5BG6/1) mottled fine sand; some medium to coarse sand, granules, and fine pebbles (combined total of ~15-20%); little silt (~10-15%); relatively homogeneous and well-sorted; localized areas of well-defined sub-horizontal stratification (1-4 cm thick); slightly moist to dry; slightly to moderately bioturbated, with some rootlets and krotovina; charcoal relatively uncommon.

Unit 20 (Trench 1): Gray (2.5Y6/1) pebbly sand (pebbles fine to medium; sand fine to medium); some silt, coarse sand, and coarse pebbles (combined total of ~15-20%); poorly-sorted; faint laminations in sand and fine pebbles

comprising lower portion of unit; dry; slightly to moderately bioturbated, with some rootlets and krotovina; charcoal relatively uncommon.

Unit 19 (Trenches 1, 3, and 4): Gray (2.5Y4.5/1), silty, fine sand; some medium to coarse sand (~10-15%); some fine to coarse pebbles (~15-20%); dry; stiff to crumbly; heavily bioturbated, with abundant rootlets and krotovina; moderate to well-developed granular soil structure; charcoal abundant (buried A horizon).

Unit 18 (Trenches 1, 3, and 4): Light-yellowish-brown (2.5Y6/5), silty, fine sand; little medium to coarse sand (~5-10%); few fine to medium pebbles (~5-10%); dry; friable; heavily bioturbated, with abundant rootlets and krotovina; moderate to well-developed granular soil structure; charcoal common.

Unit 17/18 (Trench 1): Thin (1-2 cm), relatively continuous layer of very dusky-red (2.5YR2.5/4) silty clay; dry; stiff; charcoal common (in-situ burn).

Unit 17 (Trenches 1 and 3): Pale-yellow (2.5Y7/4) very fine to fine sand; some silt, granules, and fine pebbles (combined total of ~15-20%); little medium sand (~5-10%); well-sorted; localized fine stratification (3-8 mm thick); dry; friable; moderately to heavily bioturbated, with abundant rootlets and krotovina; some development of vague granular soil structure; charcoal relatively uncommon.

Unit 10a (Trench 1): Yellow (2.5Y7/6) very fine to fine sand; homogeneous; well-sorted; moderately bioturbated; constitutes a thin (3-4 cm), discontinuous layer located in the lower portion of Unit 10.

Unit 10 (Trenches 1, 3, and 4): Dark-reddish-gray (2.5YR4/1), silty, fine sand; some medium to coarse sand (~10-15%); some fine to coarse pebbles (~10-15%); dry; stiff to crumbly; heavily bioturbated, with abundant rootlets and krotovina; moderate to well-developed granular soil structure; charcoal relatively uncommon (A horizon).

Units Exposed in Trench 2

Unit I: Very dark-grayish-brown (2.5Y3/2) to light-gray (5Y7/2) pebbly sand to sandy pebbles, with lenses of dark-gray (N4), sandy, pebbly clay in lower portion of unit (sand fine to coarse; pebbles medium to coarse); some silt, particularly in upper portion of unit (~15-20%); some fine pebbles (~10-15%); pebble content variable, with higher proportions and generally coarser clasts in lower portion of unit, and lower proportions and generally finer clasts in upper portion (normally graded sequence); contains rusty-brown hardpan horizon and large piece of broken glass (4-5 cm in diameter) in central portion of unit; slightly moist to moist; bioturbation slight throughout most of unit, but moderate in uppermost portion; charcoal rare (channel deposit).

Unit H: Dark-gray (N4) sandy clay (sand fine); some silt and medium to coarse sand (combined total of ~15-20%); trace fine pebbles (~1-5%); very moist to wet; sticky; plastic; little bioturbation; charcoal abundant.

Unit G: Light-brownish-gray (2.5Y6/3) and strong-brown (7.5YR4/6) mottled sand with variable amounts of pebbles (sand fine to medium; pebbles medium); few fine pebbles (~5-10%); trace clay (~1-5%); large proportion of pebbles are substantially weathered, with some altered to clay; slightly moist to damp; eastern half of unit contains a few thin (1-3 cm), relatively continuous layers of dark-gray clay; little bioturbation; charcoal relatively rare.

Unit F: Yellowish-red (5YR4.5/7), light-gray (2.5Y7/2), and gray (N6) mottled fine sand; some medium sand (~10-15%); trace coarse sand and silt (combined total of ~1-5%); well-sorted; localized vague planar cross-stratification; damp to slightly moist; contains a few thin (3-8 cm), relatively continuous layers of dark-bluish-gray (5B4/1) clay; little bioturbation; charcoal common.

Unit E2: Red (2.5YR4/8) and dark-brown (7.5YR3/2) mottled clayey silt; some fine sand (~10-15%); trace coarse sand (~1-5%); homogeneous and uniform; damp to slightly moist; slightly sticky; slightly plastic; slightly to moderately bioturbated, with some rootlets and krotovina; pervasive, well-developed granular soil structure, but with some relatively unaltered lenses of Unit F (yellowish-red and gray mottled fine sand); charcoal common (buried B horizon).

Unit E1: Grayish-brown (2.5Y5/3), fine, sandy silt; some medium to coarse sand (~15-20%); some fine to medium pebbles (~15-20%); some elongate lenses of yellowish-brown (10YR5/8) and gray (10YR5/1) mottled, silty, fine sand; dry; crumbly; moderately to heavily bioturbated, with widespread rootlets and krotovina; moderately-developed granular soil structure; charcoal abundant (buried A horizon).

Unit D: Grayish-brown (2.5Y5/2) sandy pebbles (pebbles medium; sand medium to coarse); some silt (~15-20%); little fine sand (~5-10%); few fine pebbles (~5-10%); locally vague to well-developed planar cross-stratification (strata 1-2 cm thick) within sandy material; dry; moderately bioturbated, with some rootlets and krotovina; charcoal rare.

Unit C: Pale-yellow (2.5Y7/4) and gray (2.5Y5/1) mottled, silty, fine sand; little medium to coarse sand and medium pebbles (combined total of ~5-10%); trace fine pebbles (~1-5%); trace clay (~1-5%); moderately well-sorted; locally well-developed planar cross-stratification (strata 1-3 cm thick); dry; moderately to heavily bioturbated, with widespread rootlets and krotovina; moderately-developed granular soil structure; charcoal relatively rare.

Unit B: Grayish-brown (2.5Y5/2) to light-brownish-gray (2.5Y6/2) sandy pebbles to pebbly sand (pebbles medium to coarse; sand fine to coarse); some fine pebbles (~15-20%); some silt (~10-15%); locally vague to moderately-developed subhorizontal stratification within sandy material; dry; moderately to

heavily bioturbated, with widespread rootlets and krotovina; moderately-developed granular soil structure; charcoal rare.

Unit A: Gray (2.5Y5/1) pebbly sandy silt to silty sand (sand fine; pebbles medium to coarse); some medium to coarse sand (~15-20%); few fine pebbles (~5-10%); little clay (~5-10%); dry; crumbly; heavily bioturbated, with abundant roots, rootlets, and krotovina; moderate to well-developed granular soil structure; charcoal common (A horizon).

APPENDIX B:

LABORATORY ANALYTICAL RESULTS

Appendix B lists the raw laboratory data for all the radiocarbon samples that were analyzed. Analysis of all samples was performed at the Center for Accelerator Mass Spectrometry at Lawrence Livermore National Laboratory in Livermore, California. Sample locations are shown on the trench logs (Plates 2-5).

CENTER FOR ACCELERATOR MASS SPECTROMETRY

Lawrence Livermore National Lab.

^{14}C results G.Heingartner August 24, 1995

CAMS #	Sample Name	Other ID	$\delta^{13}C$	fraction Modern	±	$D^{14}C$	±	^{14}C age	±
22056	T1-95-12BS -19	N10072	-25	0.9811	0.0065	-18.9	6.5	150	60
22057	T1-95-10CS—100	N10073	-25	0.8831	0.0056	-116.9	5.6	1000	60
22058	T1-95-12CN—25	N10074	-25	0.8709	0.0056	-129.1	5.6	1110	60
22059	T1-95-11CS—25	N10075	-25	0.9269	0.0059	-73.1	5.9	610	60
22060	T1-95-11CS—50	N10076	-25	0.8924	0.0057	-107.6	5.7	910	60
22061	T1-95-11CN—40	N10077	-25	0.9175	0.0061	-82.5	6.1	690	60
22062	T1-95-10CS — 40	N10078	-25	0.9476	0.0090	-52.4	9.0	430	80

1) Delta ^{13}C values are the assumed values according to Stuiver and Polach (Radiocarbon, v. 19, p.355, 1977) when given without decimal places. Values measured for the material itself are given with a single decimal place.

2) The quoted age is in radiocarbon years using the Libby half life of 5568 years and following the conventions of Stuiver and Polach (ibid.).

3) Radiocarbon concentration is given as fraction Modern, $D^{14}C$, and conventional radiocarbon age.

4) Sample preparation backgrounds have been subtracted, based on measurements of samples of ^{14}C-free coal. Backgrounds were scaled relative to sample size.

CENTER FOR ACCELERATOR MASS SPECTROMETRY
Lawrence Livermore National Laboratory

^{14}C results G. Heingartner October 10, 1995

CAMS #	Sample Name	Other ID	$\delta^{13}C$	fraction Modern	±	$D^{14}C$	±	^{14}C age	±
22850	TI-95-10BS -25	N10193	-25	0.9498	0.0088	-50.2	8.8	410	80
22851	TI-95-12CS -22	N10194	-25	0.9491	0.0063	-50.9	6.3	420	60
22852	TI-95-16CN-22a	N10214	-25	0.9398	0.0063	-60.2	6.3	500	60
22853	TI-95-21DN -25a	N10215	-25	0.9330	0.0053	-67.0	5.3	560	50
22854	TI-95-10DS -100	N10455	-25	0.8765	0.0058	-123.5	5.8	1060	60
22855	TI-95-9CN-40a	N10217	-25	0.9419	0.0062	-58.1	6.2	480	60
22856	TI-95-17BN-18a	N10218	-25	0.9587	0.0065	-41.3	6.5	340	60

1) Delta ^{13}C values are the assumed values according to Stuiver and Polach (Radiocarbon, v. 19, p.355, 1977) when given without decimal places. Values measured for the material itself are given with a single decimal place.

2) The quoted age is in radiocarbon years using the Libby half life of 5568 years and following the conventions of Stuiver and Polach (ibid.).

3) Radiocarbon concentration is given as fraction Modern, $D^{14}C$, and conventional radiocarbon age.

4) Sample preparation backgrounds have been subtracted, based on measurements of samples of ^{14}C-free coal. Backgrounds were scaled relative to sample size.

CENTER FOR ACCELERATOR MASS SPECTROMETRY

Lawrence Livermore National Laboratory

^{14}C results G. Heingartner October 10, 1995

CAMS #	Sample Name	Other ID	$\delta^{13}C$	fraction Modern	±	$D^{14}C$	±	^{14}C age	±
22884	T1-95-7CS-100A	N10219	-25	0.8884	0.0049	-111.6	4.9	950	50
22885	T1-95-11CS-50C	N10220	-25	0.9800	0.0064	-20.0	6.4	160	60
22886	T1-95-13BS-19A	N10221	-25	1.0086	0.0065	8.6	6.5	>Modern	
22887	T1-95-11BN-25A	N10222	-25	0.9535	0.0062	-46.5	6.2	380	60
22888	T1-95-12BN-22A	N10223	-25	0.9597	0.0062	-40.3	6.2	330	60
22889	T1-95-14BS-19A	N10478	-25	0.9839	0.0064	-16.1	6.4	130	60

1) Delta ^{13}C values are the assumed values according to Stuiver and Polach (Radiocarbon, v. 19, p.355, 1977) when given without decimal places. Values measured for the material itself are given with a single decimal place.

2) The quoted age is in radiocarbon years using the Libby half life of 5568 years and following the conventions of Stuiver and Polach (ibid.).

3) Radiocarbon concentration is given as fraction Modern, $D^{14}C$, and conventional radiocarbon age.

4) Sample preparation backgrounds have been subtracted, based on measurements of samples of ^{14}C-free coal. Backgrounds were scaled relative to sample size.

CENTER FOR ACCELERATOR MASS SPECTROMETRY

Lawrence Livermore National Laboratory

^{14}C results

Heingartner

January 17, 1996

CAMS #	Sample Name	Other ID	$\delta^{13}C$	fraction Modern	±	$D^{14}C$	±	^{14}C age	±
24684	T2-95-26AS-A	N11043	-25	0.9715	0.0070	-28.5	7.0	230	60
24685	T2-95-4AS-C	N11044	-25	0.9897	0.0066	-10.3	6.6	80	60
24686	T2-95-16AS-A	N11046	-25	0.8595	0.0057	-140.5	5.7	1220	60
24687	T2-95-13BS-E	N11047	-25	0.9836	0.0063	-16.4	6.3	130	60
24688	T2-95-5CS-F	N11048	-25	0.9695	0.0062	-30.5	6.2	250	60
24689	T2-95-33CS-G	N11049	-25	0.9012	0.0050	-98.8	5.0	840	50
24690	T2-95-42CS-G	N11050	-25	0.8897	0.0056	-110.3	5.6	940	60

1) Delta ^{13}C values are the assumed values according to Stuiver and Polach (Radiocarbon, v. 19, p.355, 1977) when given without decimal places. Values measured for the material itself are given with a single decimal place.

2) The quoted age is in radiocarbon years using the Libby half life of 5568 years and following the conventions of Stuiver and Polach (ibid.).

3) Radiocarbon concentration is given as fraction Modern, $D^{14}C$, and conventional radiocarbon age.

4) Sample preparation backgrounds have been subtracted, based on measurements of samples of ^{14}C-free coal. Backgrounds were scaled relative to sample size.

CENTER FOR ACCELERATOR MASS SPECTROMETRY

Lawrence Livermore National Laboratory

^{14}C results Heingartner February 25, 1996

CAMS #	Sample Name	Other ID	$\delta^{13}C$	fraction Modern	±	$D^{14}C$	±	^{14}C age	±
25577	T2-95-36BS-C	N11361	-25	0.9815	0.0050	-18.5	5.0	150	50
25578	T2-95-4AS-C	N11362	-25	0.9881	0.0069	-11.9	6.9	100	60
25579	T2-95-13BS-EI	N11363	-25	0.9649	0.0065	-35.1	6.5	290	60
25580	T2-95-5CS- F	N11364	-25	0.9011	0.0069	-98.9	6.9	840	70
25581	T2-95-12BS-C	N11365	-25	0.9803	0.0065	-19.7	6.5	160	60
25582	T2-95-6BS-EI	N11366	-25	0.9857	0.0051	-14.3	5.1	120	50
25583	T2-95-25BS-EI	N11367	-25	0.9709	0.0064	-29.1	6.4	240	60

1) Delta ^{13}C values are the assumed values according to Stuiver and Polach (Radiocarbon, v. 19, p.355, 1977) when given without decimal places. Values measured for the material itself are given with a single decimal place.

2) The quoted age is in radiocarbon years using the Libby half life of 5568 years and following the conventions of Stuiver and Polach (ibid.).

3) Radiocarbon concentration is given as fraction Modern, $D^{14}C$, and conventional radiocarbon age.

4) Sample preparation backgrounds have been subtracted, based on measurements of samples of ^{14}C-free wood. Backgrounds were scaled relative to sample size.

CENTER FOR ACCELERATOR MASS SPECTROMETRY
Lawrence Livermore National Laboratory

^{14}C results — Heingartner — March 19, 1996

CAMS #	Sample Name	Other ID	$\delta^{13}C$	fraction Modern	±	$D^{14}C$	±	^{14}C age	±
26206	T1-95-16BS-18/19	N11634	-25	0.9743	0.0063	-25.7	6.3	210	60
26207	T1-95-16BN-17a	N11635	-25	0.9698	0.0063	-30.2	6.3	250	60
26208	T1-95-13BS-17a	N11636	-25	0.9792	0.0058	-20.8	5.8	170	50
26209	T1-95-18AN-10a	N11637	-25	0.9854	0.0065	-14.6	6.5	120	60
26210	T1-95-7AS-10	N11638	-25	0.9813	0.0064	-18.7	6.4	150	60
26211	T1-95-13BS-19b	N11639	-25	0.9876	0.0065	-12.4	6.5	100	60
23212	T1-95-14BN-19a	N11640	-25	0.9803	0.0064	-19.7	6.4	160	60
26213	T1-95-14BS-18b	N11641	-25	0.9719	0.0054	-28.1	5.4	230	50
26238	TI-95-14BS-18A	N11644	-25	0.9533	0.0062	-46.7	6.2	380	60
26239	TI-95-13BN-19	N11645	-25	0.9738	0.0064	-26.2	6.4	210	60
26240	TI-95-13BS-18/19	N11646	-25	0.9773	0.0084	-22.7	8.4	180	70
26241	TI-95-15BN-18A	N11643	-25	0.7310	0.0059	-269.0	5.9	2520	70
26242	TI-95-17BS-19A	N11642	-25	0.7928	0.0055	-207.2	5.5	1870	60

1) Delta ^{13}C values are the assumed values according to Stuiver and Polach (Radiocarbon, v. 19, p.355, 1977) when given without decimal places. Values measured for the material itself are given with a single decimal place.

2) The quoted age is in radiocarbon years using the Libby half life of 5568 years and following the conventions of Stuiver and Polach (ibid.).

3) Radiocarbon concentration is given as fraction Modern, $D^{14}C$, and conventional radiocarbon age.

4) Sample preparation backgrounds have been subtracted, based on measurements of samples of ^{14}C-free coal or wood. Backgrounds were scaled relative to sample size.

CENTER FOR ACCELERATOR MASS SPECTROMETRY
Lawrence Livermore National Laboratory

^{14}C results

G.Heingartner

May 2, 1996

CAMS #	Sample Name	Other ID	$\delta^{13}C$	fraction Modern	±	$D^{14}C$	±	^{14}C age	±
27246	T1-95-12*CS*-22	N12318	-25	0.9056	0.0056	-94.4	5.6	800	50
27247	T1-95-13BS-17b	N12319	-25	0.9473	0.0066	-52.7	6.6	430	60
27248	T1-95-18BN-18a	N12320	-25	0.8595	0.0048	-140.5	4.8	1220	50

1) Delta ^{13}C values are the assumed values according to Stuiver and Polach (Radiocarbon, v. 19, p.355, 1977) when given without decimal places. Values measured for the material itself are given with a single decimal place.

2) The quoted age is in radiocarbon years using the Libby half life of 5568 years and following the conventions of Stuiver and Polach (ibid.).

3) Radiocarbon concentration is given as fraction Modern, $D^{14}C$, and conventional radiocarbon age.

4) Sample preparation backgrounds have been subtracted, based on measurements of samples of ^{14}C-free coal. Backgrounds were scaled relative to sample size.

CENTER FOR ACCELERATOR MASS SPECTROMETRY

Lawrence Livermore National Laboratory

^{14}C results Heingartner June 4, 1996

CAMS #	Sample Name	Other ID	$\delta^{13}C$	fraction Modern	±	$D^{14}C$	±	^{14}C age	±
27951	T1-95-19CS-18A	N12446	-25	0.9724	0.0061	-27.6	6.1	220	60
27952	T1-95-13BS-18	N12447	-25	0.9649	0.0061	-35.1	6.1	290	60
27953	T1-95-23BS-10A	N12448	-25	0.9784	0.0061	-21.6	6.1	180	60
27954	T1-95-19CN-18/19	N12449	-25	0.9762	0.0061	-23.8	6.1	190	60
27955	T1-95-18BN-19A	N12450	-25	0.7328	0.0046	-267.2	4.6	2500	60
27956	T1-95-21CN-19A	N12451	-25	0.6512	0.0056	-348.8	5.6	3450	70
27957	T1-95-5AN-10	N12452	-25	0.9546	0.0060	-45.4	6.0	370	60
27958	T1-95-11CN-25	N12453	-25	0.6784	0.0043	-321.6	4.3	3120	60
27959	T1-95-20CN-19A	N12454	-25	0.9448	0.0059	-55.2	5.9	460	60
27960	T1-95-9BS-25	N12455	-25	0.7512	0.0070	-248.8	7.0	2300	80
27961	QL4766	N12456	-25	0.0023	0.0001	-997.7	0.1	48790	400

1) Delta ^{13}C values are the assumed values according to Stulver and Polach (Radiocarbon, v. 19, p.355, 1977) when given without decimal places. Values measured for the material itself are given with a single decimal place.

2) The quoted age is in radiocarbon years using the Libby half life of 5568 years and following the conventions of Stulver and Polach (ibid.).

3) Radiocarbon concentration is given as fraction Modern, $D^{14}C$, and conventional radiocarbon age.

4) Sample preparation backgrounds have been subtracted, based on measurements of samples of ^{14}C-free wood. Backgrounds were scaled relative to sample size.

CENTER FOR ACCELERATOR MASS SPECTROMETRY

Lawrence Livermore National Laboratory

^{14}C results G.Heingartner October 29, 1996

CAMS #	Sample Name	Other ID	$\delta^{13}C$	fraction Modern	±	$D^{14}C$	±	^{14}C age	±
31266	T3-96-4BS-22/25	N13549	-25	0.9613	0.0066	-38.7	6.6	320	60
31267	T3-96-5BN-25	N13552	-25	0.9529	0.0065	-47.1	6.5	390	60
31268	T3-96-4BS-18/19a	N13555	-25	0.9770	0.0068	-23.0	6.8	190	60
31269	T3-96-3BS-19a	N13561	-25	0.9815	0.0068	-18.5	6.8	150	60
31270	T3-96-5BS-19	N13562	-25	0.9801	0.0068	-19.9	6.8	160	60
31271	T3-96-3CN-22	N13564	-25	0.9381	0.0055	-61.9	5.5	510	50

1) Delta ^{13}C values are the assumed values according to Stulver and Polach (Radiocarbon, v. 19, p.355, 1977) when given without decimal places. Values measured for the material itself are given with a single decimal place.

2) The quoted age is in radiocarbon years using the Libby half life of 5568 years and following the conventions of Stulver and Polach (ibid.).

3) Radiocarbon concentration is given as fraction Modern, $D^{14}C$, and conventional radiocarbon age.

4) Sample preparation backgrounds have been subtracted, based on measurements of samples of ^{14}C-free coal.

CENTER FOR ACCELERATOR MASS SPECTROMETRY

Lawrence Livermore National Laboratory

^{14}C results G.Heingartner November 11, 1996

CAMS #	Sample Name	Other ID	$\delta^{13}C$	fraction Modern	±	$D^{14}C$	±	^{14}C age	±
31475	T3-96-4AS-18 0.1mgC	N13551	-25	0.9625	0.0117	-37.5	11.7	310	100
31476	T3-96-4BS-22/25	N13554	-25	0.9666	0.0063	-33.4	6.3	270	60
31477	T3-96-3CN-22	N13565	-25	0.9161	0.0051	-83.9	5.1	700	50

1) Delta ^{13}C values are the assumed values according to Stuiver and Polach (Radiocarbon, v. 19, p.355, 1977) when given without decimal places. Values measured for the material itself are given with a single decimal place.

2) The quoted age is in radiocarbon years using the Libby half life of 5568 years and following the conventions of Stuiver and Polach (ibid.).

3) Radiocarbon concentration is given as fraction Modern, $D^{14}C$, and conventional radiocarbon age.

4) Sample preparation backgrounds have been subtracted, based on measurements of samples of ^{14}C-free coal. Backgrounds were scaled relative to sample size.

5) Comment: The relatively large uncertainty for the -4As-18 sample is due to the small size.

CENTER FOR ACCELERATOR MASS SPECTROMETRY
Lawrence Livermore National Laboratory

^{14}C results G.Heingartner November 19, 1996

CAMS #	Sample Name	Other ID	$\delta^{13}C$	fraction Modern	±	$D^{14}C$	±	^{14}C age	±
31846	T1 -96-13BN-17/18	N13556	-25	0.9764	0.0051	-23.6	5.1	190	50
31847	T1 -96-14BN-17/18	N13557	-25	0.9634	0.0053	-36.6	5.3	300	50
31848	T1 -96-14BS 17/18a	N13558	-25	0.9782	0.0062	-21.8	6.2	180	60
31849	T1 -96-14BS 17/18b	N13559	-25	0.9675	0.0061	-32.5	6.1	270	60
31850	T3-96-3CS 22/25	N13560	-25	0.9407	0.0059	-59.3	5.9	490	60
31851	T3-96-4BS 22/25b	N13563	-25	0.9435	0.0059	-56.5	5.9	470	60
31852	T3-96-6BN 22/25	N14054	-25	0.9785	0.0053	-21.5	5.3	170	50
31853	T1 -96-14BS-18	N14055	-25	0.9902	0.0063	-9.8	6.3	80	60
31854	T1 -96-12BS-19b	N14056	-25	0.9939	0.0054	-6.1	5.4	50	50
31855	T1 -96-12BS-19a	N14057	-25	0.9845	0.0053	-15.5	5.3	130	50
31856	T1-95-22BN-19a	N14058	-25	0.9783	0.0053	-21.7	5.3	180	50
31857	Coal	N14061	-25	0.0017	0.0001	-998.3	0.1	51060	340

1) Delta ^{13}C values are the assumed values according to Stuiver and Polach (Radiocarbon, v. 19, p.355, 1977) when given without decimal places. Values measured for the material itself are given with a single decimal place.

2) The quoted age is in radiocarbon years using the Libby half life of 5568 years and following the conventions of Stuiver and Polach (ibid.).

3) Radiocarbon concentration is given as fraction Modern, $D^{14}C$, and conventional radiocarbon age.

4) Sample preparation backgrounds have been subtracted, based on measurements of samples of ^{14}C-free coal.

CENTER FOR ACCELERATOR MASS SPECTROMETRY

Lawrence Livermore National Laboratory

^{14}C results Heingartner December 5, 1996

CAMS #	Sample Name	Other ID	$\delta^{13}C$	fraction Modern	±	$D^{14}C$	±	^{14}C age	±
32182	T4-96-5BN-19A	N14252	-25	0.9790	0.0065	-21.0	6.5	170	60
32183	T4-96-5BN-19B	N14253	-25	0.9575	0.0064	-42.5	6.4	350	60
32184	T4-96-4BN-22/25B	N14254	-25	0.9562	0.0063	-43.8	6.3	360	60
32185	T1 -96-15BN-18B	N14255	-25	0.9856	0.0065	-14.4	6.5	120	60
32186	T3-96-4AS-18	N14256	-25	0.9653	0.0051	-34.7	5.1	280	50
32187	T3-96-2BN-19A	N14257	-25	0.9757	0.0063	-24.3	6.3	200	60
32188	T1 -96-13BN-17A	N14258	-25	0.9544	0.0042	-45.6	4.2	370	40

1) Delta ^{13}C values are the assumed values according to Stuiver and Polach (Radiocarbon, v. 19, p.355, 1977) when given without decimal places. Values measured for the material itself are given with a single decimal place.

2) The quoted age is in radiocarbon years using the Libby half life of 5568 years and following the conventions of Stuiver and Polach (ibid.).

3) Radiocarbon concentration is given as fraction Modern, $D^{14}C$, and conventional radiocarbon age.

4) Sample preparation backgrounds have been subtracted, based on measurements of samples of ^{14}C-free coal. Backgrounds were scaled relative to sample size.

CENTER FOR ACCELERATOR MASS SPECTROMETRY
Lawrence Livermore National Laboratory

^{14}C results — Helngartner — January 7, 1997

CAMS #	Sample Name	Other ID	$\delta^{13}C$	fraction Modern	±	$D^{14}C$	±	^{14}C age	±
33089	T3-96-3BS-18	N14525	-25	0.9731	0.0055	-26.9	5.5	220	50
33090	T3-96-5BN-25	N14526	-25	0.9245	0.0054	-75.5	5.4	630	50
33091	T1 -96-14CS-22b	N14528	-25	0.9621	0.0057	-37.9	5.7	310	50
33092	T1 -96-13BS-18b	N14529	-25	0.9622	0.0068	-37.8	6.8	310	60
33093	T1 -96-15BN-18a	N14530	-25	0.9662	0.0058	-33.8	5.8	280	50
33094	T1 -96-13DS-25	N14531	-25	0.9090	0.0044	-91.0	4.4	770	40
33095	T1 -96-14CS-22a	N14532	-25	0.9579	0.0055	-42.1	5.5	350	50

1) Delta ^{13}C values are the assumed values according to Stuiver and Polach (Radiocarbon, v. 19, p.355, 1977) when given without decimal places. Values measured for the material itself are given with a single decimal place.

2) The quoted age is in radiocarbon years using the Libby half life of 5568 years and following the conventions of Stuiver and Polach (ibid.).

3) Radiocarbon concentration is given as fraction Modern, $D^{14}C$, and conventional radiocarbon age.

4) Sample preparation backgrounds have been subtracted, based on measurements of samples of ^{14}C-free coal. Backgrounds were scaled relative to sample size.

CENTER FOR ACCELERATOR MASS SPECTROMETRY

Lawrence Livermore National Laboratory

^{14}C results G. Heingartner February 4, 1997

CAMS #	Sample Name	Other ID	$\delta^{13}C$	fraction Modern	±	$D^{14}C$	±	^{14}C age	±
33923	T4-96-5BS-19		-25	1.0137	0.0069	13.7	6.9	>Modern	0
33924	T3-96-2AN-17		-25	1.0011	0.0056	1.1	5.6	0	50

1) Delta ^{13}C values are the assumed values according to Stuiver and Polach (Radiocarbon, v. 19, p.355, 1977) when given without decimal places. Values measured for the material itself are given with a single decimal place.

2) The quoted age is in radiocarbon years using the Libby half life of 5568 years and following the conventions of Stuiver and Polach (ibid.).

3) Radiocarbon concentration is given as fraction Modern, $D^{14}C$, and conventional radiocarbon age.

4) Sample preparation backgrounds have been subtracted, based on measurements of samples of ^{14}C-free coal. Backgrounds were scaled relative to sample size.

APPENDIX C:

TABLE OF INDIVIDUAL RADIOCARBON SAMPLE AGES

Appendix C lists the ages of all the individual radiocarbon samples analyzed from the trenches. Under the heading "Sample Number", the identification number of the sample is listed. The first denotation of this number (**T1**-95-15AS-25a) refers to the trench from which the sample was obtained, the second denotation (T1-**95**-15AS-25a) refers to the year in which the trench was excavated, the third denotation (T1-95-**15AS**-25a) refers to the location of the sample within the trench, and the fourth denotation (T1-95-15AS-**25**a) refers to the unit within which the sample was found. The suffix at the end of the unit number (T1-95-15AS-25**a**), where present, is used to differentiate between samples located in close proximity to one another. The number one in parentheses following the sample identification number denotes the first run of a split sample, whereas the number two in parentheses denotes the second run.

Under the heading "Radiocarbon Yrs. B.P.", the age of the sample in radiocarbon years before present is shown. The expressed errors represent one standard deviation. Under the heading "2 σ Cal. Yrs. B.P. (Highest Prob.)", the highest probability 2 sigma age range of the sample in calendar years before present is shown. Under the heading "2 σ Cal. Age (Highest Prob.)", the highest probability 2 sigma calendric age range of the sample (A.D. or B.C.) is shown. Under the heading "% Probability (within 2 σ)", the percent probability of the calendric age representing the true age of the sample, within the limits of the 2 sigma interval (i.e. at the 95 percent confidence level), is shown. Samples were calibrated by using the 3.0.3c version of the Calib calibration program (Stuiver and Reimer, 1993). Sample locations are shown on the trench logs (Plates 2-5).

AGES OF INDIVIDUAL RADIOCARBON SAMPLES

Sample Number Trench 1	Radiocarbon Yrs. B.P.	2σ Cal. Yrs. B.P. (Highest Prob.)	2σ Cal. Age (Highest Prob.)	% Probability (within 2σ)
T1-95-18AN-10a	120±60	79±75	1796-1946 AD	60
T1-95-7AS-10	150±60	223±60	1668-1787 AD	45
T1-95-23BS-10a	180±60	178±121	1652-1893 AD	82
T1-95-5AN-10	370±60	406±102	1442-1646 AD	100
T1-95-16BN-17a	250±60	358±111	1481-1703 AD	59
T1-95-13BS-17a	170±50	208±83	1660-1825 AD	66
T1-95-13BS-17b	430±60	481±60	1410-1529 AD	68
T1-96-13BN-17a	370±40	407±92	1452-1635 AD	100
T1-96-13BN-17/18	190±50	214±87	1649-1823 AD	71
T1-96-14BN-17/18	300±50	379±101	1470-1672 AD	96
T1-96-14BS-17/18a	180±60	178±121	1652-1893 AD	82
T1-96-14BS-17/18b	270±60	370±110	1470-1690 AD	75
T1-95-17BN-18a	340±60	398±106	1446-1659 AD	100
T1-95-14BS-18b	230±50	183±53	1714-1820 AD	41
T1-95-14BS-18a	380±60	409±102	1439-1643 AD	100
T1-95-15BN-18a	2520±70	2587±164	800-473 BC	92
T1-95-18BN-18a	1220±50	1160±106	684-896 AD	93
T1-95-19CS-18a	220±60	192±133	1626-1891 AD	78
T1-95-13BS-18	290±60	380±111	1459-1681 AD	88
T1-96-15BN-18b	120±60	79±75	1796-1946 AD	60
T1-96-14BS-18	80±60	79±70	1801-1941 AD	67
T1-96-13BS-18b	310±60	389±113	1449-1674 AD	96
T1-96-15BN-18a	280±50	371±101	1478-1680 AD	87

AGES OF INDIVIDUAL RADIOCARBON SAMPLES (cont.)

Sample Number Trench 1	Radiocarbon Yrs. B.P.	2σ Cal. Yrs. B.P. (Highest Prob.)	2σ Cal. Age (Highest Prob.)	% Probability (within 2σ)
T1-95-13BS-18/19	180±70	153±153	1644-1955 AD	100
T1-95-16BS-18/19	210±60	187±132	1632-1895 AD	80
T1-95-19CN-18/19	190±60	181±125	1645-1894 AD	82
T1-95-12BS-19	150±60	223±60	1668-1787 AD	45
T1-95-14BS-19a	130±60	80±77	1794-1947 AD	59
T1-95-13BS-19b	100±60	79±73	1798-1944 AD	64
T1-95-14BN-19a	160±60	171±115	1664-1894 AD	82
T1-95-13BN-19	210±60	187±132	1632-1895 AD	80
T1-95-17BS-19a	1870±60	1811±122	18-261 AD	95
T1-95-18BN-19a	2500±60	2583±159	791-474 BC	92
T1-95-21CN-19a	3450±70	3712±164	1925-1598 BC	97
T1-95-20CN-19a	460±60	488±67	1395-1529 AD	81
T1-96-12BS-19b	50±50	80±63	1807-1933 AD	76
T1-96-12BS-19a	130±50	80±75	1796-1945 AD	59
T1-95-22BN-19a	180±50	211±85	1655-1824 AD	68
T1-95-12CS-22 (1)	420±60	476±55	1419-1530 AD	63
T1-95-12CS-22 (2)	800±50	722±70	1159-1298 AD	99
T1-95-16CN-22a	500±60	506±70	1374-1514 AD	84
T1-95-12BN-22a	330±60	394±110	1446-1666 AD	100
T1-96-14CS-22a	350±50	400±97	1454-1647 AD	100
T1-96-14CS-22b	310±50	385±103	1463-1668 AD	99
T1-95-12CN-25	1110±60	1044±116	790-1022 AD	100
T1-95-11CS-25	610±60	593±66	1291-1424 AD	100

AGES OF INDIVIDUAL RADIOCARBON SAMPLES (cont.)

Sample Number Trench 1	Radiocarbon Yrs. B.P.	2σ Cal. Yrs. B.P. (Highest Prob.)	2σ Cal. Age (Highest Prob.)	% Probability (within 2σ)
T1-95-10BS-25	410±80	421±123	1406-1653 AD	100
T1-95-21DN-25a	560±50	545±33	1372-1439 AD	57
T1-95-11BN-25a	380±60	409±102	1439-1643 AD	100
T1-95-11CN-25	3120±60	3335±130	1515-1255 BC	97
T1-95-9BS-25	2300±80	2281±215	545-116 BC	95
T1-96-13DS-25	770±40	697±46	1207-1299 AD	100
T1-95-11CN-40	690±60	628±80	1242-1403 AD	100
T1-95-10CS-40	430±80	426±128	1396-1653 AD	100
T1-95-9CN-40a	480±60	495±67	1388-1522 AD	85
T1-95-11CS-50	910±60	817±113	1020-1246 AD	100
T1-95-11CS-50c	160±60	171±115	1664-1894 AD	82
T1-95-10CS-100	1000±60	873±122	955-1200 AD	98
T1-95-10DS-100	1060±60	983±97	870-1065 AD	91
T1-95-7CS-100a	950±50	839±98	1013-1210 AD	100

Sample Number Trench 2	Radiocarbon Yrs. B.P.	2σ Cal. Yrs. B.P. (Highest Prob.)	2σ Cal. Age (Highest Prob.)	% Probability (within 2σ)
T2-95-26AS-A	230±60	229±102	1620-1823 AD	68
T2-95-16AS-A	1220±60	1161±109	680-898 AD	89
T2-95-4AS-C	100±60	79±73	1798-1944 AD	64
T2-95-12BS-C	160±60	171±115	1664-1894 AD	82

AGES OF INDIVIDUAL RADIOCARBON SAMPLES (cont.)

Sample Number Trench 2	Radiocarbon Yrs. B.P.	2σ Cal. Yrs. B.P. (Highest Prob.)	2σ Cal. Age (Highest Prob.)	% Probability (within 2σ)
T2-95-36BS-C	150±50	223±59	1669-1786 AD	46
T2-95-13BS-E1	290±60	380±111	1459-1681 AD	88
T2-95-6BS-E1	120±50	79±73	1798-1944 AD	62
T2-95-25BS-E1	240±60	183±53	1714-1820 AD	34
T2-95-5CS-F	840±70	732±68	1150-1286 AD	70
T2-95-33CS-G	840±50	731±66	1153-1285 AD	83
T2-95-42CS-G	940±60	836±112	1003-1226 AD	100

Sample Number Trench 3	Radiocarbon Yrs. B.P.	2σ Cal. Yrs. B.P. (Highest Prob.)	2σ Cal. Age (Highest Prob.)	% Probability (within 2σ)
T3-96-4AS-18	280±50	371±101	1478-1680 AD	87
T3-96-3BS-18	220±50	184±56	1711-1822 AD	45
T3-96-3BS-19a	150±60	223±60	1668-1787 AD	45
T3-96-5BS-19	160±60	171±115	1664-1894 AD	82
T3-96-2BN-19a	200±60	182±131	1637-1899 AD	82
T3-96-3CN-22 (1)	510±50	519±49	1383-1480 AD	88
T3-96-3CN-22 (2)	700±50	661±41	1248-1330 AD	59
T3-96-4BS-22/25 (1)	320±60	392±112	1447-1670 AD	98
T3-96-4BS-22/25 (2)	270±60	370±110	1470-1690 AD	75
T3-96-3CS-22/25	490±60	501±69	1381-1518 AD	85
T3-96-4BS-22/25b	470±60	491±67	1392-1526 AD	83

AGES OF INDIVIDUAL RADIOCARBON SAMPLES (cont.)

Sample Number Trench 3	Radiocarbon Yrs. B.P.	2σ Cal. Yrs. B.P. (Highest Prob.)	2σ Cal. Age (Highest Prob.)	% Probability (within 2σ)
T3-96-6BN-22/25	170±50	208±83	1660-1825 AD	66
T3-96-5BN-25 (1)	390±60	412±102	1436-1640 AD	100
T3-96-5BN-25 (2)	630±50	601±59	1290-1408 AD	100

Sample Number Trench 4	Radiocarbon Yrs. B.P.	2σ Cal. Yrs. B.P. (Highest Prob.)	2σ Cal. Age (Highest Prob.)	% Probability (within 2σ)
T4-96-5BN-19a	170±60	175±118	1658-1893 AD	82
T4-96-5BN-19b	350±60	400±104	1446-1654 AD	100
T4-96-4BN-22/25b	360±60	404±103	1444-1649 AD	100

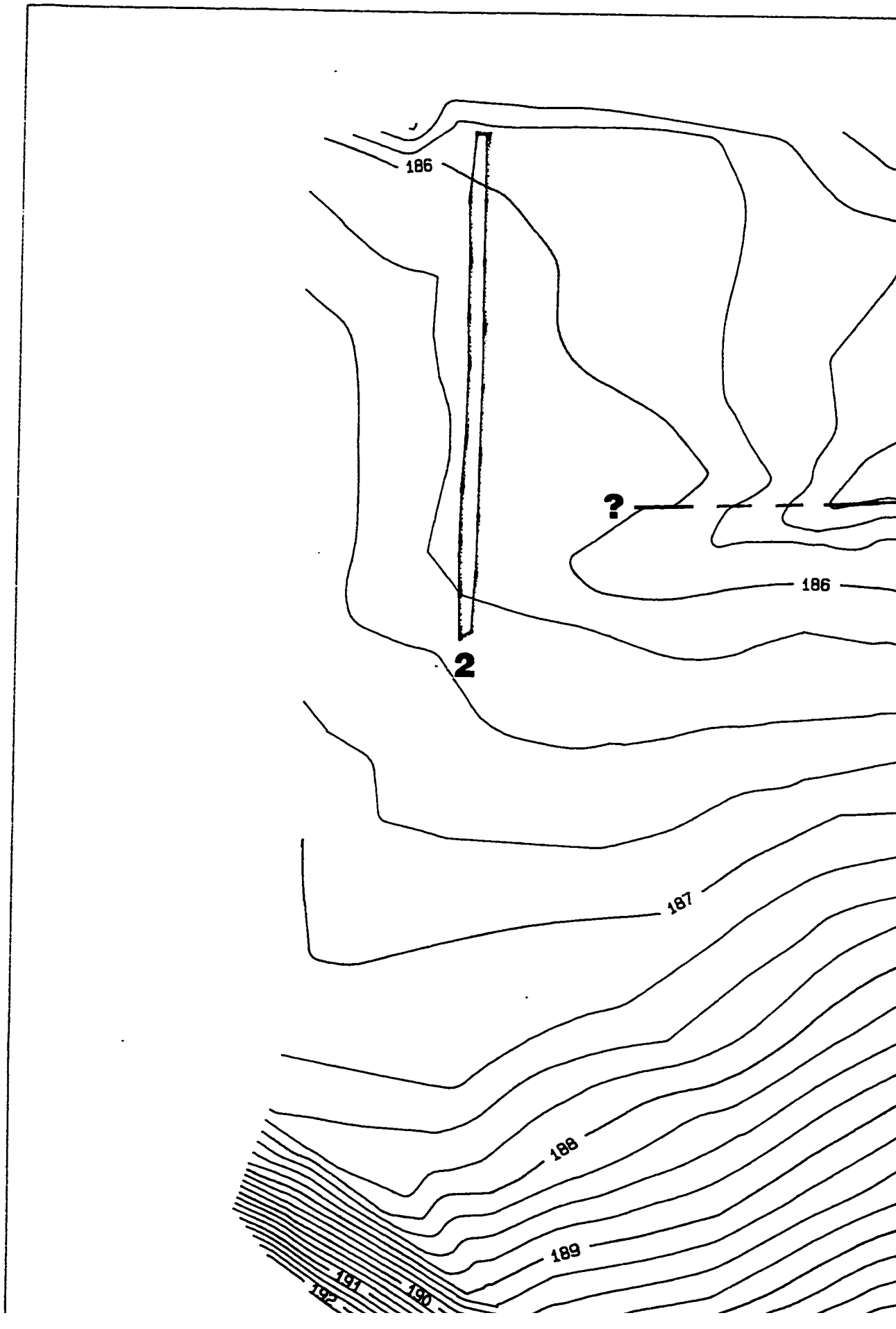
186
?
186
2
187
188
189
191
190
192

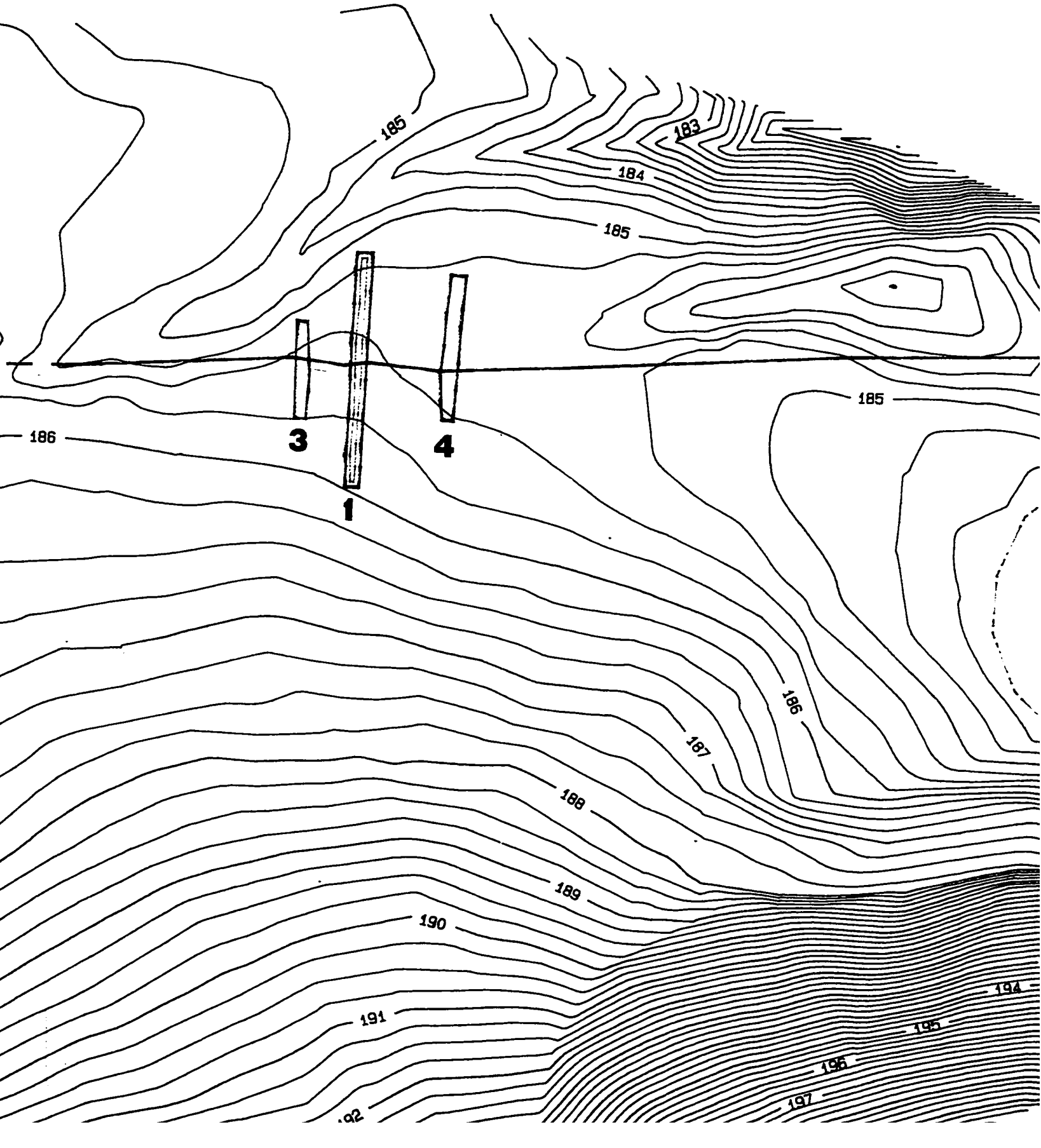
185
183
184
185
185
186
3
4
1
186
187
188
189
190
191
194
195
196
197

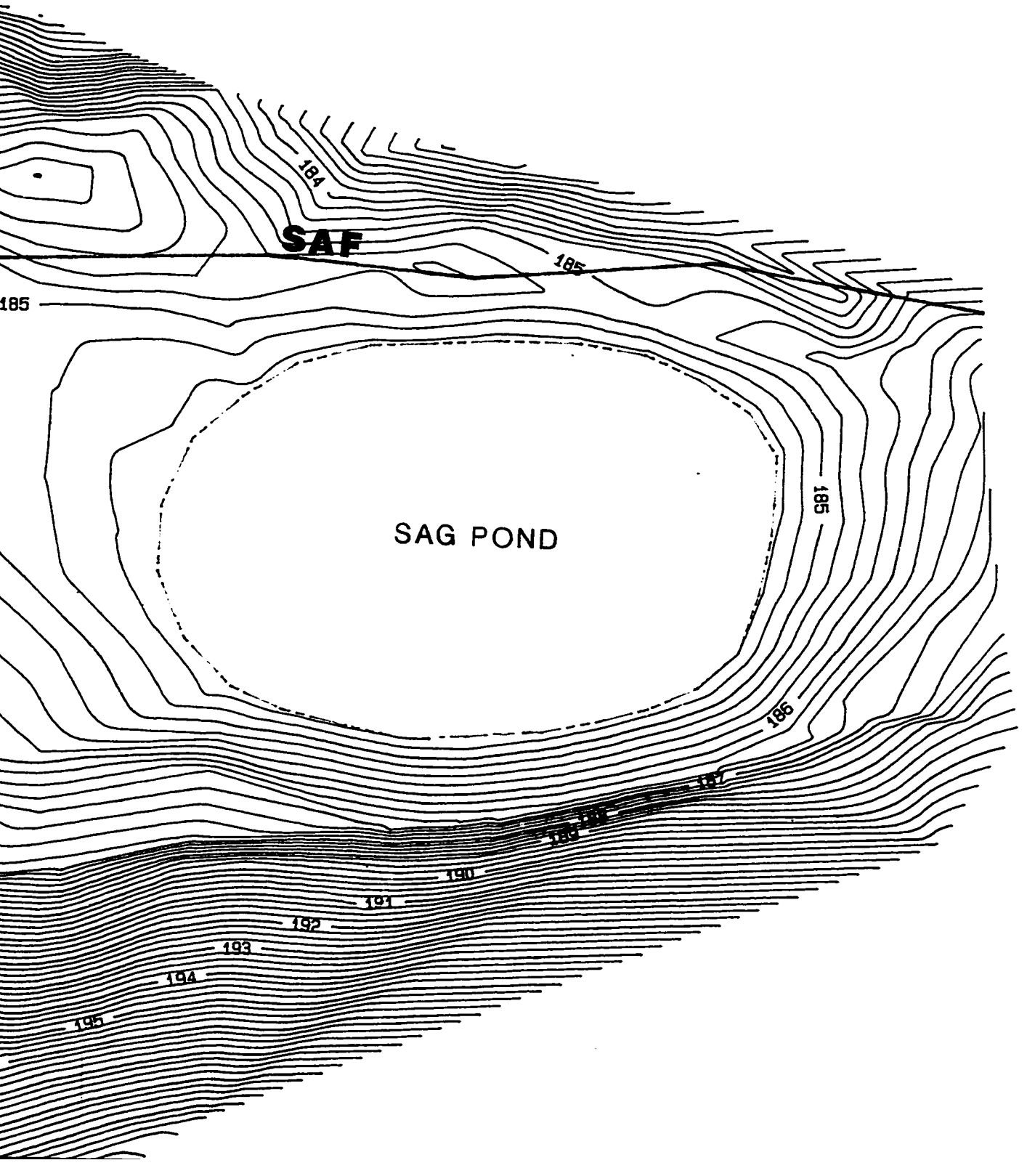
SAF
SAG POND
184
185
185
185
186
187
188
189
190
191
192
193
194
195

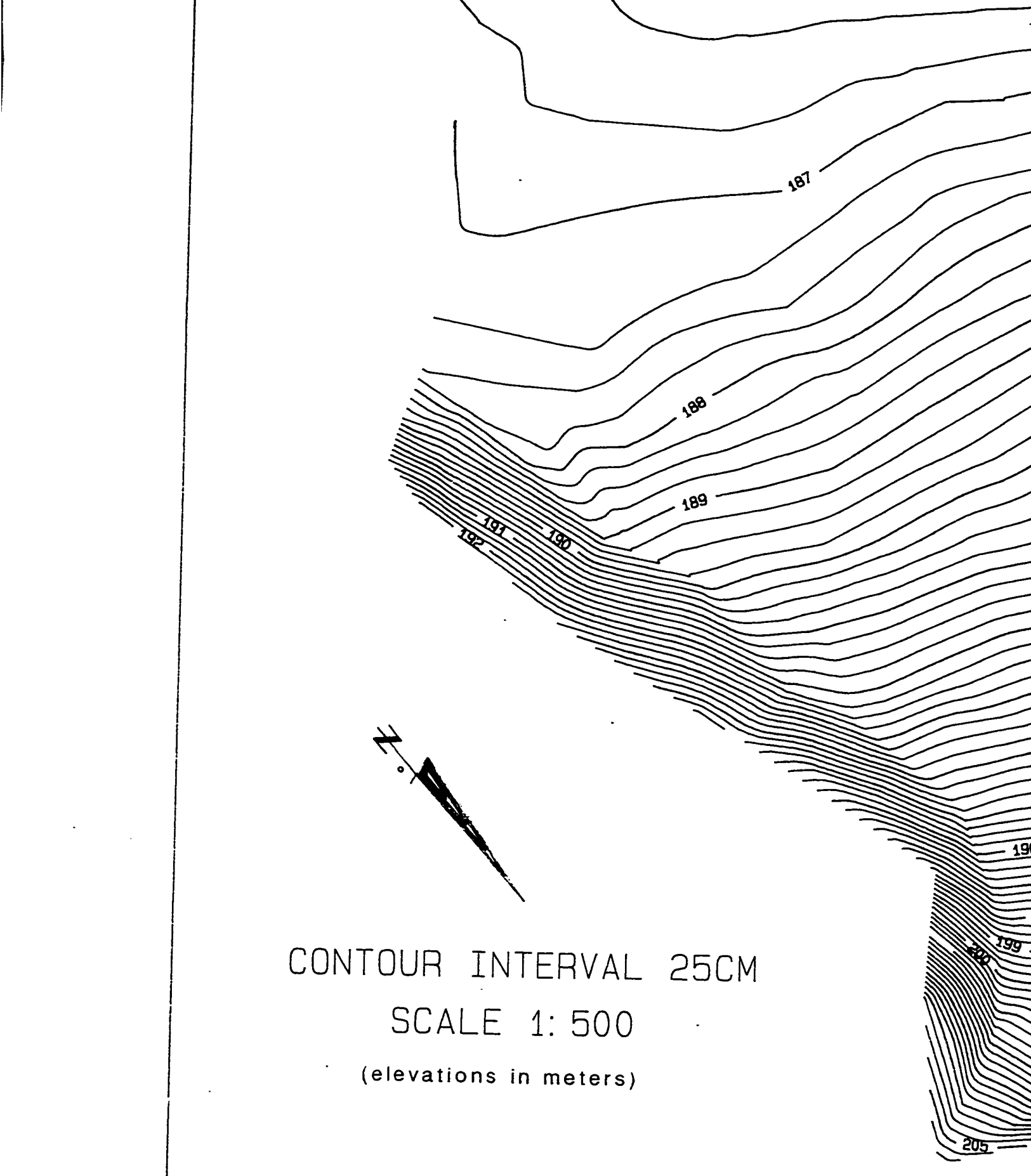

CONTOUR INTERVAL 25CM

SCALE 1: 500

(elevations in meters)

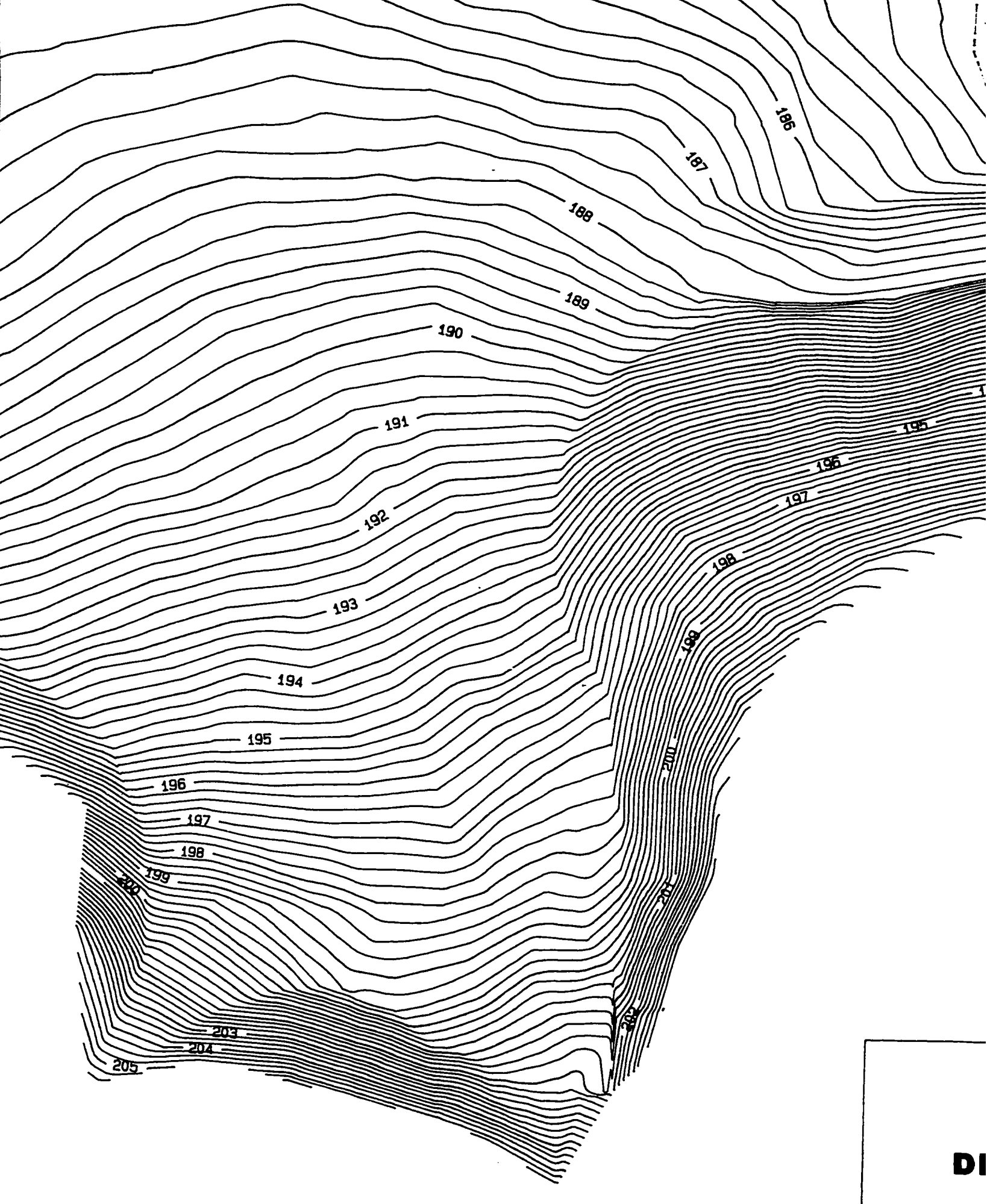
186
187
188
189
190
191
192
193
194
195
196
197
198
199
200
201
202
203
204
205

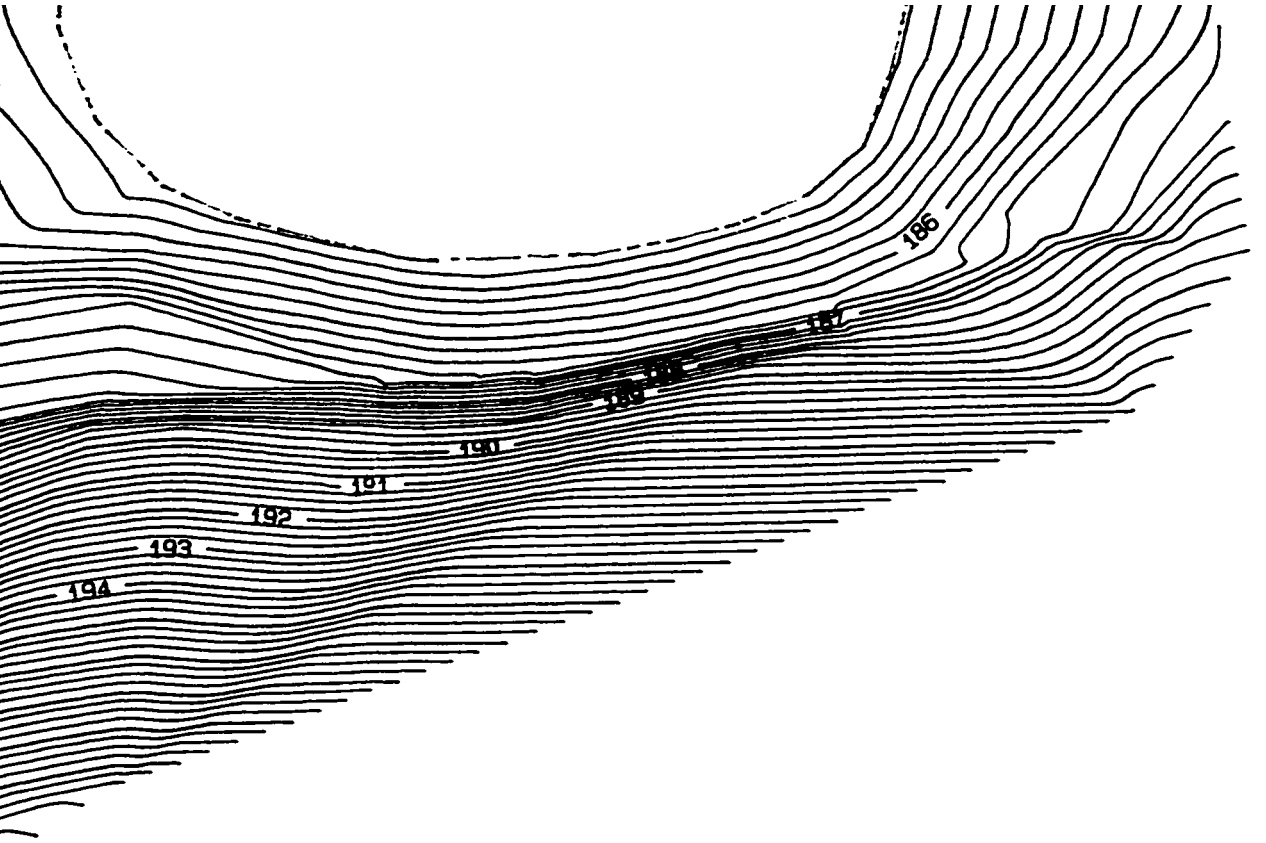

PLATE 1

DETAILED TOPOGRAPHIC MAP OF STUDY SITE

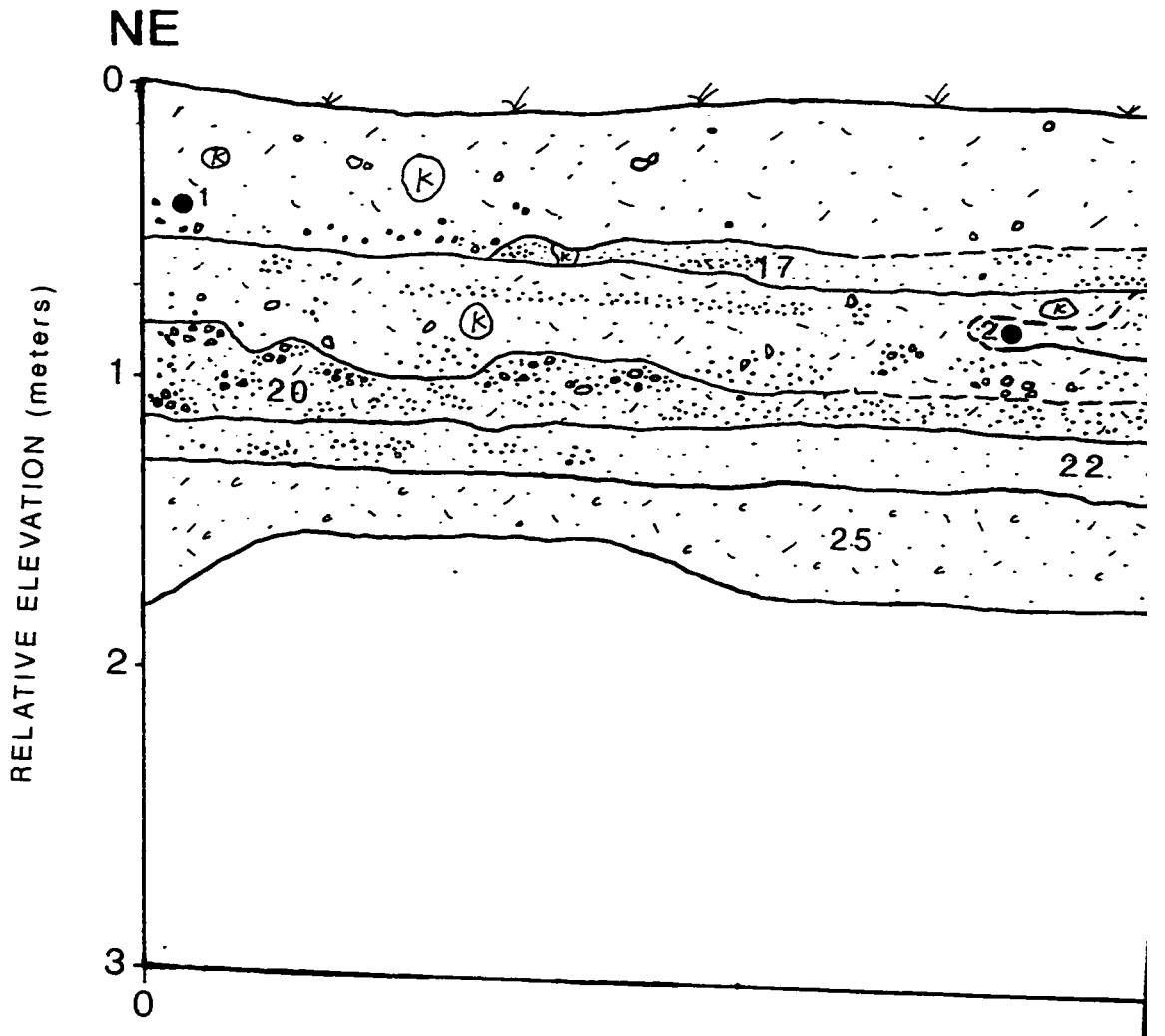
NE
0
1
2
3
0
RELATIVE ELEVATION (meters)
K
1
17
2
20
22
25

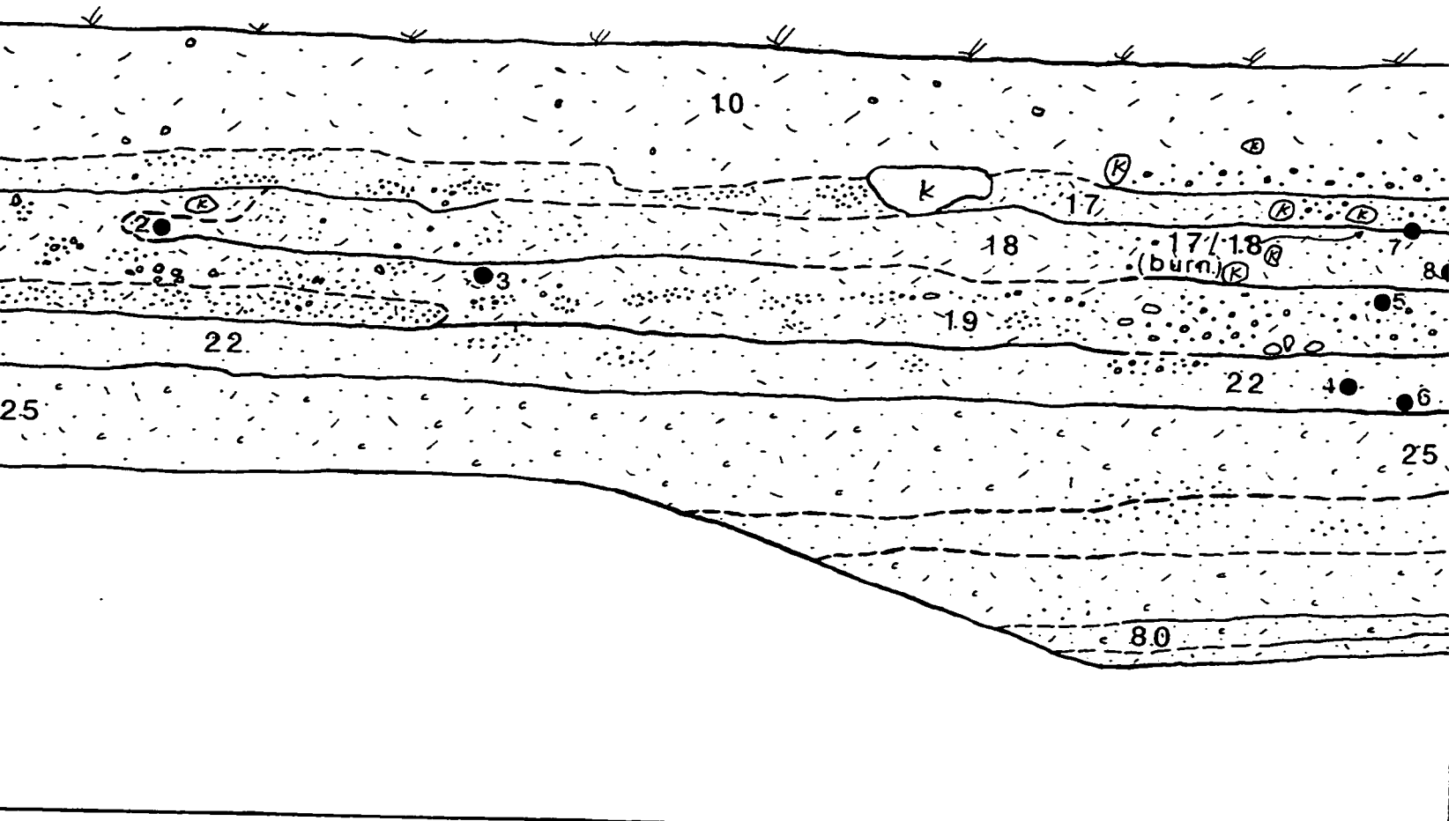

5

TRENCH 1
South Wall

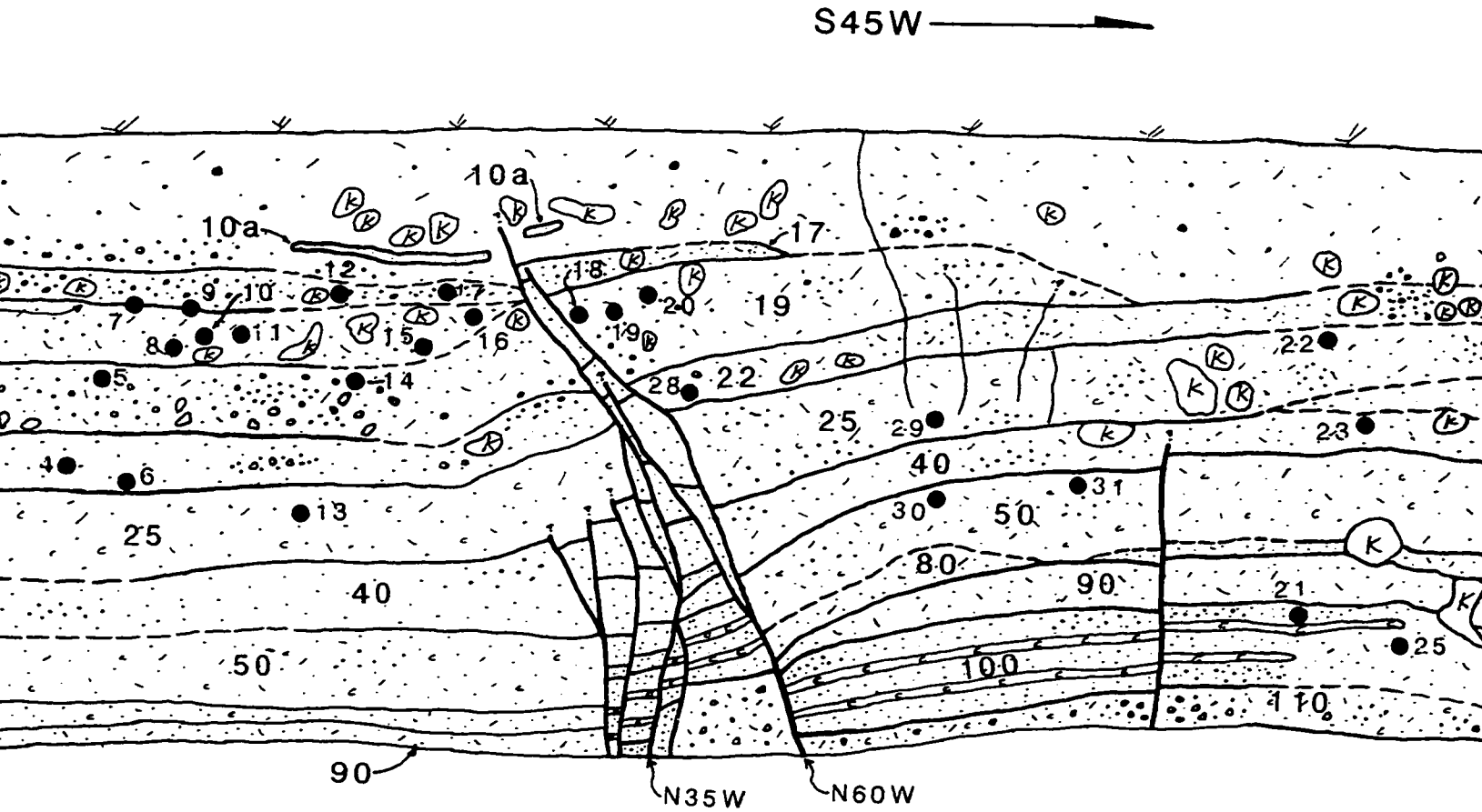

10

TRENCH 1
North Wall

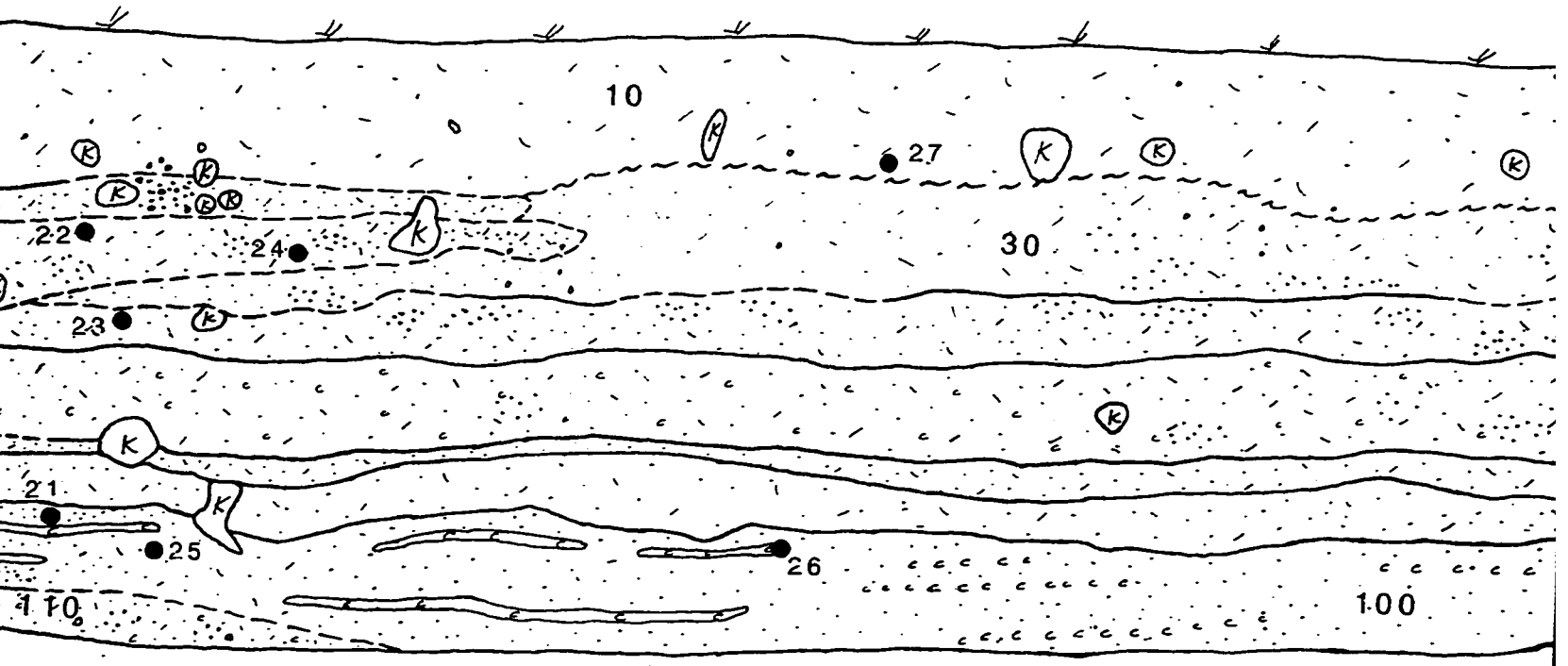

15

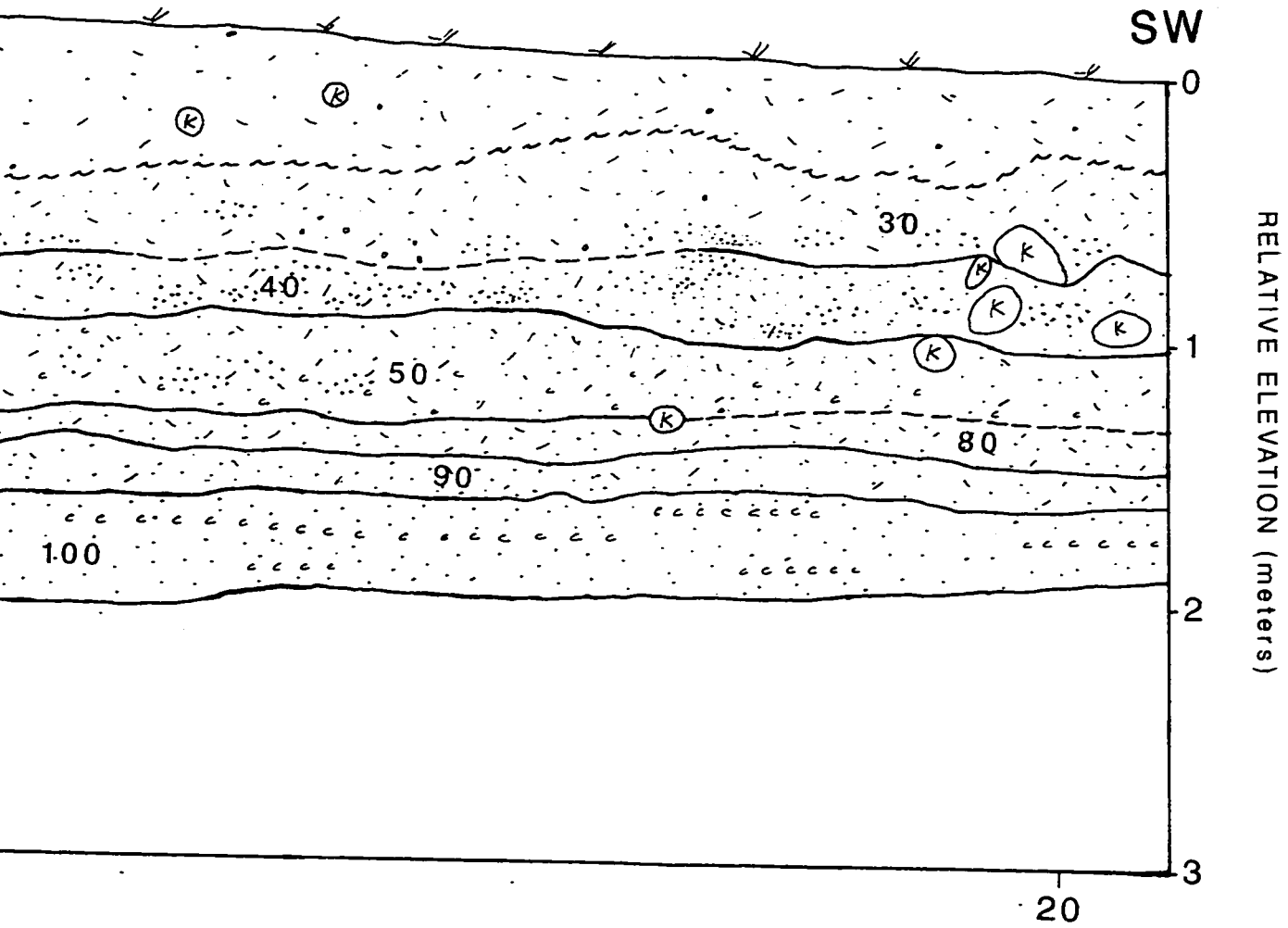
SW
0
1
2
3
20
RELATIVE ELEVATION (meters)
30
40
50
80
90
100
K

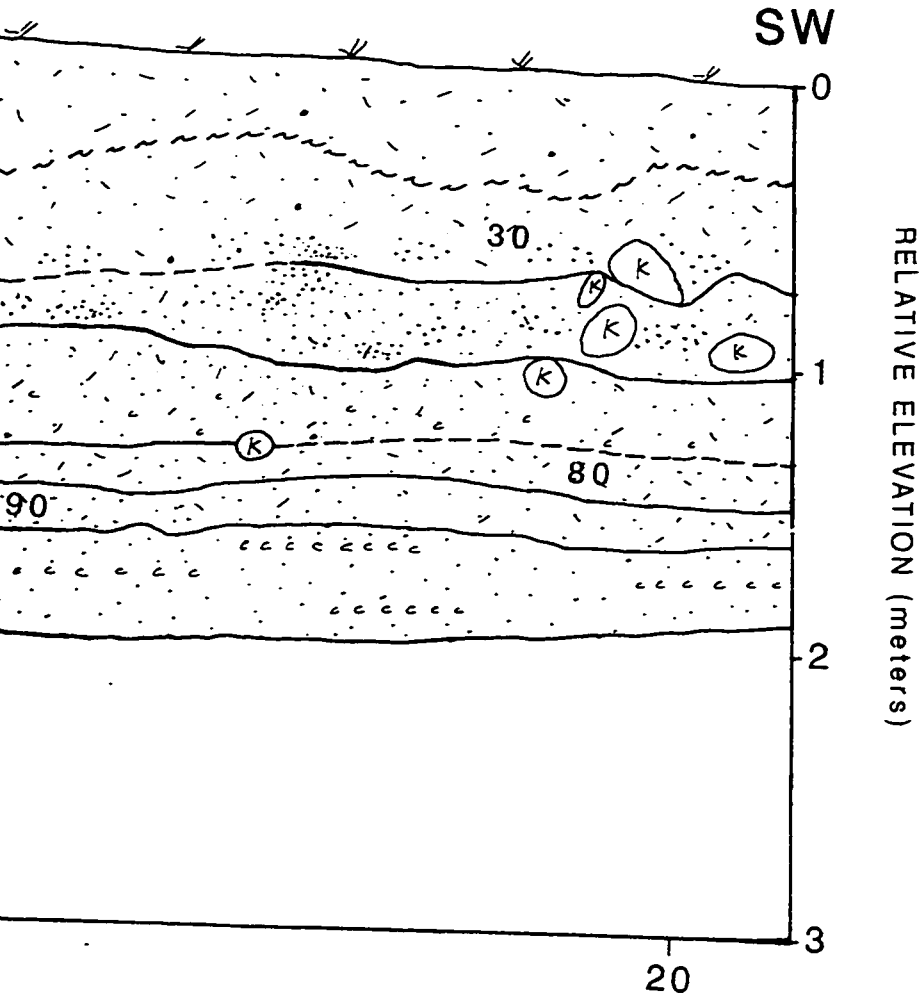
SW
0
1
2
3
30
80
90
K
20
RELATIVE ELEVATION (meters)

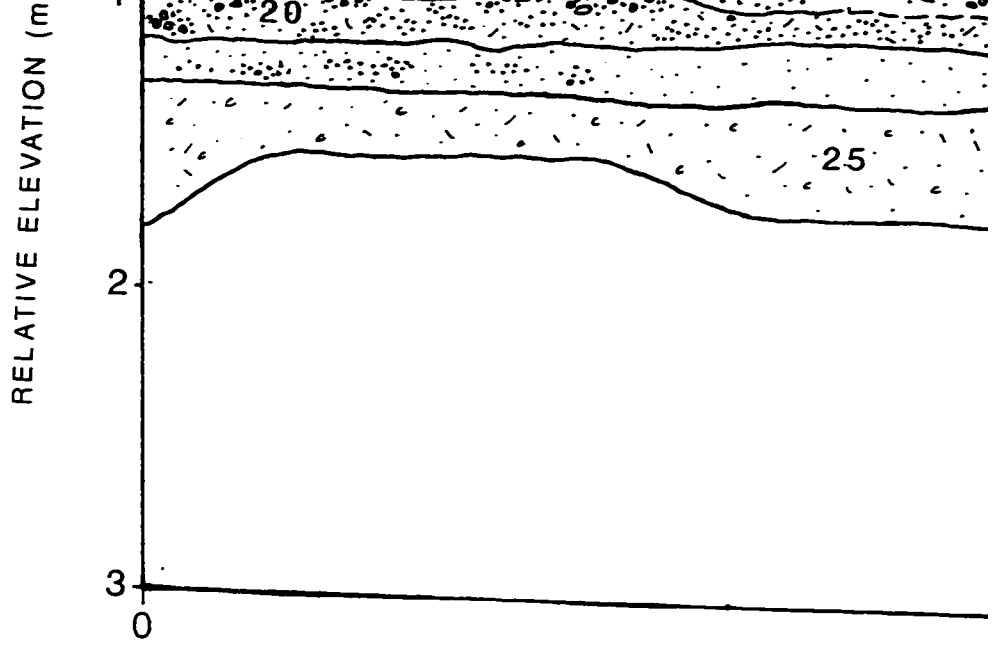
RELATIVE ELEVATION (m
20
25
2
3
0

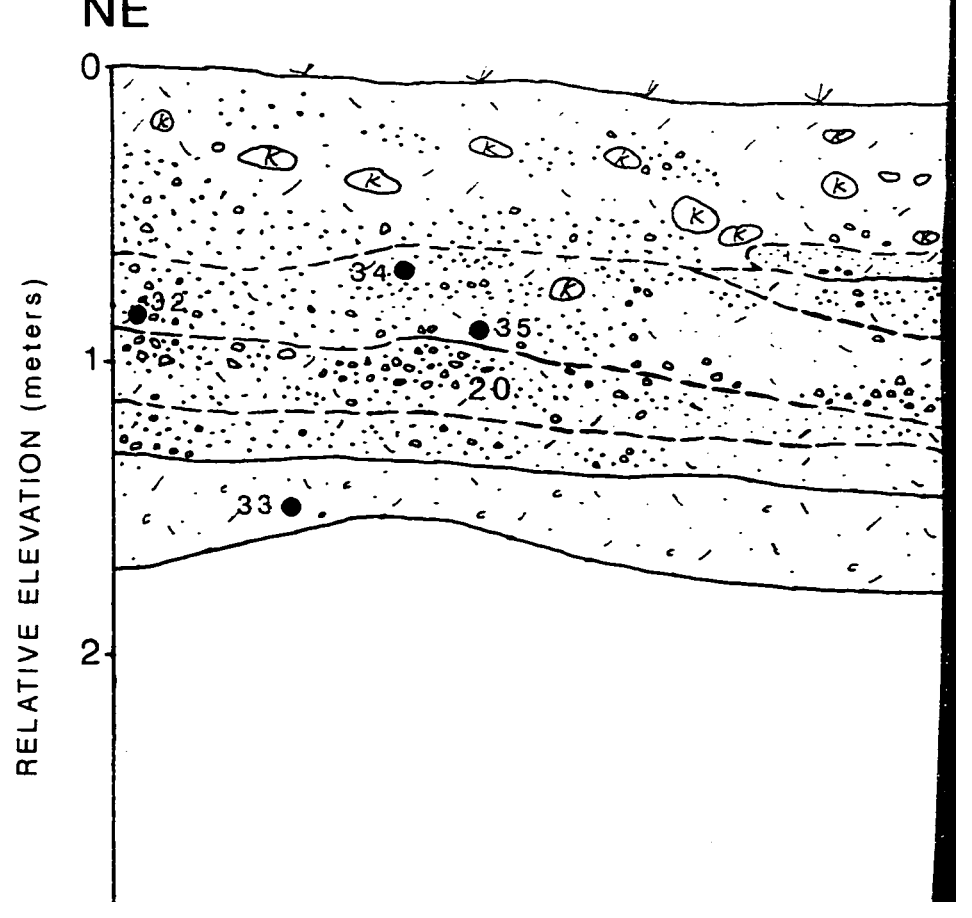
NE
0
RELATIVE ELEVATION (meters)
34
32
35
20
33
1
2

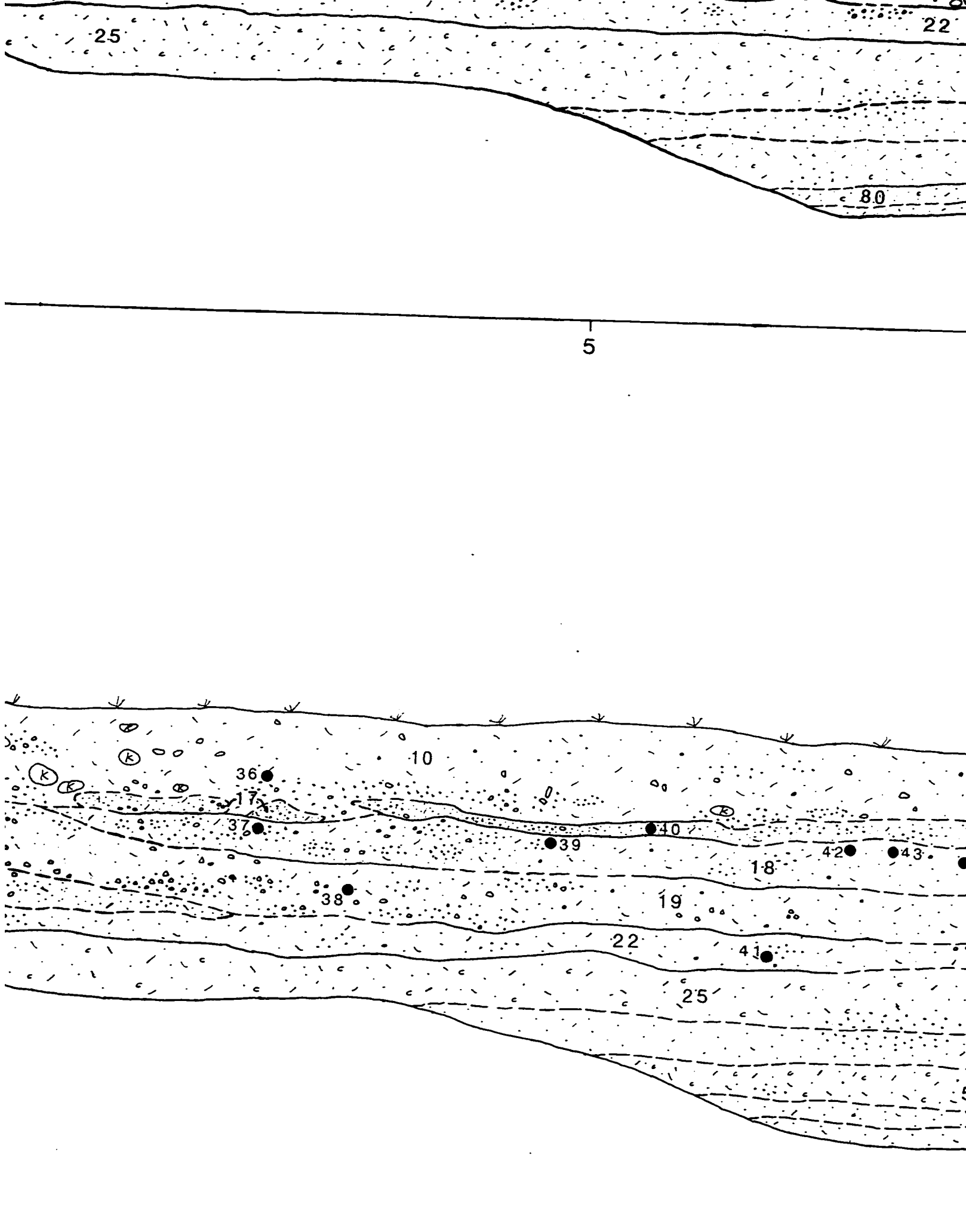
25
22
80
5
10
36
17
37
39
40
42
43
18
38
19
22
41
25

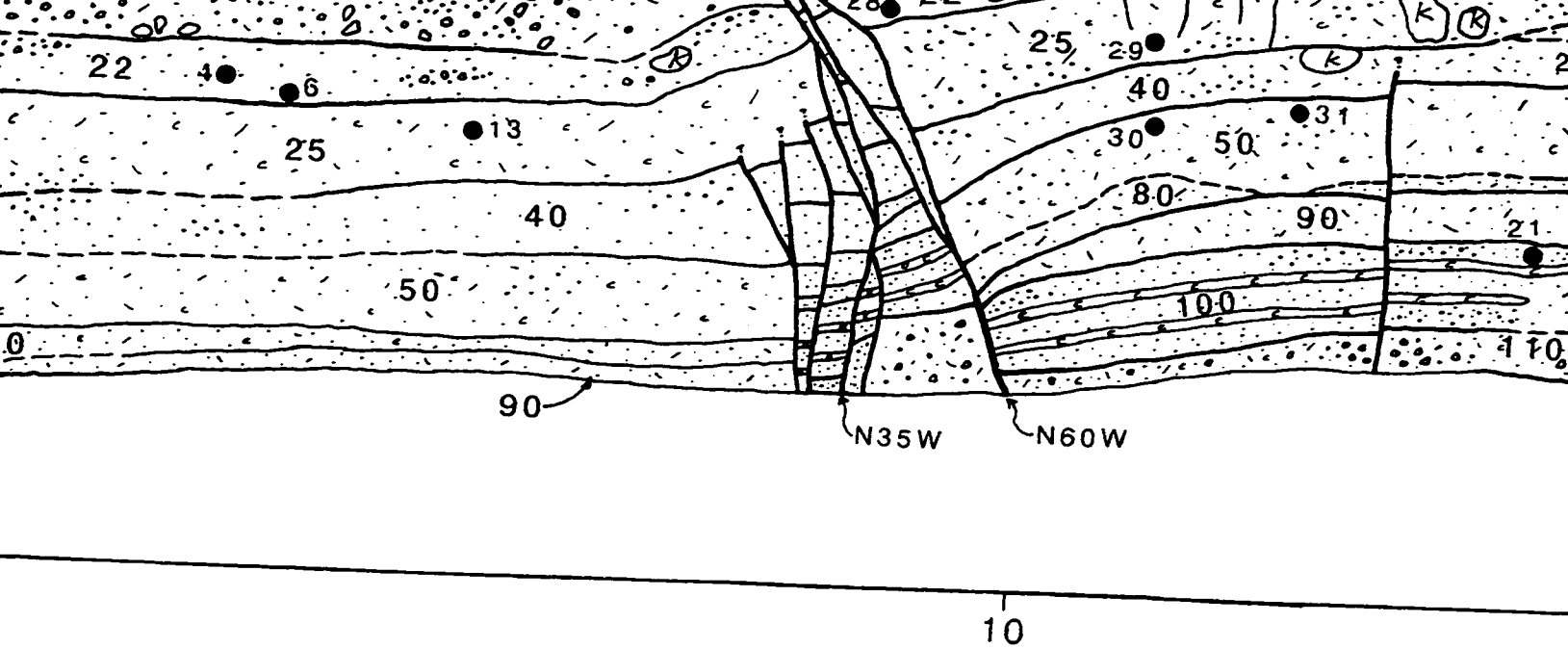

10

TRENCH 1
North Wall

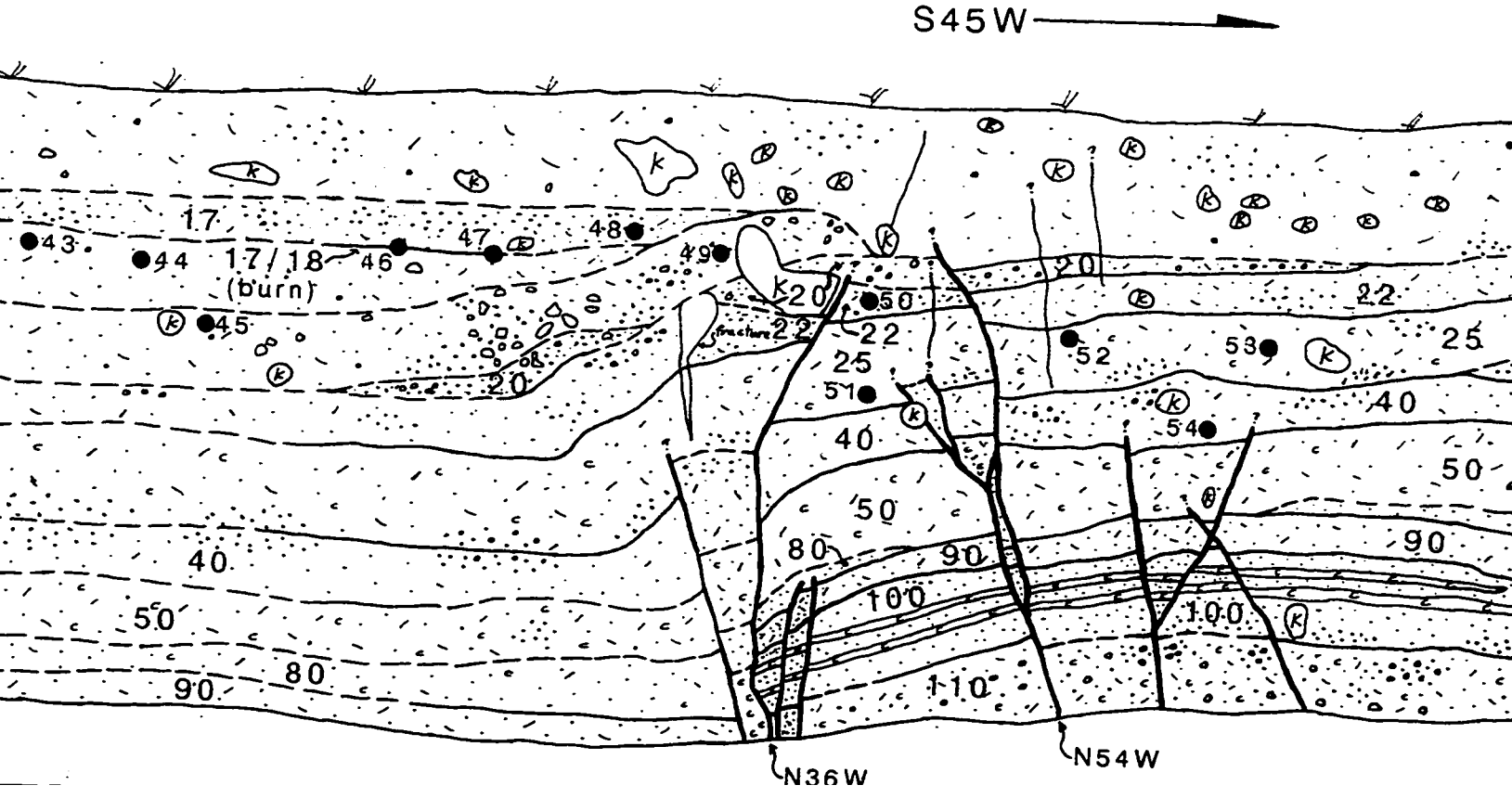

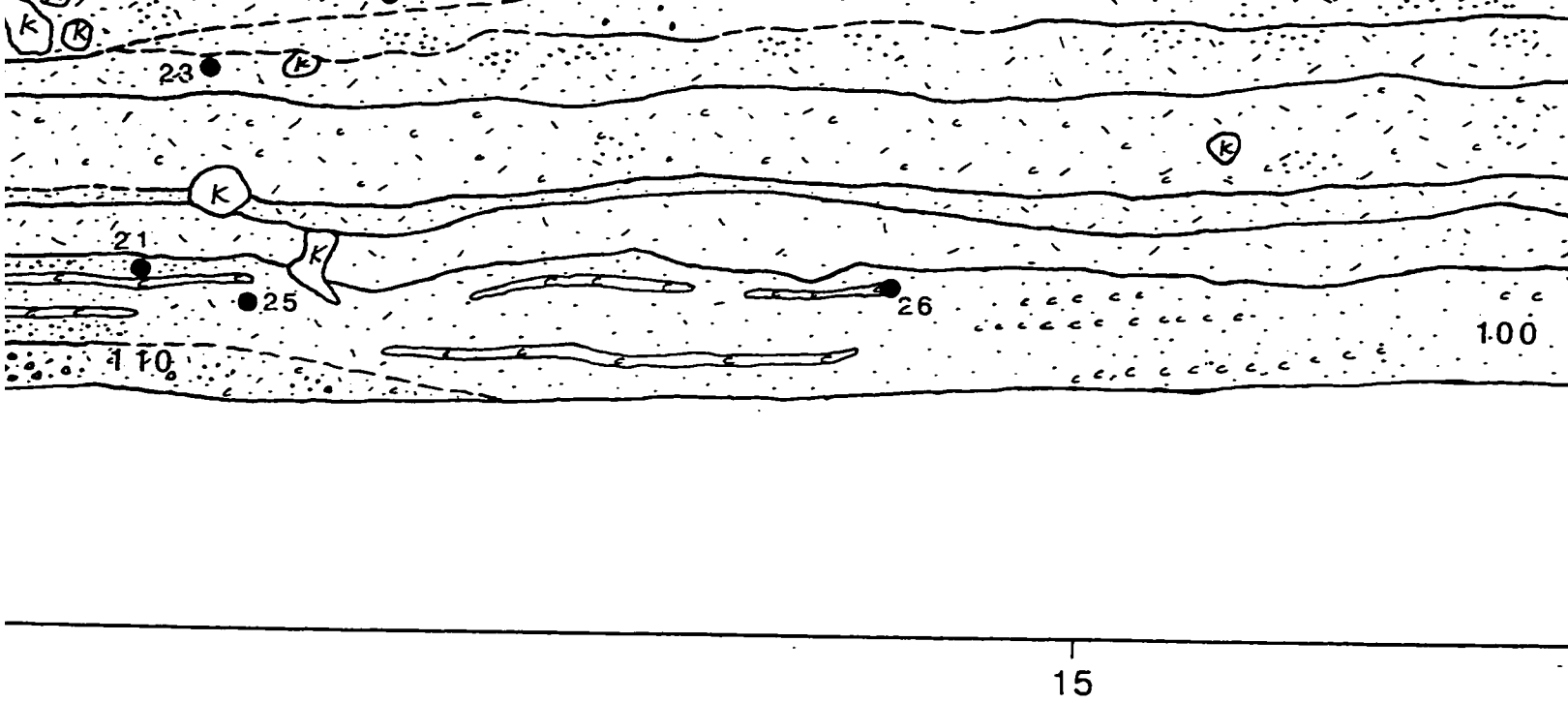

15

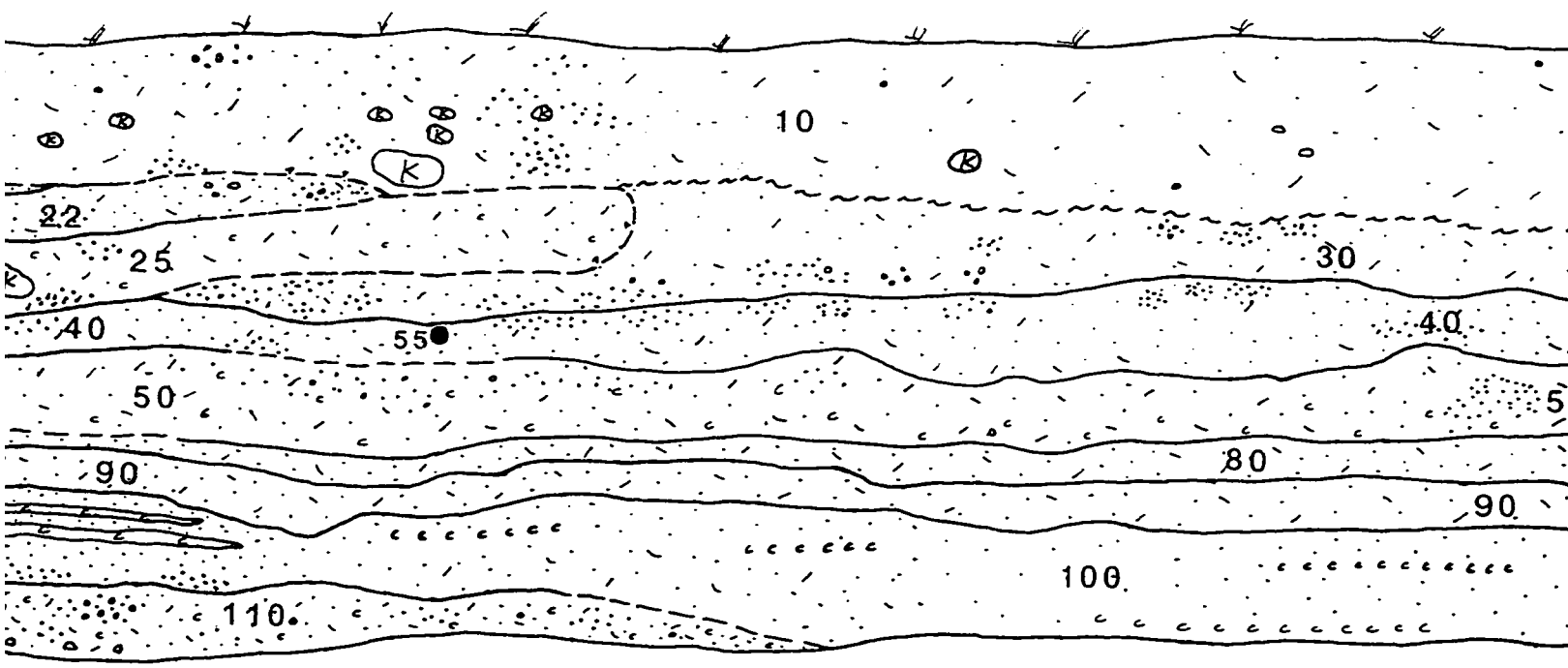

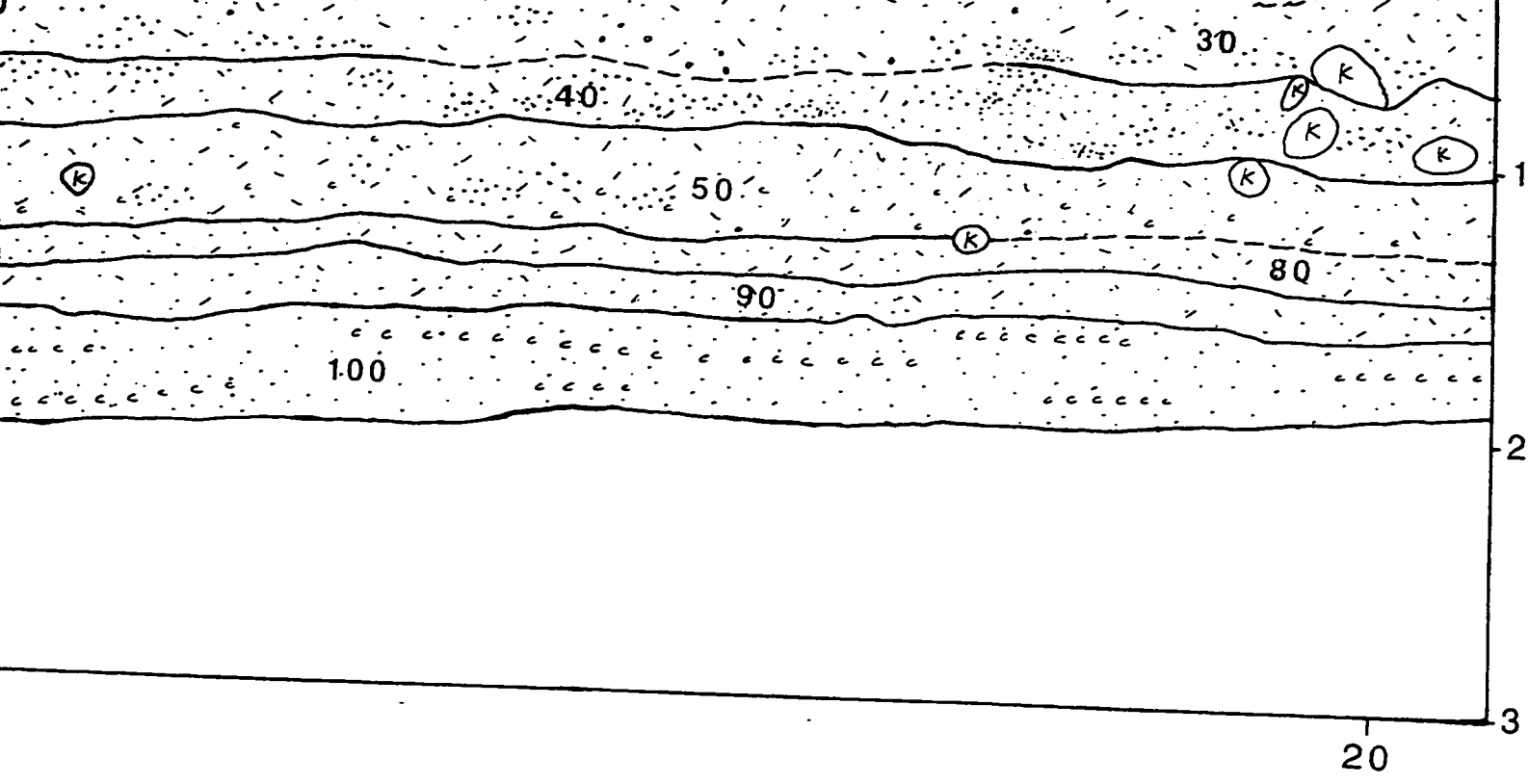
30
40
50
80
90
100
K
1
2
3
20

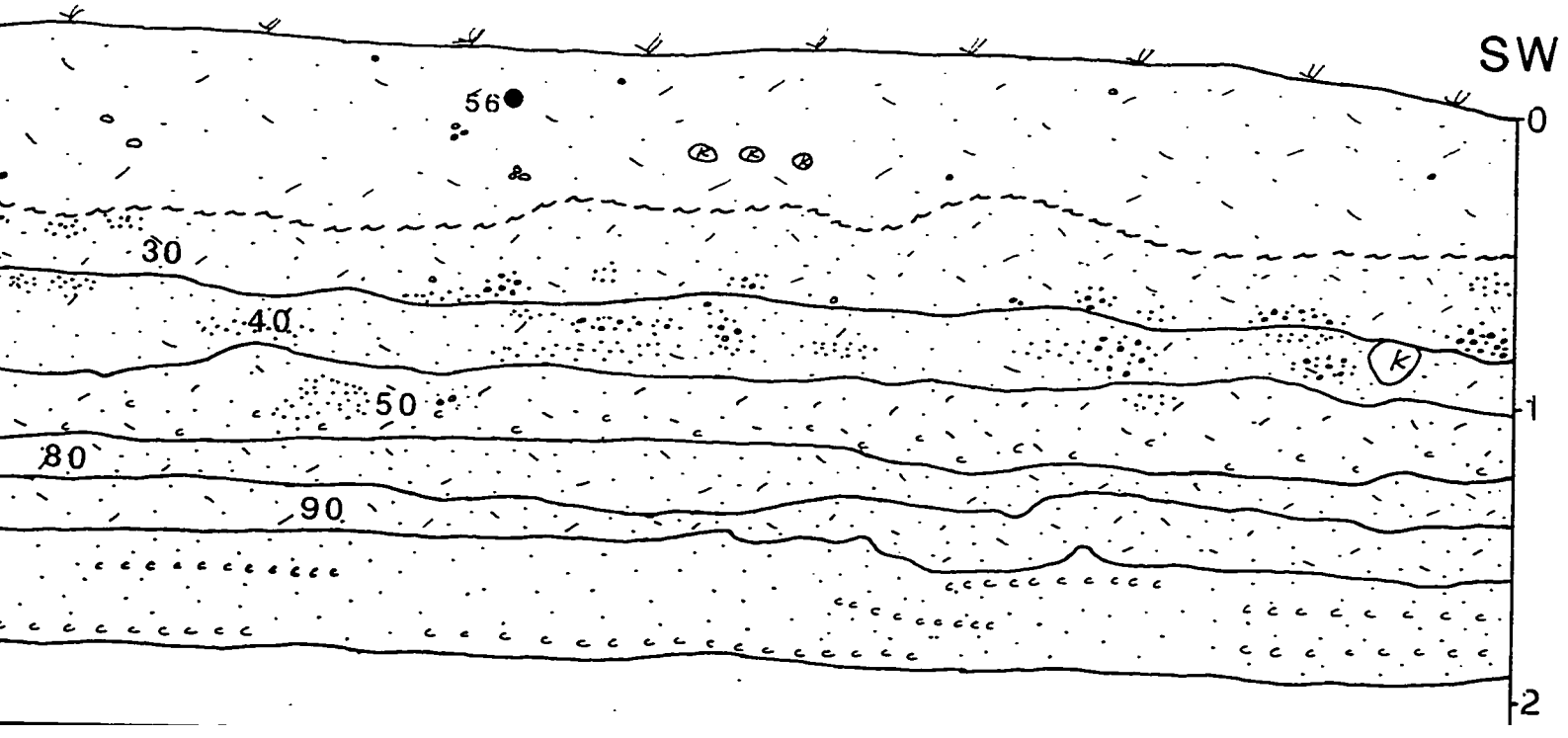
SW
56
30
40
50
80
90
K
0
1
2

RELATIVE ELEVATION (meters)

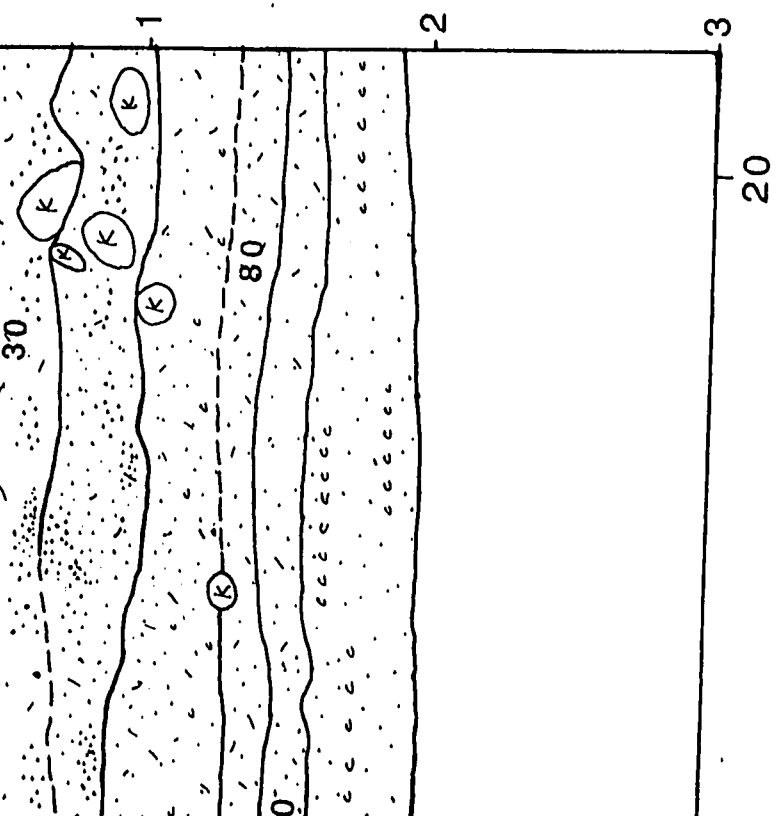

RELATIVE ELEVATION (mete

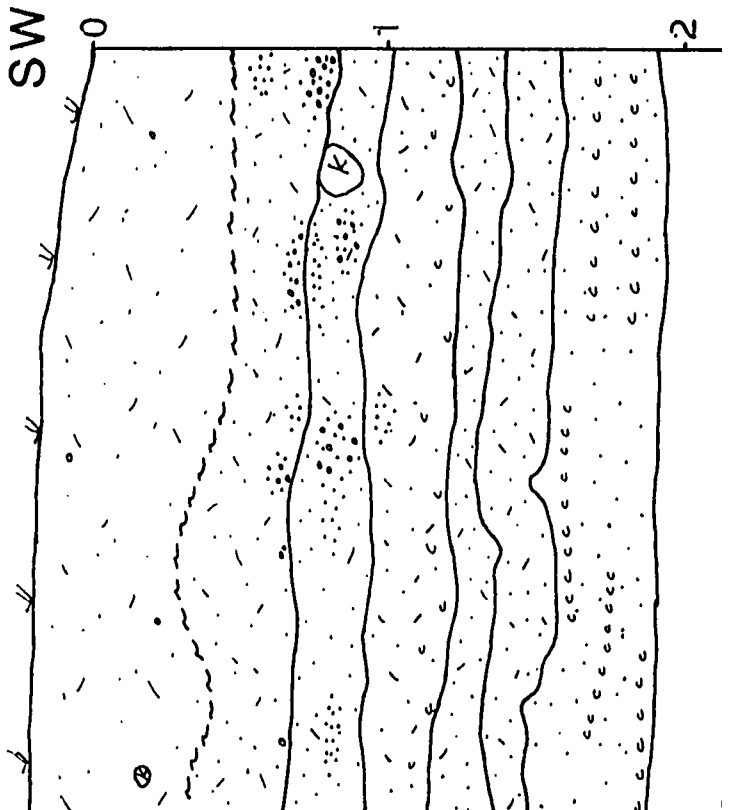

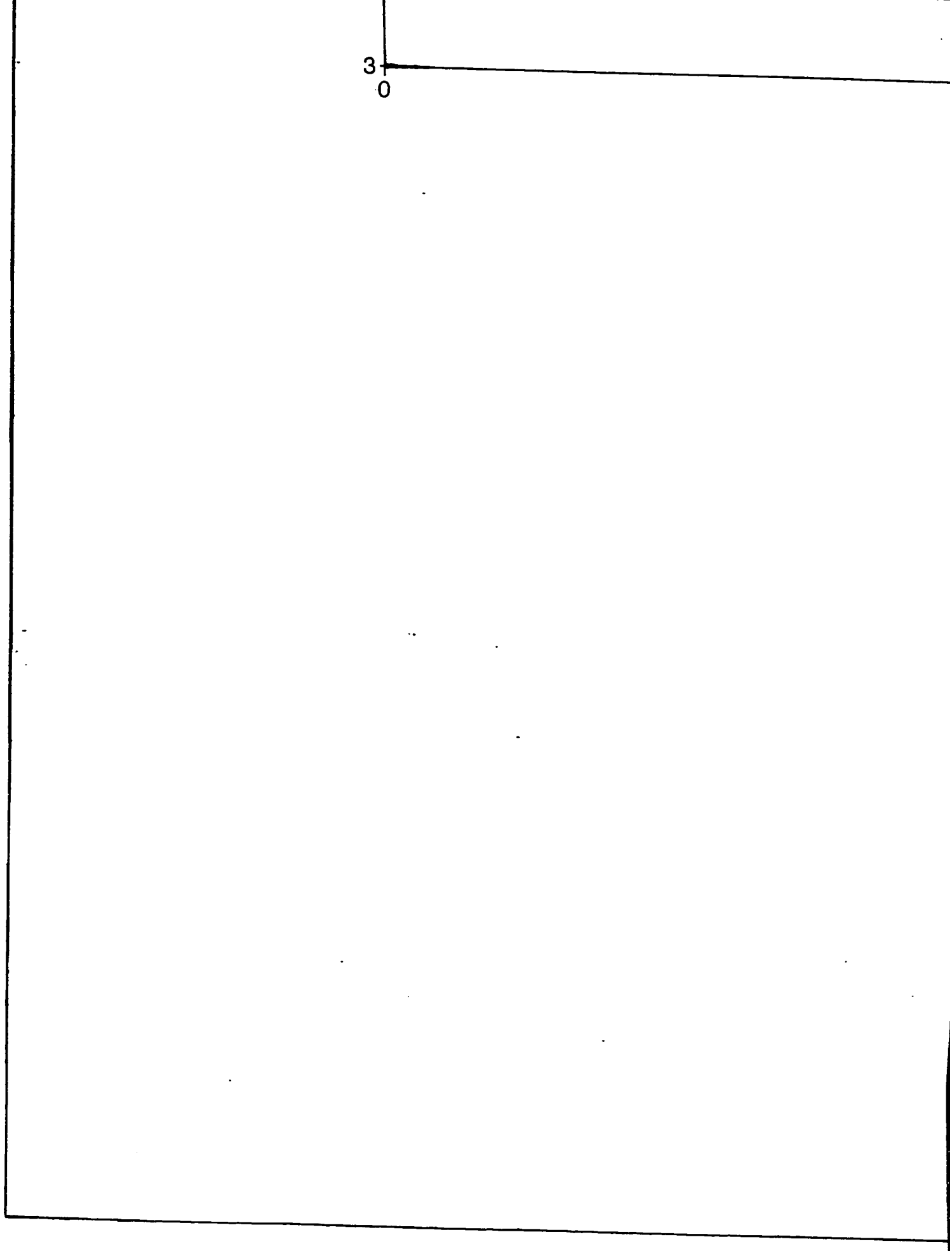
3
0

RADIOCARBON SAMPLE IDENTIFICATION KEY

1 = T1-95-23BS-10a
2 = T1-95-19CS-18a
3 = T1-95-17BS-19a
4 = T1-96-14CS-22a
5 = T1-95-14BS-19a
6 = T1-96-14CS-22b
7 = T1-96-14BS-17/18a
8 = T1-95-14BS-18b
9 = T1-96-14BS-17/18b
10 = T1-95-14BS-18a
11 = T1-96-14BS-18
12 = T1-95-13BS-17a
13 = T1-96-13DS-25
14 = T1-95-13BS-19b
15 = T1-96-13BS-18b
16 = T1-95-13BS-18
17 = T1-95-13BS-17b
18 = T1-96-12BS-19a
19 = T1-95-12BS-19
20 = T1-96-12BS-19b
21 = T1-95-10CS-100
22 = T1-95-10BS-25
23 = T1-95-10CS-40
24 = T1-95-9BS-25
25 = T1-95-10DS-100
26 = T1-95-7CS-100a
27 = T1-95-7AS-10
28 = T1-95-12CS-22
29 = T1-95-11CS-25
30 = T1-95-11CS-50
31 = T1-95-11CS-50c
32 = T1-95-22B-19a
33 = T1-95-21DN-25a
34 = T1-95-21CN-19a
35 = T1-95-20CN-19a
36 = T1-95-18AN-10a
37 = T1-95-18BN-18a
38 = T1-95-18BN-19a
39 =
40 =
41 =
42 =
43 =
44 =
45 =
46 =
47 =
48 =
49 =
50 =
51 =
52 =
53 =
54 =
55 =
56 =

CATION KEY

39 = T1-95-17BN-18a
40 = T1-95-16BN-17a
41 = T1-95-16CN-22a
42 = T1-95-15BN-18a
43 = T1-96-15BN-18b
44 = T1-96-15BN-18a
45 = T1-95-14BN-19a
46 = T1-96-14BN-17/18
47 = T1-96-13BN-17/18
48 = T1-96-13BN-17a
49 = T1-95-13BN-19
50 = T1-95-12BN-22a
51 = T1-95-12CN-25
52 = T1-95-11BN-25a
53 = T1-95-11CN-25
54 = T1-95-11CN-40
55 = T1-95-9CN-40a
56 = T1-95-5AN-10

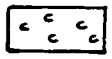
Clay

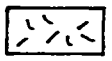
Silt

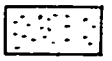
Fine sand


Medium to co


Fine gravel

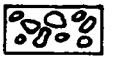
Medium to co

40 Stratigraphic u
in Appendix A

NOTES

1. Ground surface and g
2. Not all symbols may b
3. Elevations are relative
4. Horizontal distance is
5. See Figure 9 for tre
6. See Appendix C for a

EXPLANATION OF TRENCH LOGS

Clay

Silt

Fine sand

Medium to coarse sand and granules

Fine gravel

Medium to coarse gravel

Stratigraphic unit (descriptions in Appendix A)

———?Contact: dashed where approximate; queried where uncertain

~ ~ ~ Gradational soil contact

———? Shear: dashed where approximate; queried where uncertain

———?Fracture; little to no vertical offset: dashed where aproximate; queried where uncertain

● Radiocarbon sample location

15 Radiocarbon sample number

N30W Strike of prominent shear

(K) Krotovina

nd surface and geologic contacts are based on tape and level measurements.
all symbols may be present on all trench logs.
ations are relative to ground surface only.
ontal distance is in meters.
Figure 9 for trench location.
Appendix C for ages of radiocarbon samples.

3

20

nate;

te;

fset:

Additional notes

See Figure 18 for detailed log of south wall fault zone exposure.

PL

LOG OF

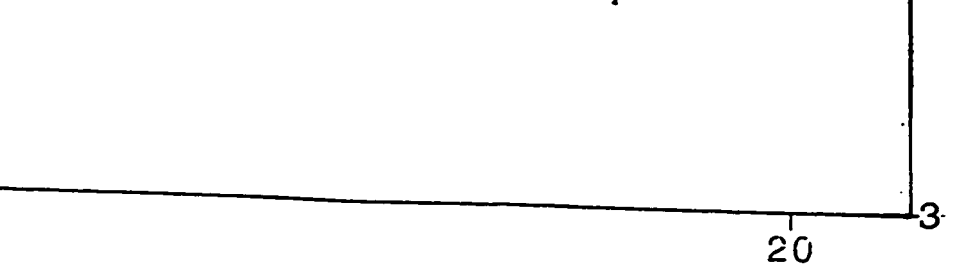

Additional notes

detailed log of south wall fault zone exposure.

PLATE 2

LOG OF TRENCH 1

PLEASE NOTE:

Oversize maps and charts are filmed in sections in the following manner:

LEFT TO RIGHT, TOP TO BOTTOM, WITH SMALL OVERLAPS

The following map or chart has been refilmed in its entirety at the end of this dissertation (not available on microfiche). A xerographic reproduction has been provided for paper copies and is inserted into the inside of the back cover.

Black and white photographic prints (17" x 23") are available for an additional charge.

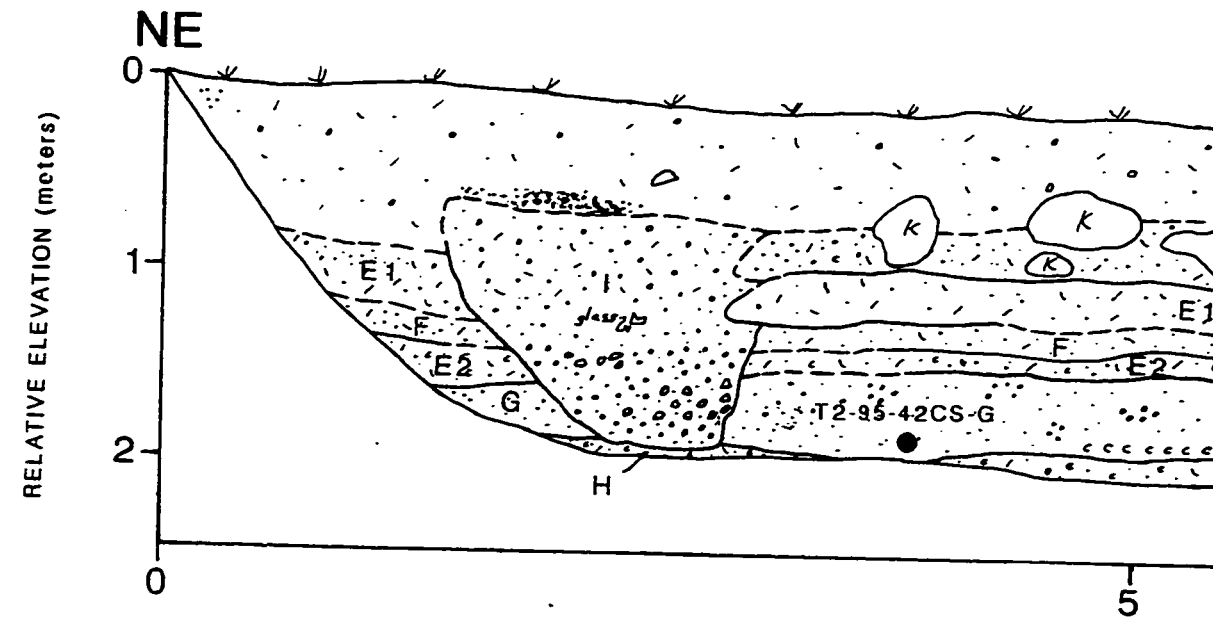
NE
RELATIVE ELEVATION (meters)
0
1
2
0
5
E1
F
E2
G
H
K
T2-95-42CS-G

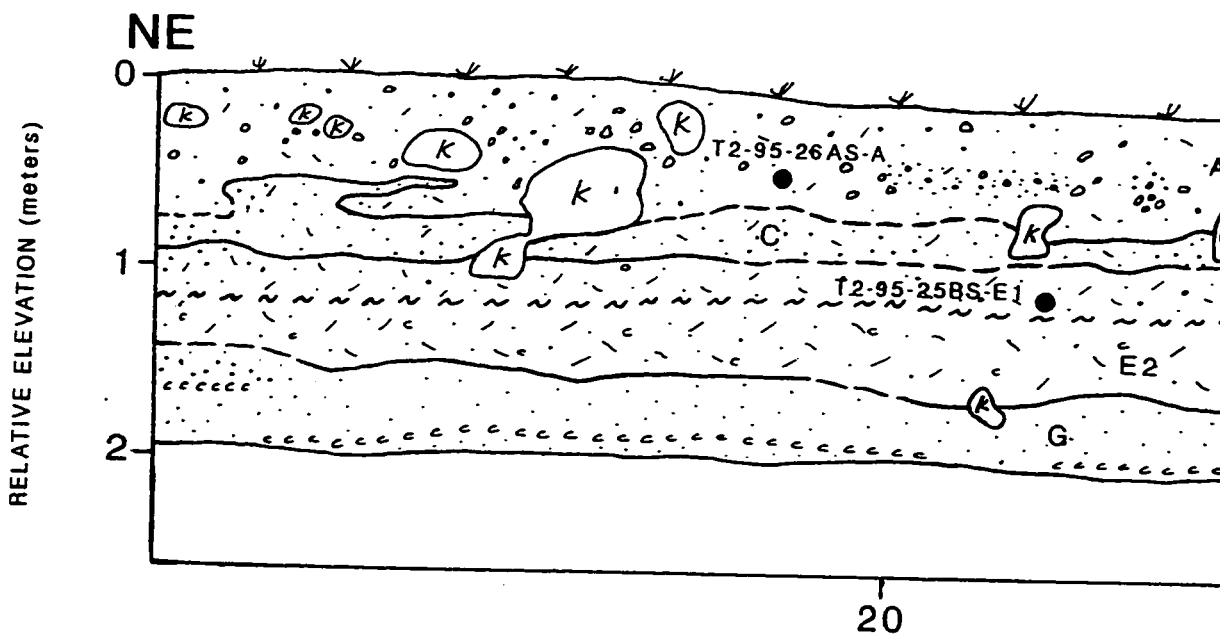
NE
RELATIVE ELEVATION (meters)
0
1
2
20
K
k
T2-95-26AS-A
C
T2-95-25BS-E1
E2
G

TRENCH 2
South Wall

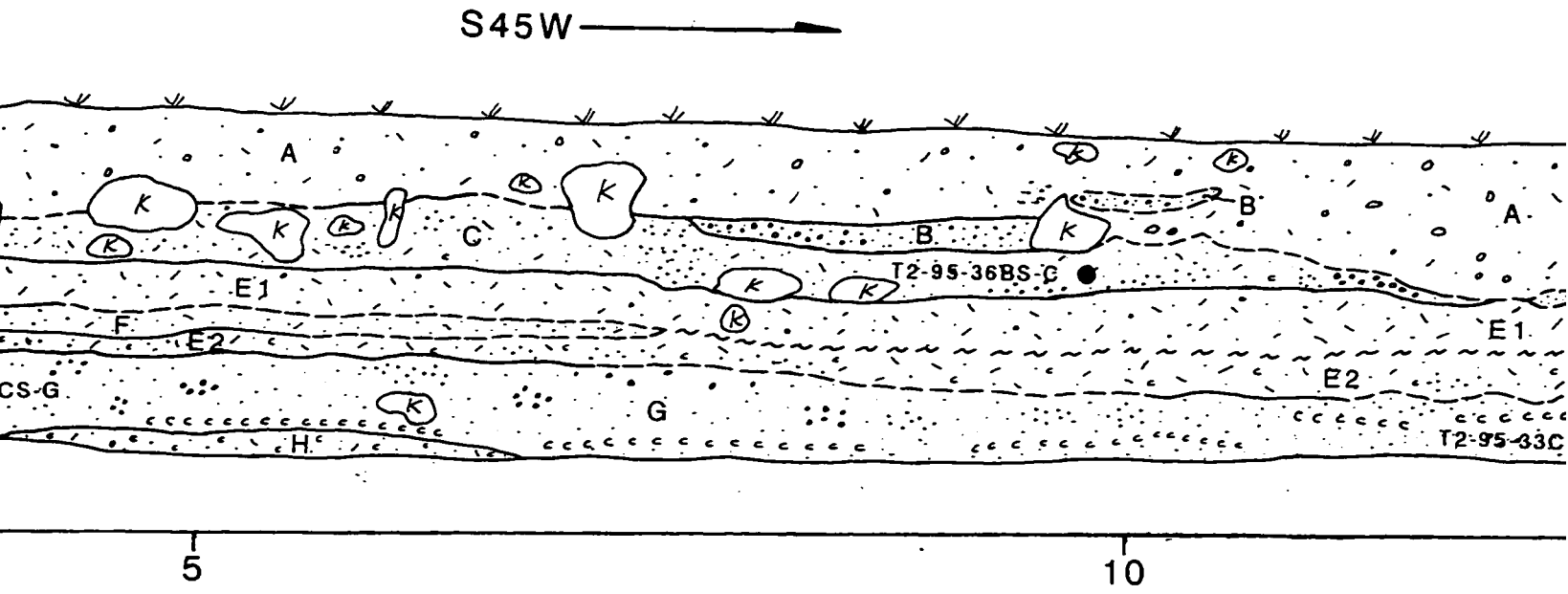

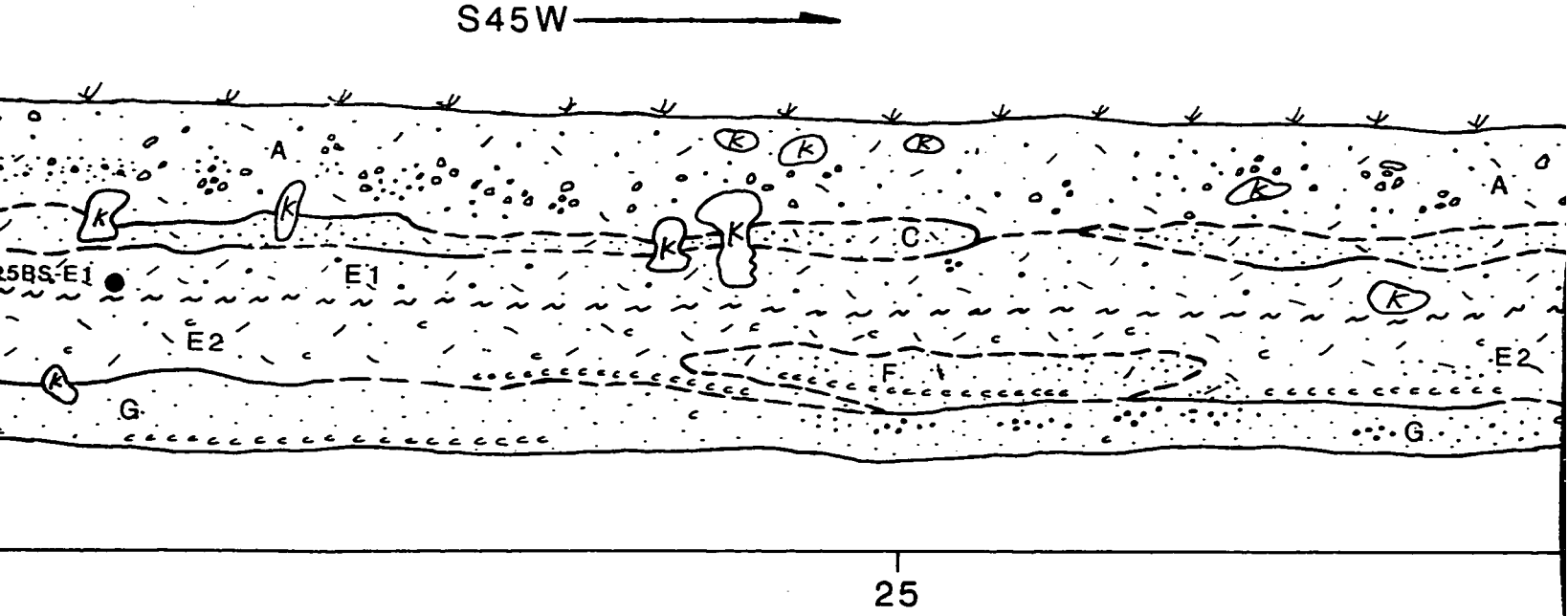

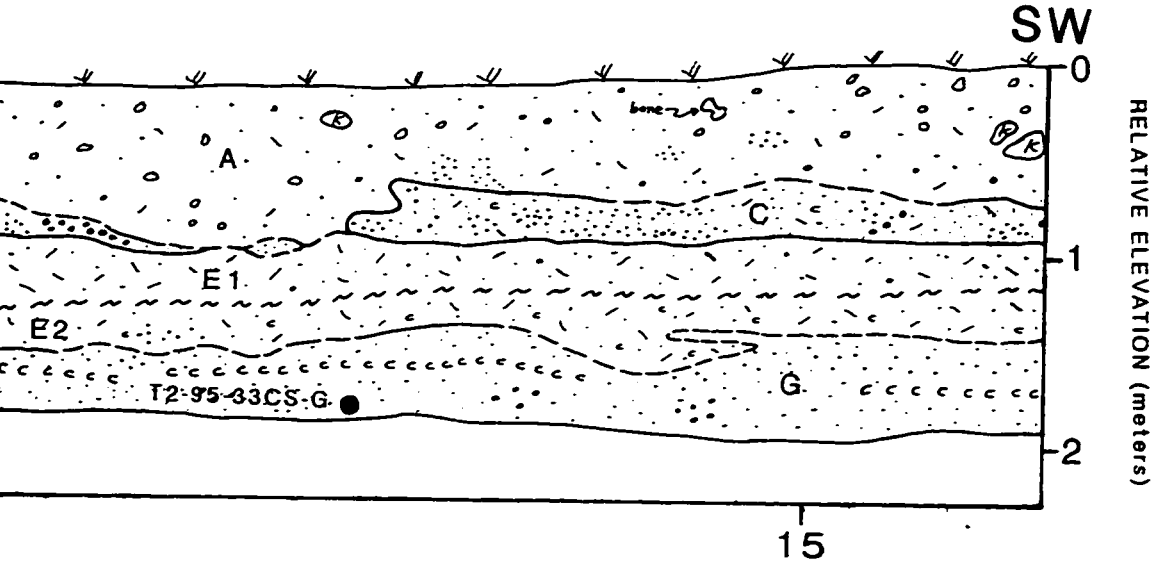
SW
0
1
2
A
C
E1
E2
G
T2-95-33CS-G
15
RELATIVE ELEVATION (meters)

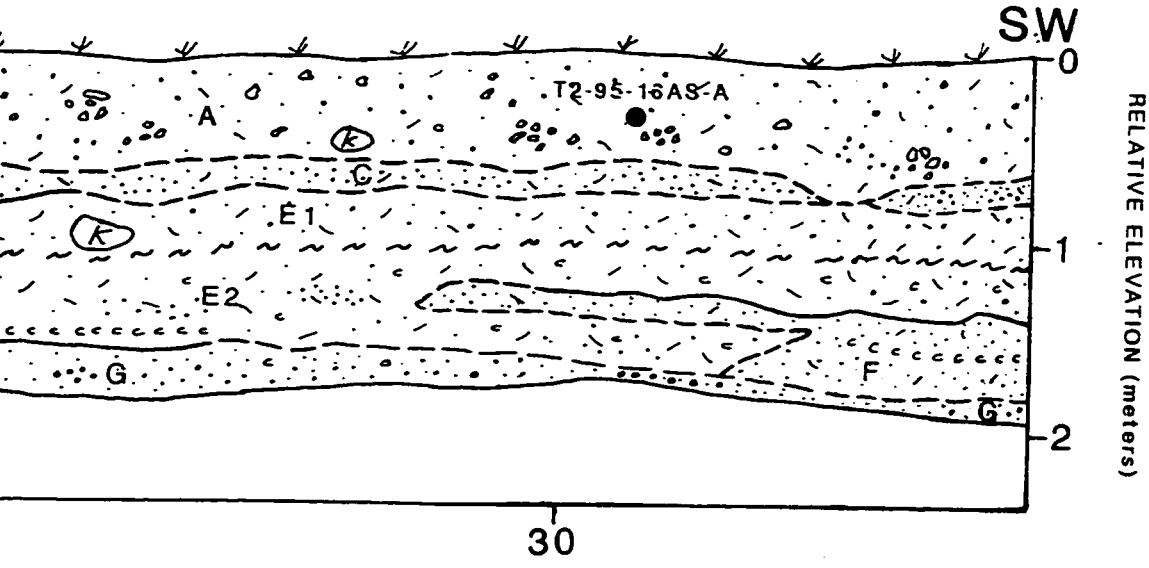
SW
0
1
2
T2-95-16AS-A
A
C
E1
E2
G
F
30
RELATIVE ELEVATION (meters)

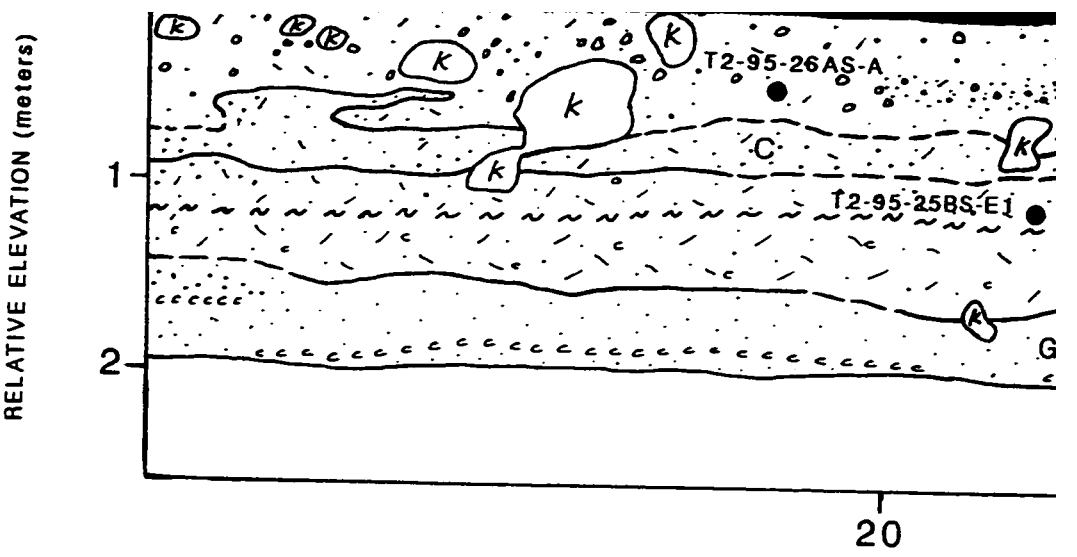
RELATIVE ELEVATION (meters)
1
2
T2-95-26AS-A
T2-95-25BS-E1
C
G
20

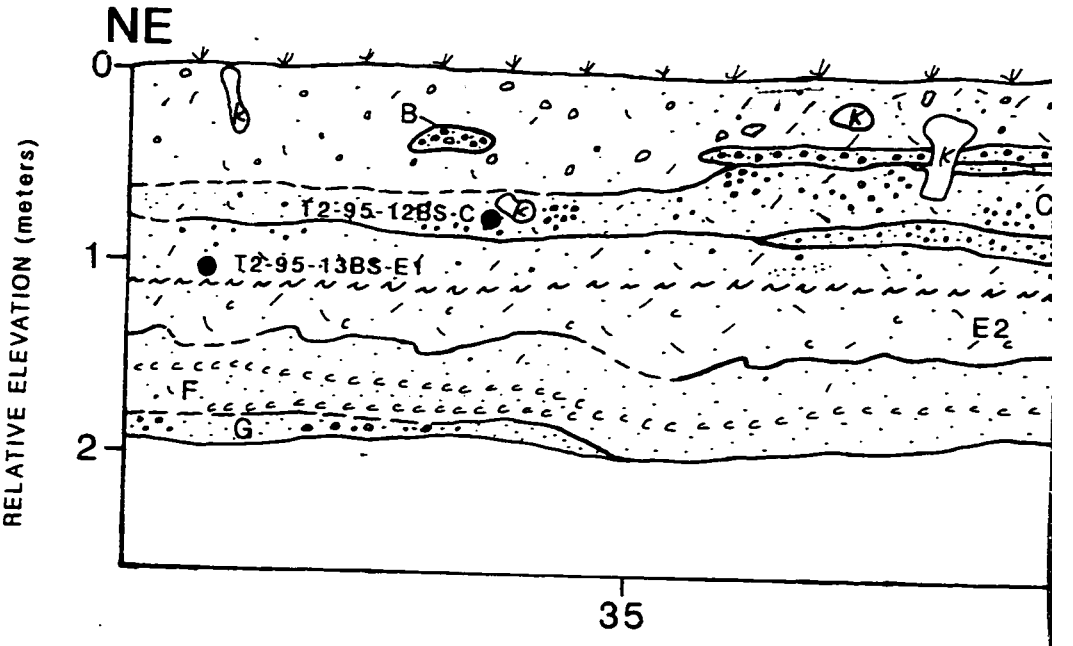
NE
0
1
2
RELATIVE ELEVATION (meters)
B
T2-95-12BS-C
T2-95-13BS-E1
E2
F
G
35

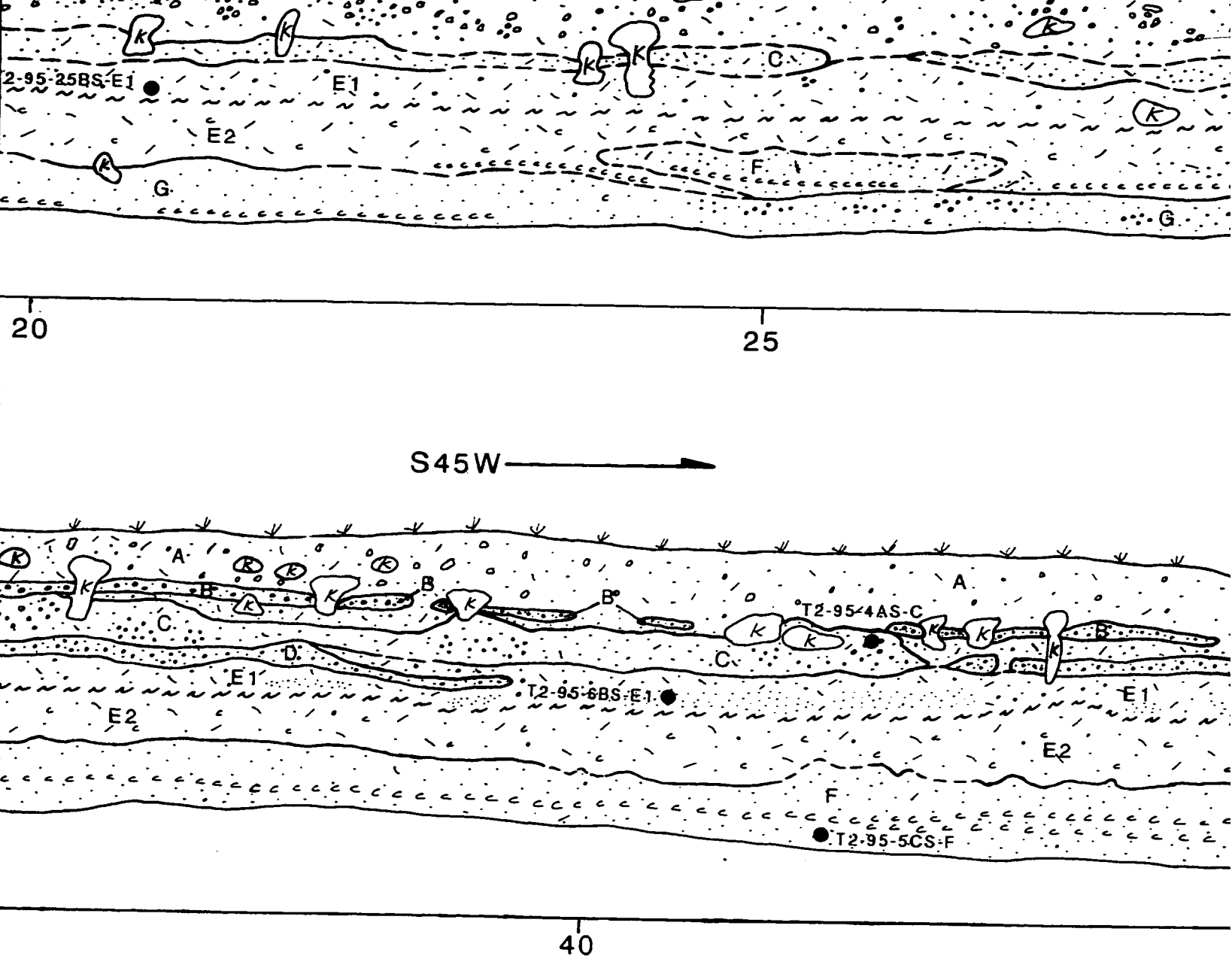

EXPLANATION OF TRENCH LOGS

- Clay
- Silt
- Fine sand
- Medium to coarse sand and granules
- Fine gravel
- Medium to coarse gravel

- Contact: dashed where approximate; queried where uncertain
- Gradational soil contact
- Shear: dashed where approximate; queried where uncertain
- Fracture; little to no vertical offset: dashed where aproximate; queried where uncertain
- Radiocarbon sample location

LATIVE ELEVATION (meters)

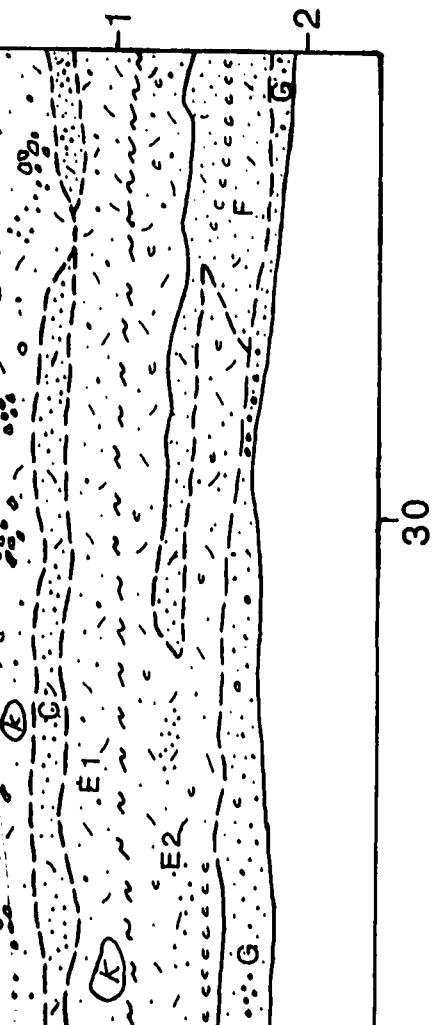

RELATIVE ELEVATION (meters)

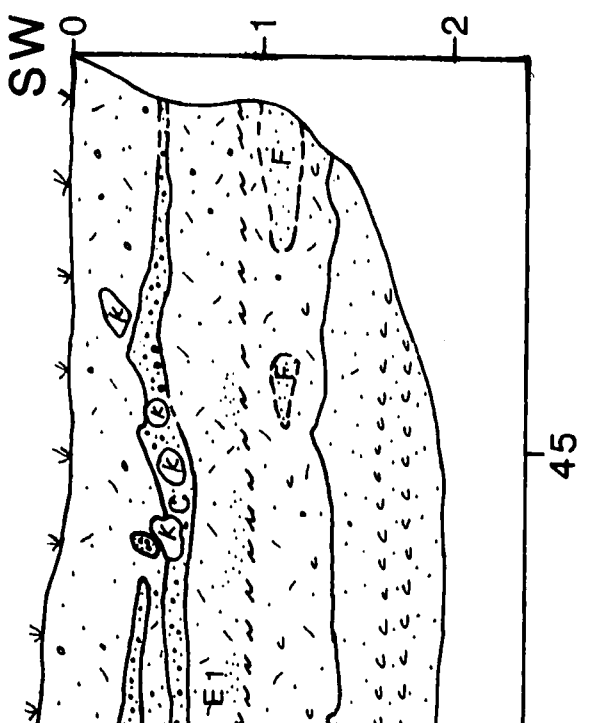

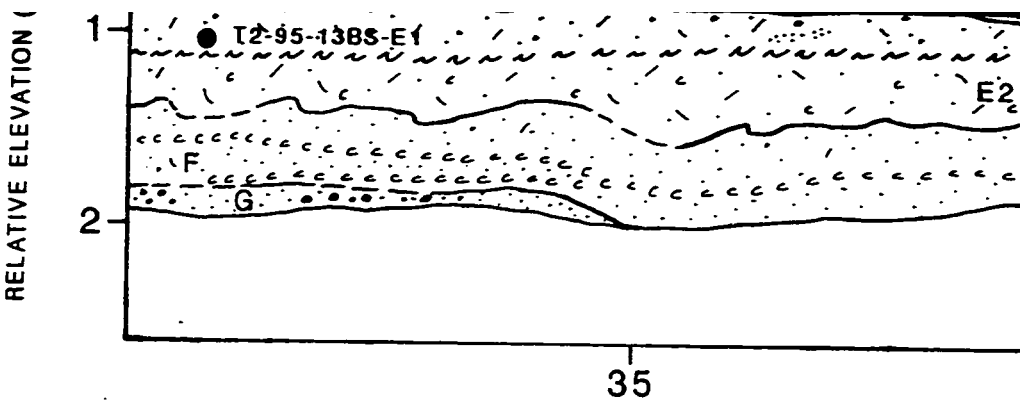

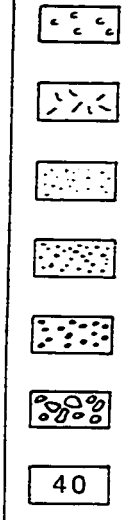

NOTES

1. Ground
2. Not all
3. Elevati
4. Horizo
5. See Fi
6. See Ap

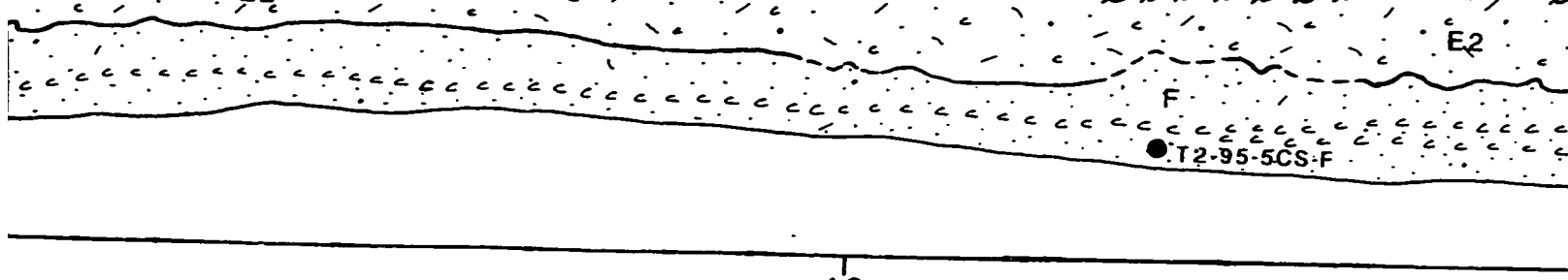

EXPLANATION OF TRENCH LOGS

Clay	Contact: dashed where approximate; queried where uncertain
Silt	Gradational soil contact
Fine sand	Shear: dashed where approximate; queried where uncertain
Medium to coarse sand and granules	Fracture; little to no vertical offset: dashed where aproximate; queried where uncertain
Fine gravel	Radiocarbon sample location
Medium to coarse gravel	15 Radiocarbon sample number
40 Stratigraphic unit (descriptions in Appendix A)	N30W Strike of prominent shear
	(K) Krotovina

NOTES

1. Ground surface and geologic contacts are based on tape and level measurements.
2. Not all symbols may be present on all trench logs.
3. Elevations are relative to ground surface only.
4. Horizontal distance is in meters.
5. See Figure 9 for trench location.
6. See Appendix C for ages of radiocarbon samples.

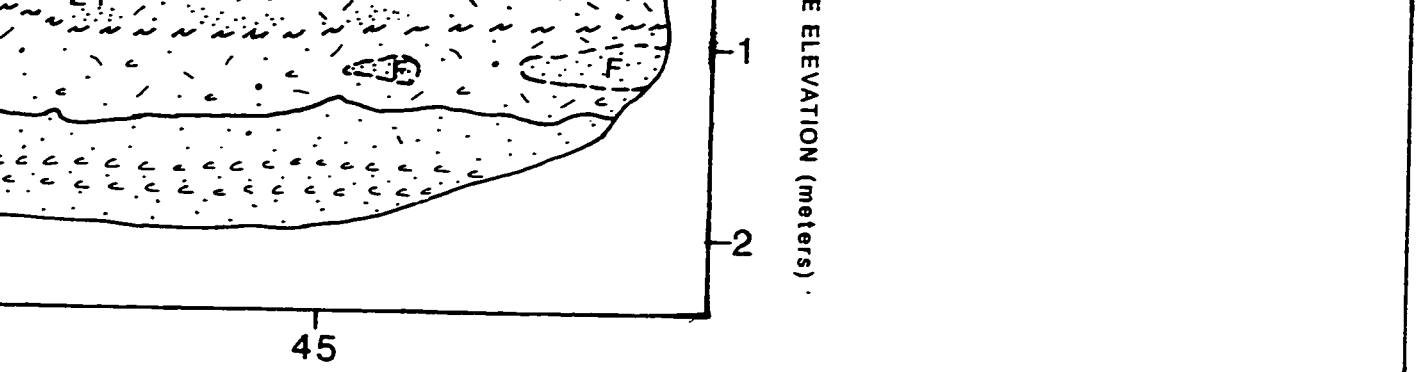

PLATE 3

LOG OF TRENCH 2

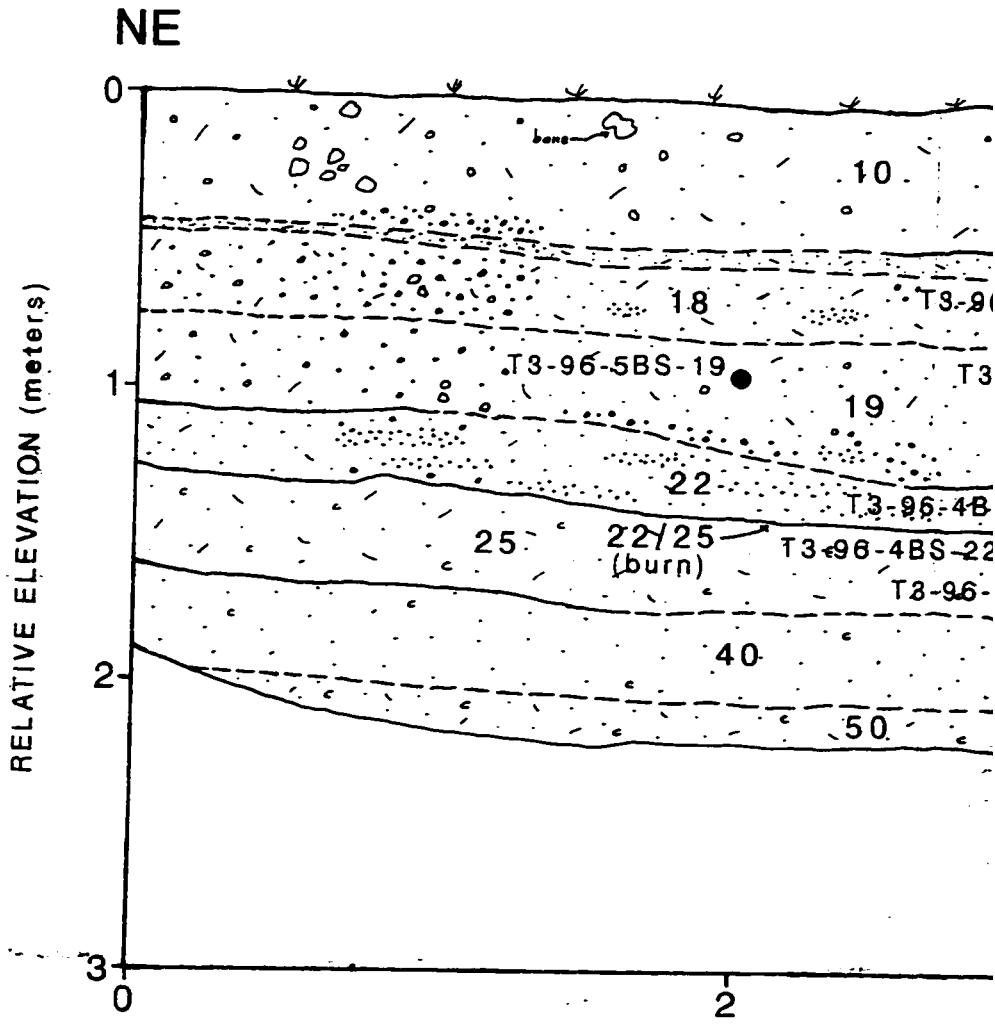
NE
RELATIVE ELEVATION (meters)
0
1
2
3
0
2
bone
10
18
T3-96-5BS-19
19
22
T3-96-4B
25
22/25
(burn)
T3-96-4BS-22
40
50

TRENCH 3
South Wall

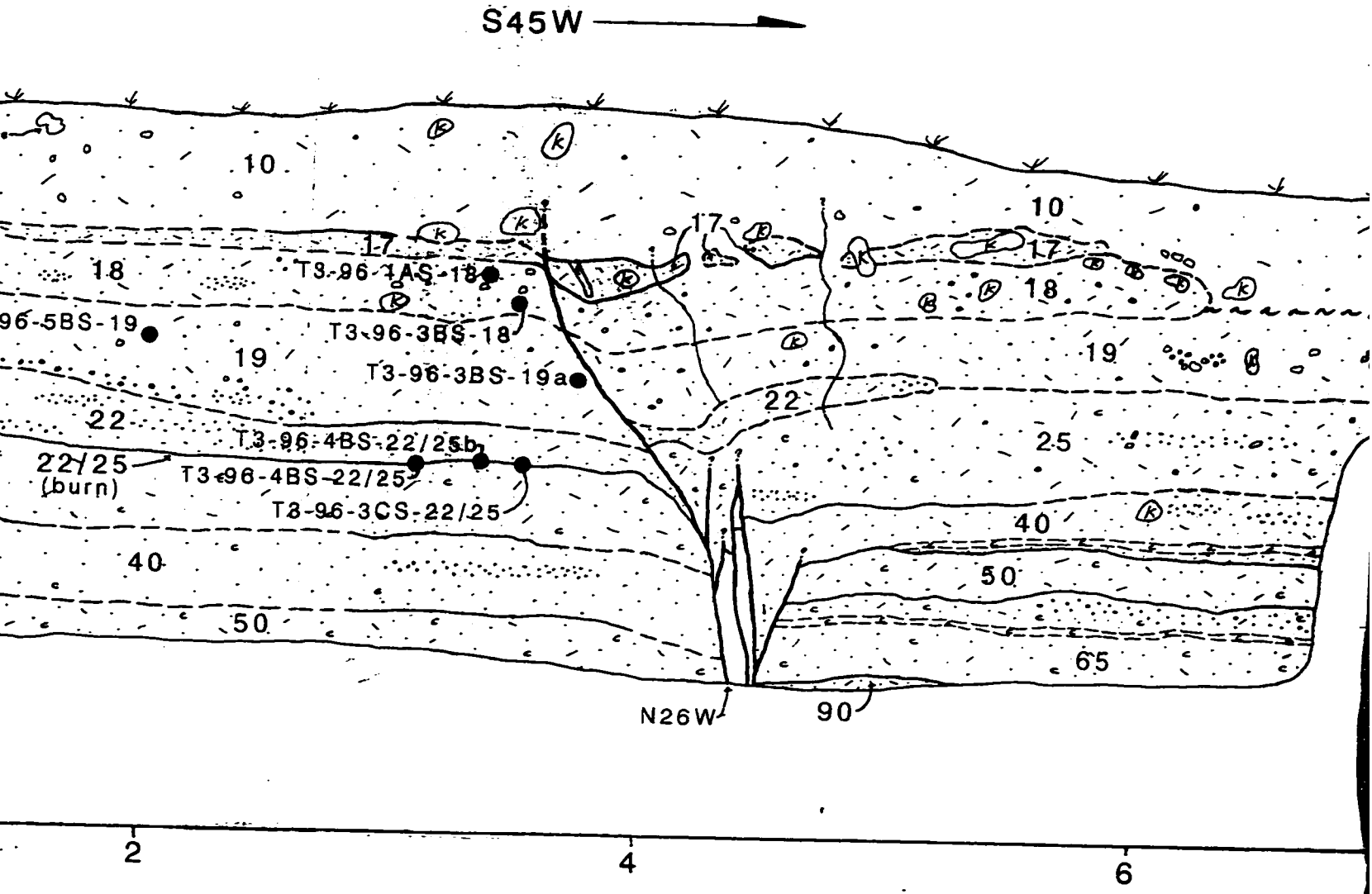

TRENCH 3
North Wall

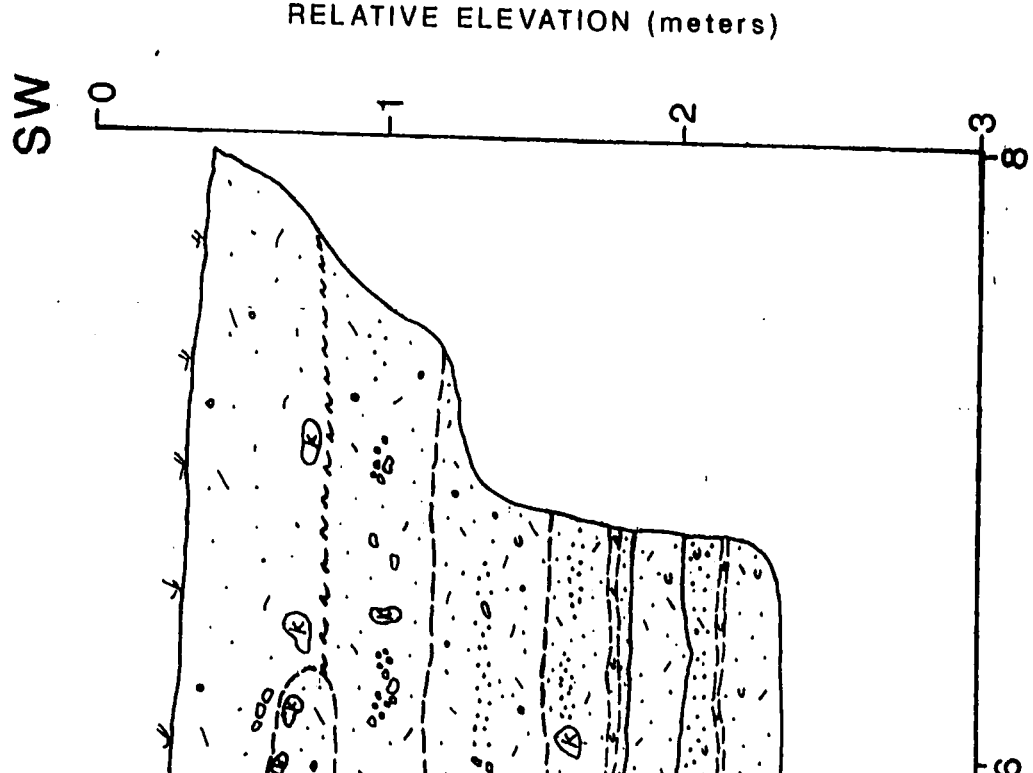
RELATIVE ELEVATION (meters)
SW
0
1
2
3
8
6

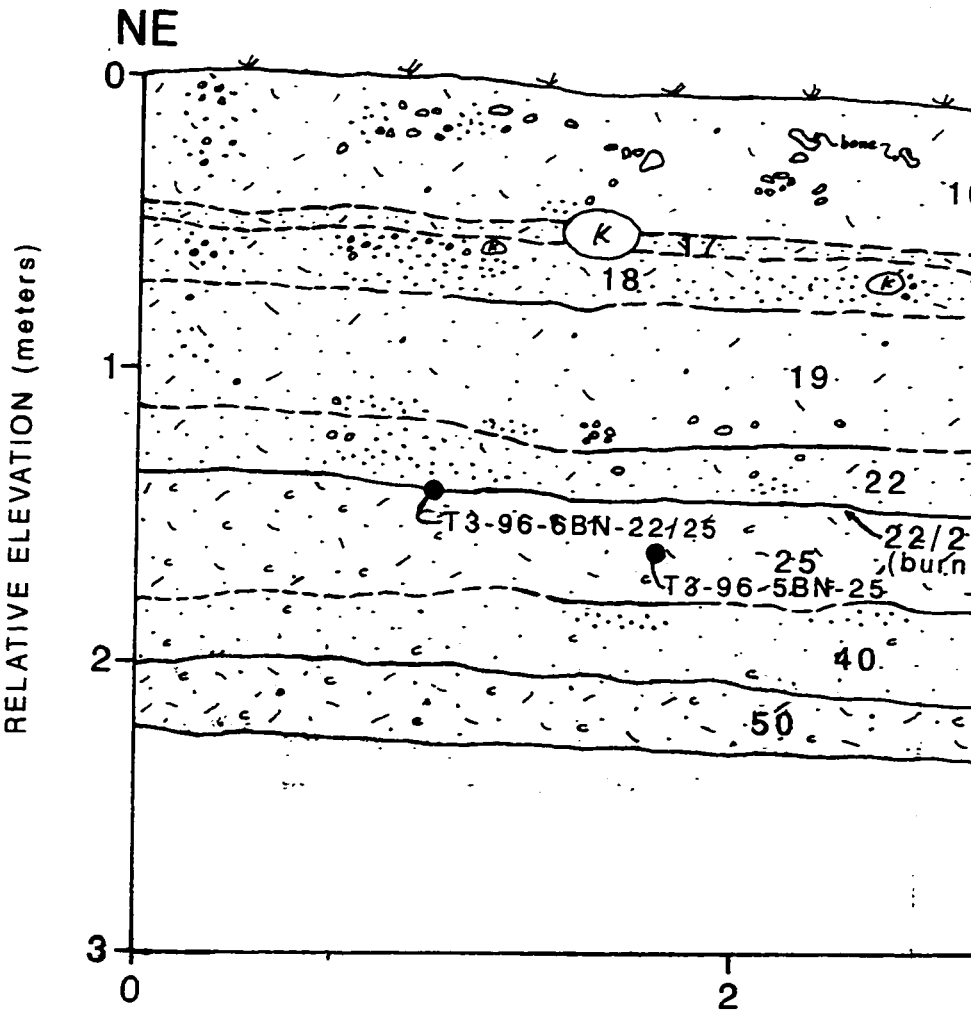

EXP

Clay

Silt

TRENCH 3
North Wall

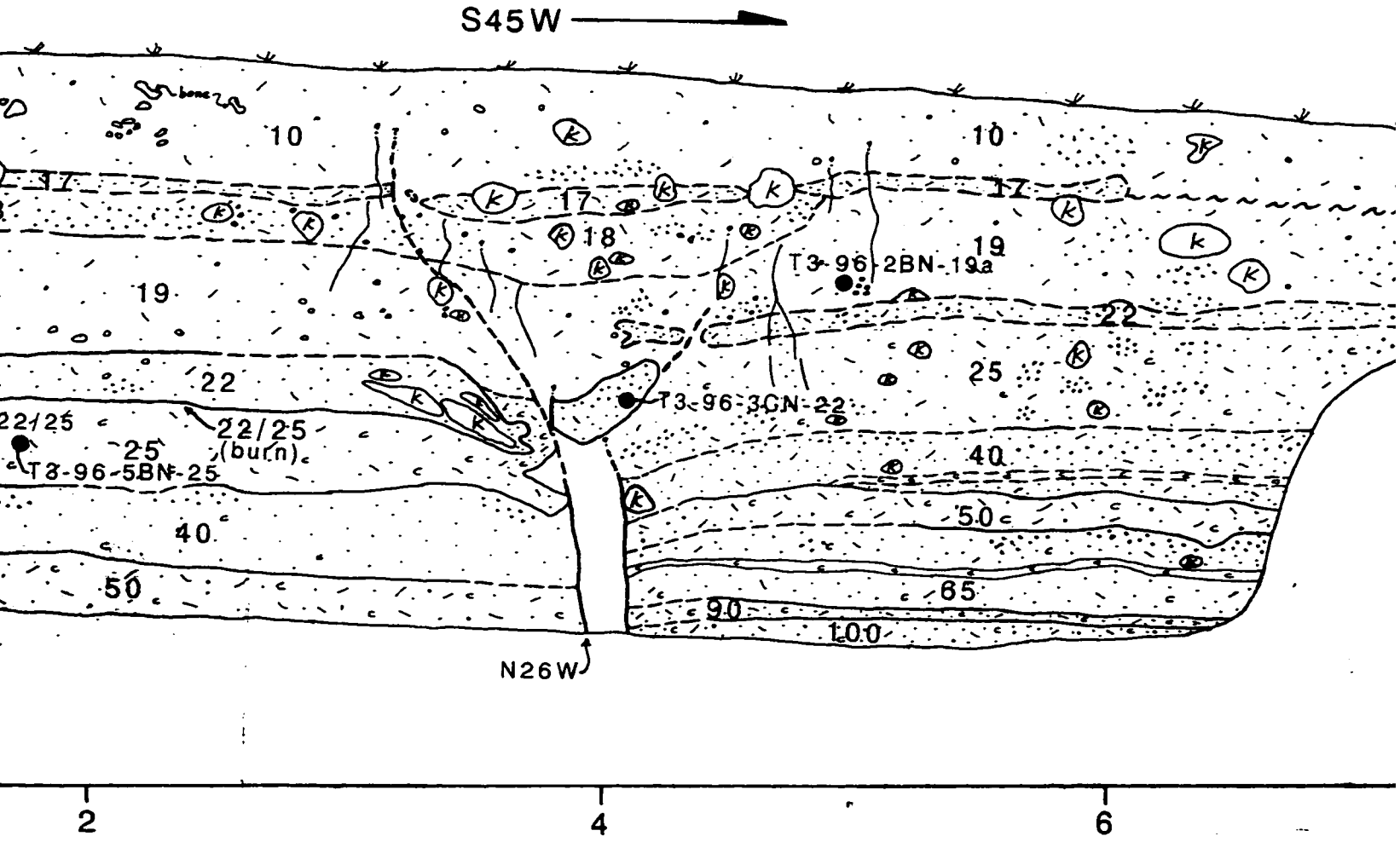

EXPLANATION OF TRENCH LOGS

Clay

Silt

———?Contact: dashed where approximate; queried where uncertain

~ ~ ~ Gradational soil contact

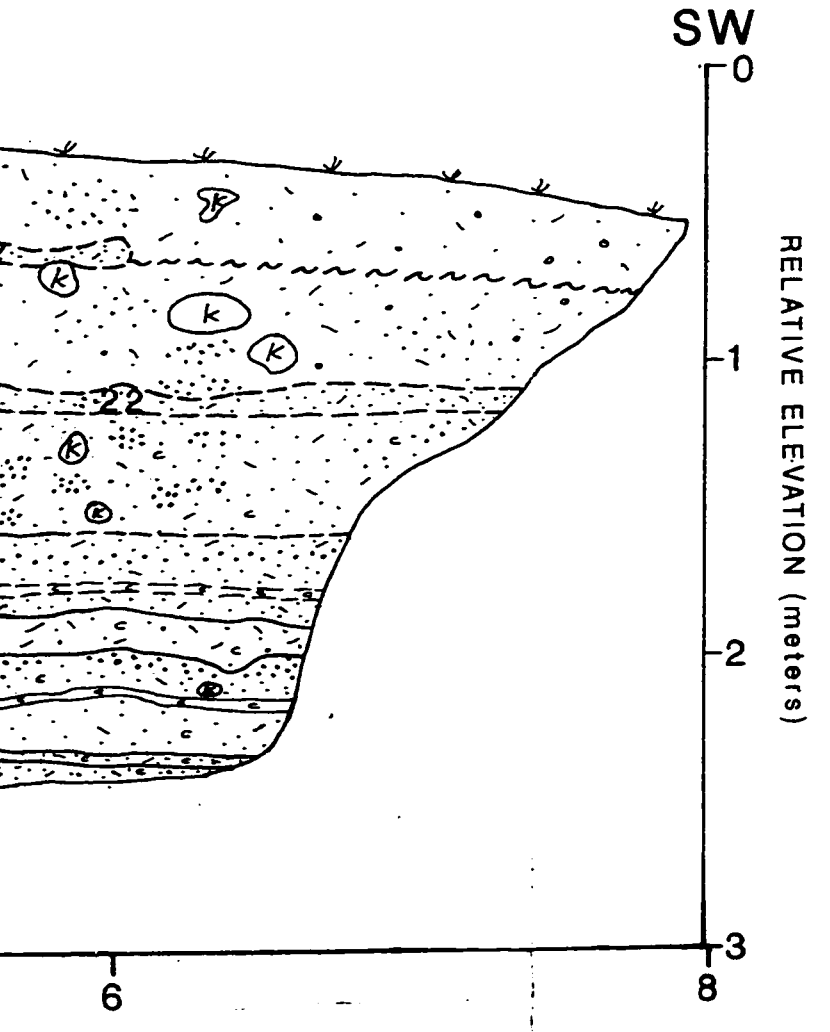

re approximate;
ain

act

EXP

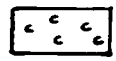
Clay

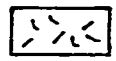
Silt

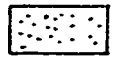
Fine sand


Medium to coars


Fine gravel

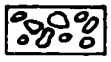
Medium to coars

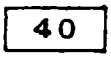

Stratigraphic unit
in Appendix A)

NOTES

1. Ground surface and geolo
2. Not all symbols may be p
3. Elevations are relative to
4. Horizontal distance is in
5. See Figure 9 for trench
6. See Appendix C for ages

Clay

Silt

Fine sand

Medium to coarse sand and granules

Fine gravel

Medium to coarse gravel

Stratigraphic unit (descriptions in Appendix A)

Contact: dashed where approximate; queried where uncertain

Gradational soil contact

Shear: dashed where approximate; queried where uncertain

Fracture; little to no vertical offset: dashed where aproximate; queried where uncertain

Radiocarbon sample location

15 Radiocarbon sample number

N30W Strike of prominent shear

(K) Krotovina

S

ound surface and geologic contacts are based on tape and level measurements.
t all symbols may be present on all trench logs.
vations are relative to ground surface only.
rizontal distance is in meters.
e Figure 9 for trench location.
e Appendix C for ages of radiocarbon samples.

pproximate;

roximate;

ical offset:

ion

ber

s.

PLATE 4

LOG OF TRENCH 3

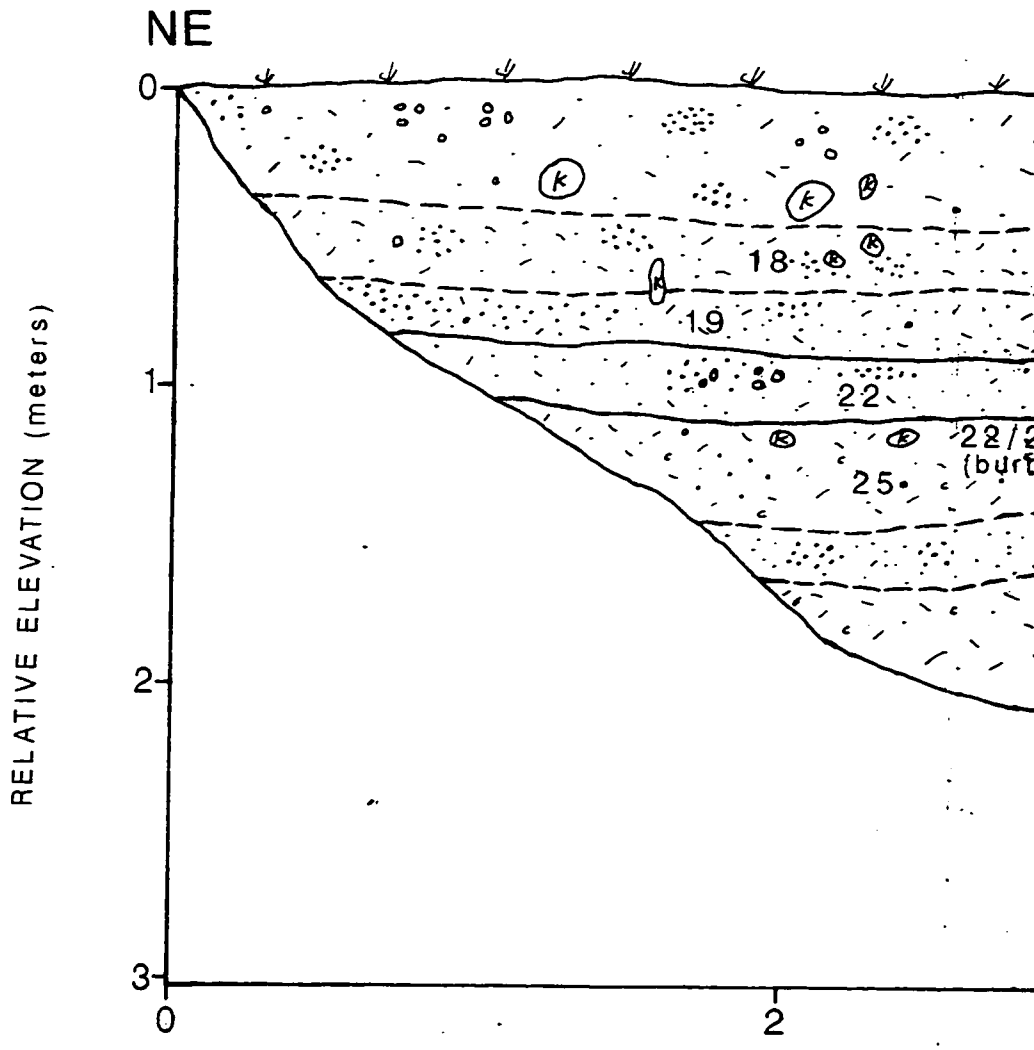
NE
0
1
2
3
RELATIVE ELEVATION (meters)
K
K
K
18
19
22
25
0
2

TRENCH 4
South Wall

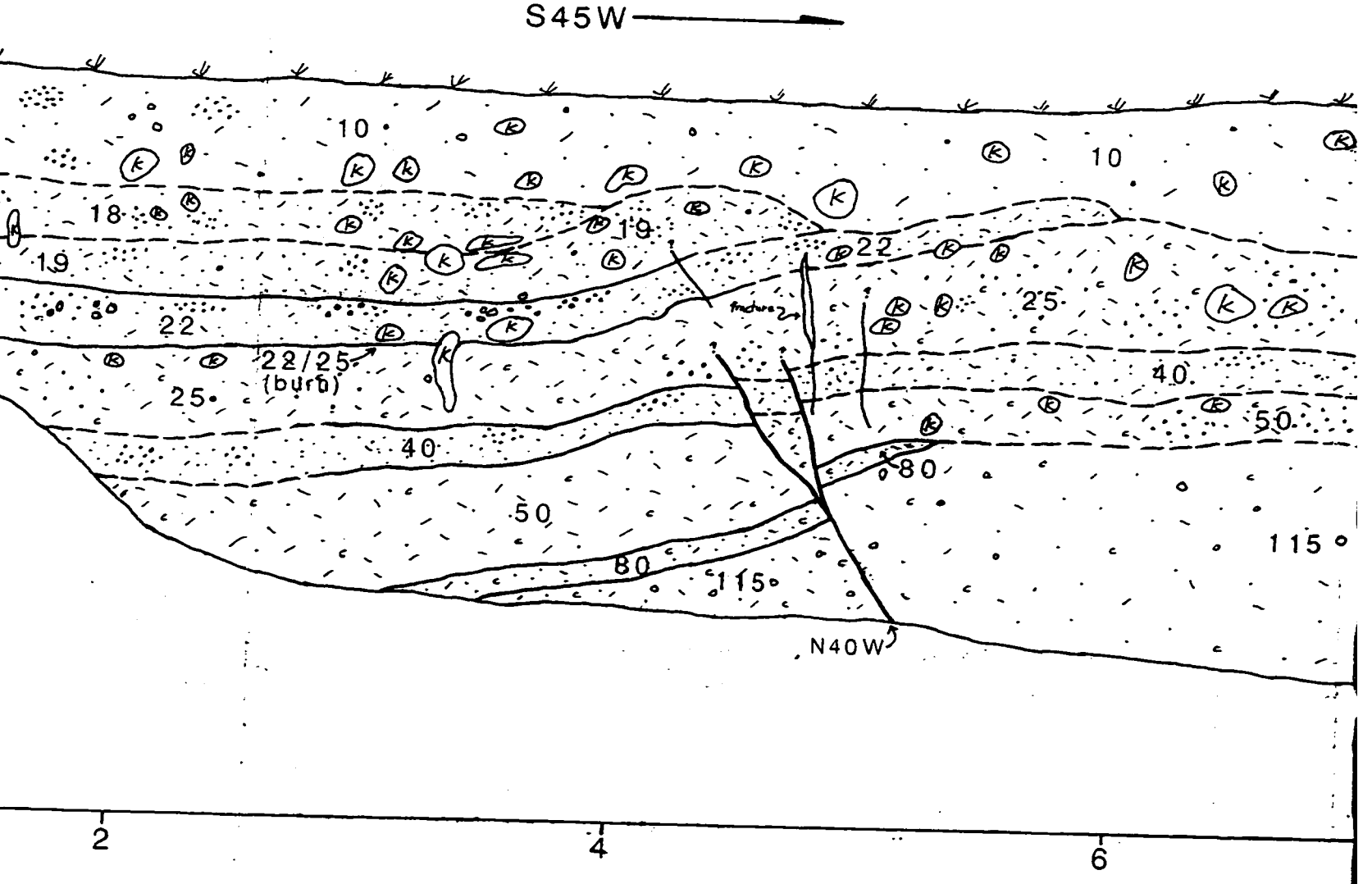

TRENCH 4
North Wall

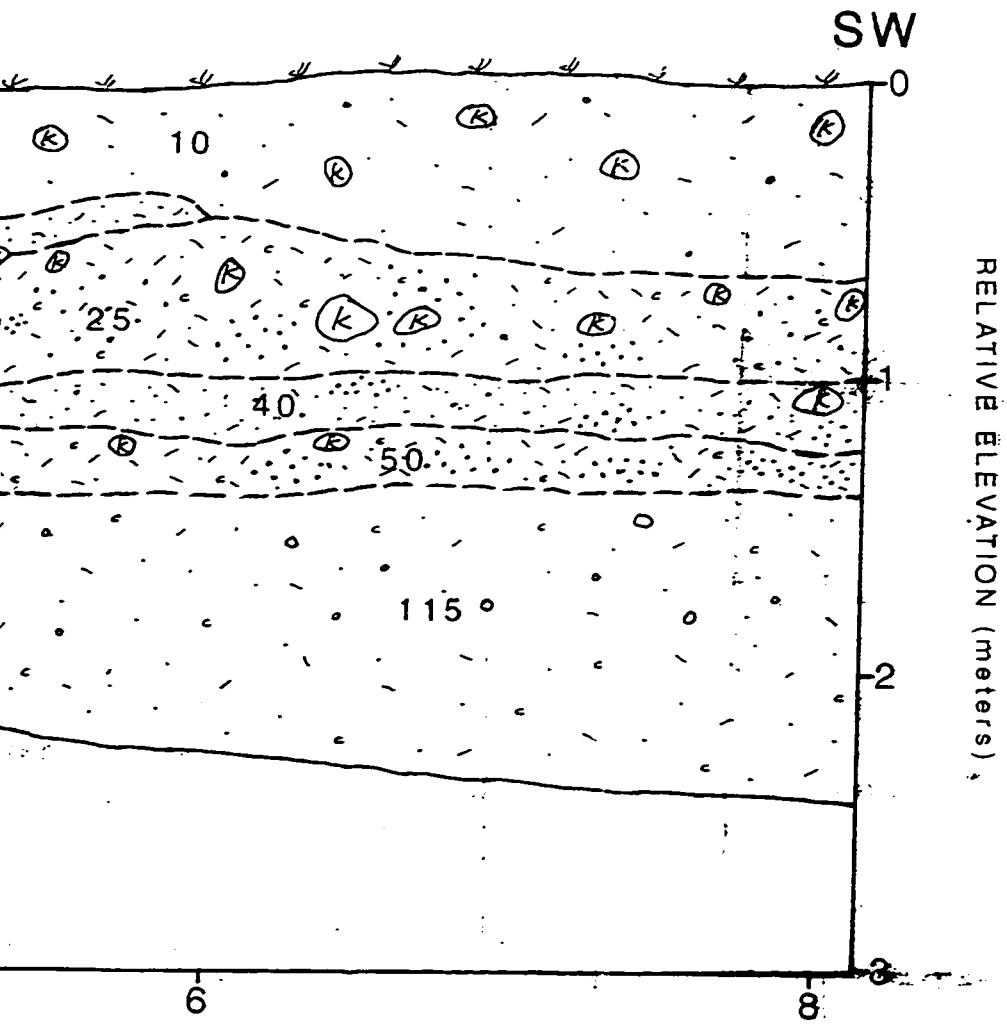
SW
0
1
2
3
10
25
40
50
115
6
8
RELATIVE ELEVATION (meters)


3
0
2

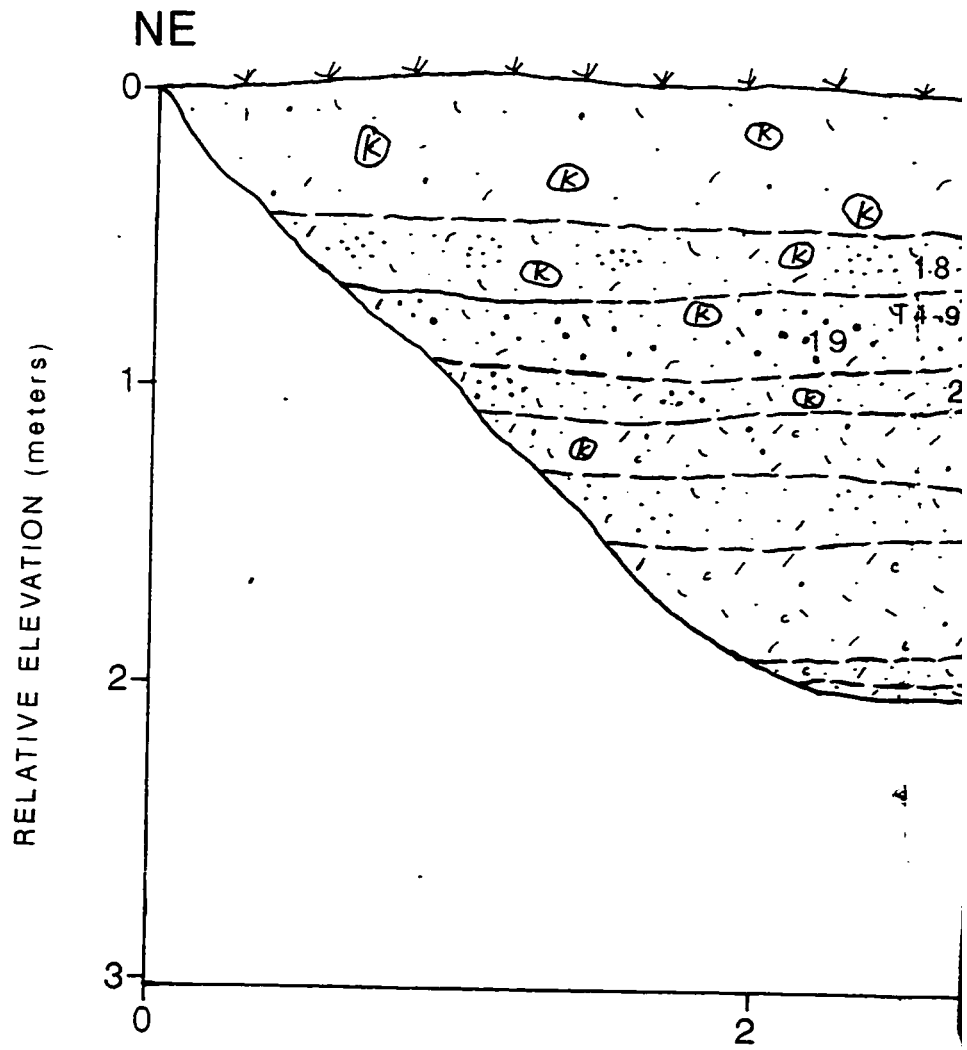
NE
0
1
2
3
0
2
RELATIVE ELEVATION (meters)
K
1.8
1.9
2

2 4 6

TRENCH 4
North Wall

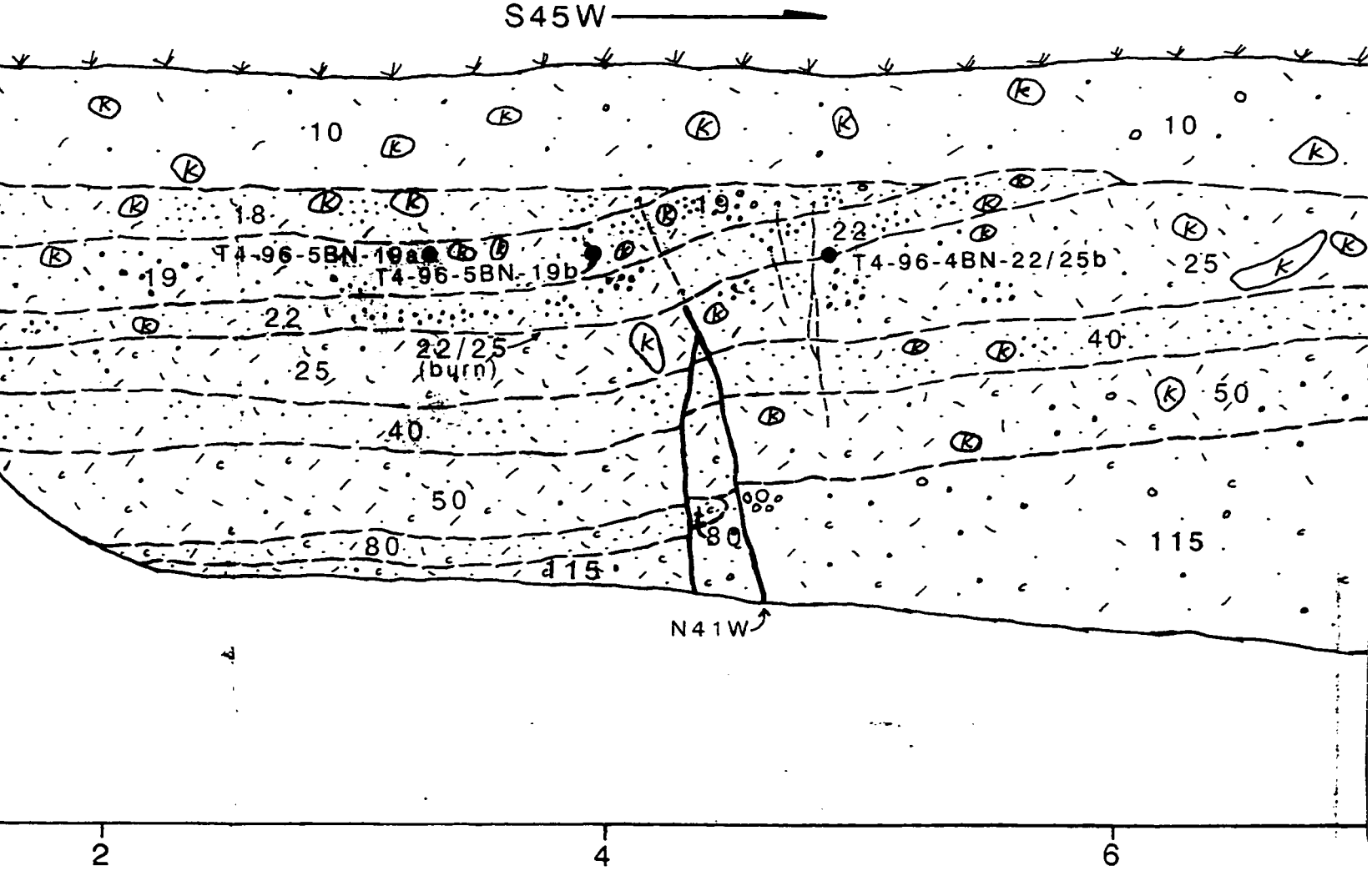

2 4 6

EXPLANATION OF TRENCH LOGS

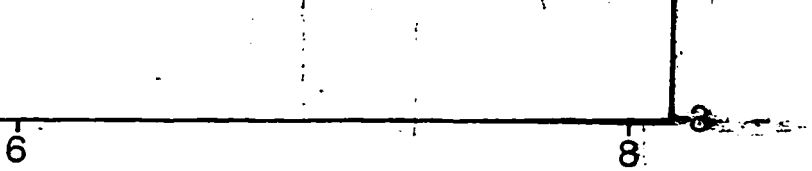

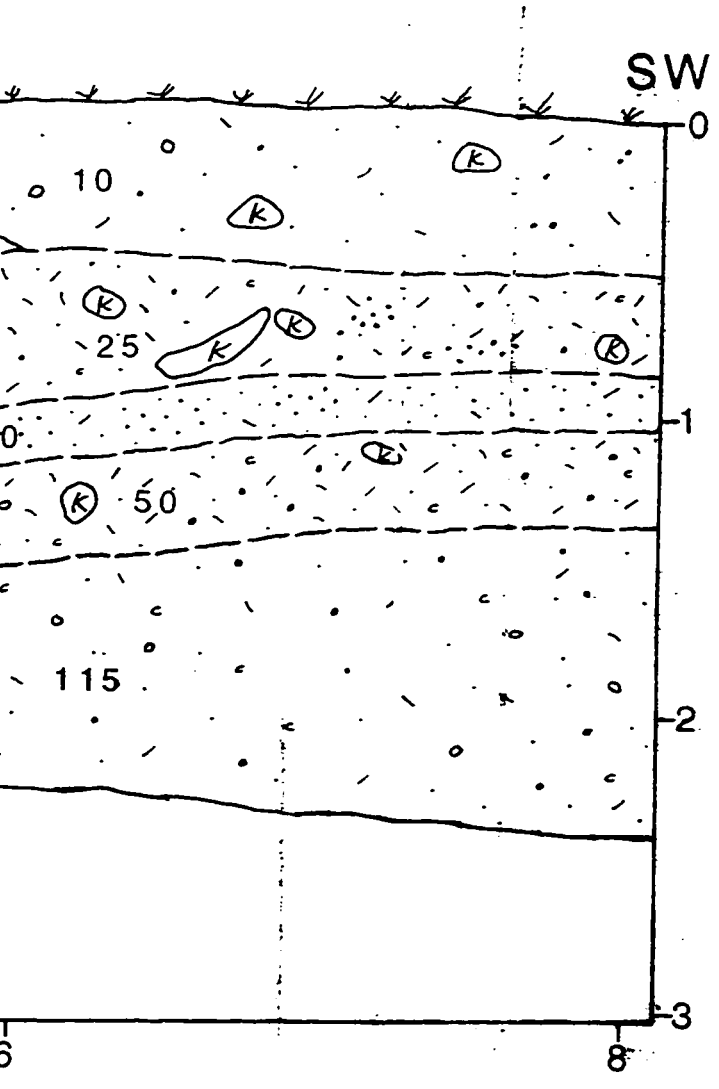

RELATIVE ELEVATION (meters)

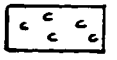

Clay

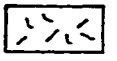

Silt

Fine sand

Medium to c

Fine gravel

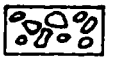

Medium to c

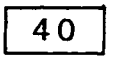

Stratigraphic
in Appendix

NOTES

1. Ground surface and g
2. Not all symbols may b
3. Elevations are relative
4. Horizontal distance is
5. See Figure 9 for tre
6. See Appendix C for a

EXPLANATION OF TRENCH LOGS

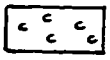
Clay

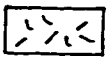
Silt


Fine sand


Medium to coarse sand and granules

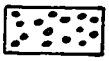
Fine gravel

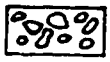
Medium to coarse gravel

40 Stratigraphic unit (descriptions in Appendix A)

———?Contact: dashed where approxim queried where uncertain

~ ~ ~ Gradational soil contact

———?Shear: dashed where approximat queried where uncertain

———?Fracture; little to no vertical off dashed where aproximate; queried where uncertain

● Radiocarbon sample location

15 Radiocarbon sample number

N30W Strike of prominent shear

(k) Krotovina

NOTES

1. Ground surface and geologic contacts are based on tape and level measurements.
2. Not all symbols may be present on all trench logs.
3. Elevations are relative to ground surface only.
4. Horizontal distance is in meters.
5. See Figure 9 for trench location.
6. See Appendix C for ages of radiocarbon samples.

re approximate;
ain

ct

approximate;
ain

vertical offset:
ate;
in

cation

umber

ear

ents.

PLATE 5

LOG OF TRENCH 4

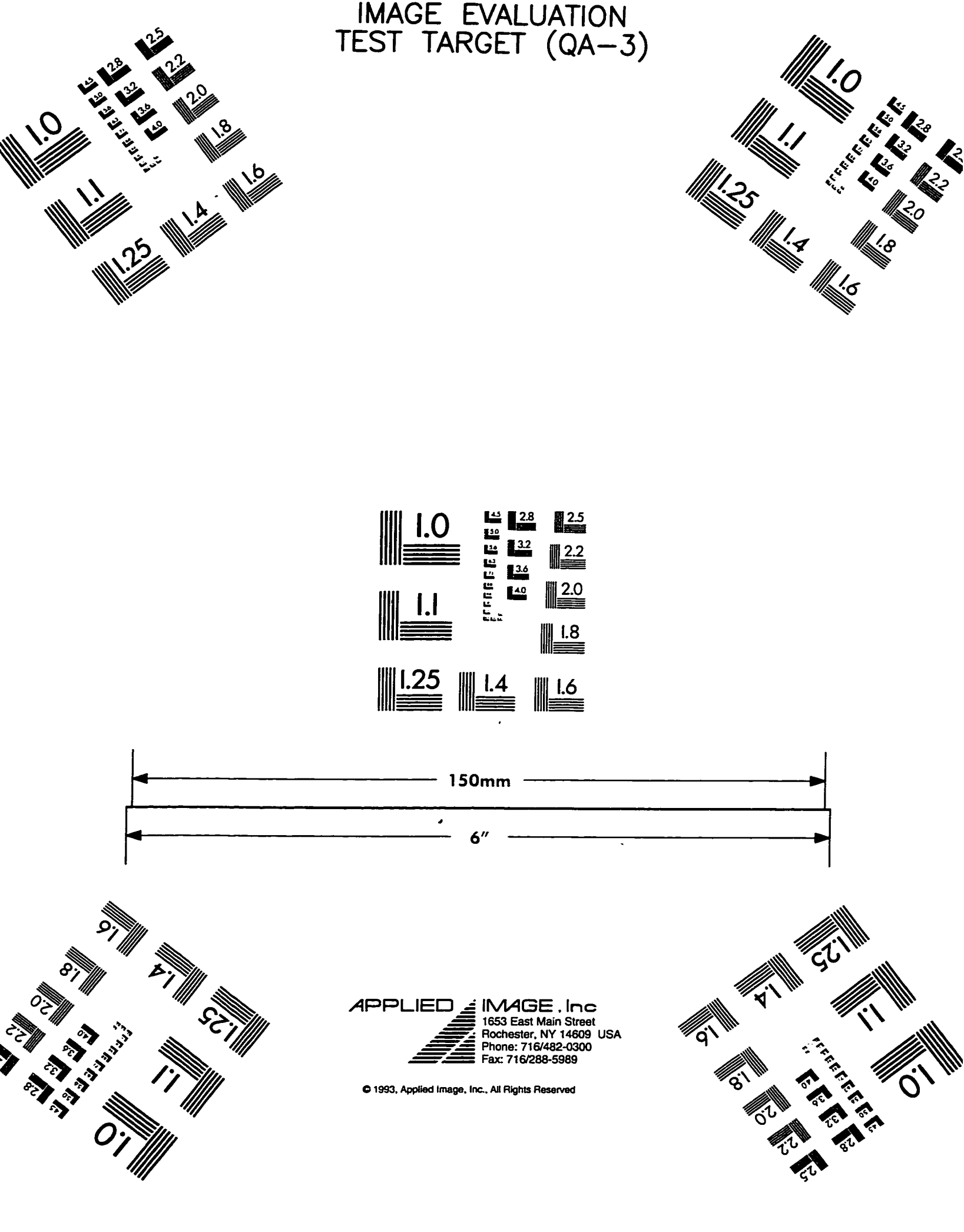
IMAGE EVALUATION
TEST TARGET (QA-3)
1.0
1.1
1.25
1.4
1.6
1.8
2.0
2.2
2.5
2.8
3.2
3.6
4.0
150mm
6"
APPLIED IMAGE, Inc
1653 East Main Street
Rochester, NY 14609 USA
Phone: 716/482-0300
Fax: 716/288-5989
© 1993, Applied Image, Inc., All Rights Reserved